The study of the complexation of Sn(II)-APDDMP and Sn(IV)-PEIMP, considered as potential therapeutic agents for bone metastases

This dissertation was submitted to the
University of Cape Town
in fulfillment of the requirements for the degree of
MASTER OF SCIENCE

By

David R. Jansen
B.Sc(Hons) University of Cape Town

UNIVERSITY
OF CAPE TOWN

necsa
We're in your world
NUCLEAR TECHNOLOGY & SERVICES

The study of the complexation of Sn(II)-APDDMP and Sn(IV)-PEIMP, considered as potential therapeutic agents for bone metastases

D.R. Jansen

Department of Radiochemistry, Necsa, PO Box 582, Pretoria, 0001, South Africa,
davidj@necsa.co.za

necsa
We're in your world
NUCLEAR TECHNOLOGY & SERVICES

The research described in this thesis was funded by Necsa (South African Nuclear Energy Corporation, Ltd.). All experiments were conducted in the department of Radiochemistry, Necsa.

TABLE OF CONTENTS

ACKNOWLEDGE MENTS

I would like express my gratitude to my supervisors Dr Jan Rijn Zeevaart and professor Graham Jackson for their guidance and contributions toward the completion of this thesis. I regard it a privilege to have been mentored by individuals such as these, with their wealth of knowledge and experience in the field. Thank you to Jan Rijn for his motivation and being an enthusiastic mentor, assisting in my understanding of the subject material and for initiating the project. Thank you to professor Jackson for his valuable input and advice.

I would also like to extend a word of thanks to NECSA management – in particular Dr Van Zyl de Villiers – for support, and for having provided a suitable environment for conducting research, and allowing me the liberty of submitting this work toward the completion of my MSc degree.

Thank you to Mrs Deidre Brooks (UCT, Department of Chemistry, administration) for her assistance and facilitation of my registration, and for being my 'mediator' within the Science Faculty and Department of Chemistry.

Special thanks to my parents for their support and fervent prayers. I am grateful for their selfless sacrifice through the years enabling me to advance toward my intended (current) career, and for having inspired me to pursue my ambitions.

And above all, I praise God for giving the strength and ability to accomplish everything I have up till now. I thank Him for having surrounded me with the right people (everyone mentioned above, and the many others that I've failed to mention) and providing me with opportunities for personal growth in all aspects of life. Thank God for His perfect design, for His love, mercy and grace. *Soli Deo Gloria*.

LIST OF ABBREVIATIONS

APD	1-Hydroxy-3-amino-propylidene-diphosphonate commercially known as Pamidronate^{TM}
APDDMP	N, N,-dimethylenephosphonate-1-hydroxy-4-aminopropylidene-diphosphonate
β	Radioactive decay by emission of an energetic beta-particle (electron)
Bq	Bequerel; unit of radioactivity, one decay per second
C	degrees Celsius
Ci	Curie; unit of radioactivity, 1 curie = $3.7 \times 10^{10}\ Bq$
Cit or cit	citrate
Cys	cysteinate
Diphosphonate or bisphosphonate	$^{2-}O_3P\text{-}C\text{-}PO_3^{2-}$ covalent bond. Not easily hydrolysed
DTPA	Diethylenetriaminepenta-acetate
E_0	electrode constant

ECCLES	Evaluation of Constituent Concentration in Large Equilibrium Systems
EDTMP	Ethylenediamine-tetramethylenephosphonate
ESTA	Equilibrium simulation for Titration Analysis; computer programs suite
γ	Radioactive decay by emission of an electromagnetic γ-ray
GEP	Glass Electrode Potentiometry
H	proton
h or hr	hour
HEDP	1-hydroxy-ethylene-diphosphonate also known as Etidronate
His or his	histidinate
HMDP	Hydroxy methylenediphosphonate
ICP	Inductive Coupled Plasma used for chemical analysis
J	Joule

keV	kilo electron volt
L	ligand
LFER	Liner Free Energy Relationships
log β	logarithm of the overall formation constant
log K	logarithm of the stepwise formation constant
LWL	Low-molecular-Weight Ligands
M	$mol.dm^{-3}$ or metal-ion
MeV	mega electron volt
MDP	Methylenediphosphonate also known Medronate
mV	milli volt
$\bar{n}$	average number of protons per ligand in the absence of metal-ion
Necsa	South African Nuclear Energy Corporation Ltd.
pA	negative logarithm of the free deprotonated ligand concentration

PEI-MP	N,N',N'-trimethylenephosphonate-polyethyleneimine
pH	negative logarithm of the free acid concentration
pK_a	negative logarithm of the acid dissociation constant
p.m.i.	Plasma Mobilisation Index
$^{32}PO_4^{3-}$	^{32}P-orthophosphate, first studies in 1935
$\overline{Q}$	deprotonation function, the average number of protons released as a result of complexation per metal-ion
Sal or sal	salicylate
^{153}Sm-EDTMP	Commercially Quadramet^{TM} since 1997. Discovered in the 1980s.
^{117m}Sn(IV)-DTPA	Radiopharmaceutical: Tin(IV)-117m - Diethylenetriaminepentaacetate
^{99m}Tc-MDP	Commercially known as MDP^{TM} or Amerscan^{TM}.
$\overline{Z}$	formation function, the average number of protons bound per metal-ion

$\overline{Z_H}$	formation protonation function, the average number of protons bound per ligand

INTRODUCTION AND THEORY

1.1 Introduction

Apart from the common understanding of the skeleton, simply being "the bony or more or less cartilaginous framework supporting the soft tissues and protecting the internal organs of a typical vertebrate", as described by the Webster dictionary, it is, in fact, in itself a rather complex organ with functions more fundamental towards sustaining the life of the organism. The skeleton facilitates mobility by providing sites of attachment for muscle, it participates in metabolism as the depository for calcium and phosphate ions, and very importantly it serves to protect the very sensitive bone marrow. During the lifetime of an organism bone tissue undergoes continual resorption (destruction) and reconstruction [1, 2] – better known as remodelling. The two opposing effects work in synch, establishing a reasonable balance within healthy individuals. As can be anticipated, this equilibrium is not always static and conditions arise to upset the harmony. One such case being osteoporosis, in which the rate of resorption exceeds the rate at which new tissue is regenerated, thus resulting in a local or systemic bone deficit. Conversely, the excessive and uncontrolled cell division within the tissue is also possible, leading to the formation of tumours (irregular growths). This disease, better known as cancer, is painful and certainly fatal if not diagnosed and treated early. A secondary form of cancer also occurs in which the cells from a certain tumour are separated from the organ of origin and transported in the body to a different site/organ where it develops [3]. These secondary tumours are referred to as metastases. The skeleton is a common site for metastases. Metastatic bone cancer usually originates from breast, prostate and lung cancers.

Interest has mounted in recent years in developing radiopharmaceuticals for specifically targeting bone where tissue is over-expressed, as is typical of bone tumours. The hope is to identify a drug for effective pain palliative therapy and treatment. These studies are geared towards identifying chemical structures that exhibit an affinity for bone tissue, as well as – and very importantly – low levels of toxicity to the more sensitive healthy bone marrow. Radiopharmaceuticals make it

possible to render an anti-tumour effect at low chemical levels. These therapeutic agents are comprised of two key components: a radionuclide (radioactive metal-ion) and a ligand with which it is complexed. The individual entities, or/and their combination, should exhibit an affinity for hydroxyapatite and its components (i.e. the main mineral phase of bone) allowing for the selective accumulation in bone, particularly concentrating in the affected areas with high bone-turnover. The radionuclide is the 'active' ingredient and is responsible for rendering relief upon selective uptake at the target site – ideally with negligible damage to healthy tissue.

Key factors to consider when selecting an effective radionuclide include: (i) the ability to produce the radionuclide with high enough specific activity (i.e. high amount of radioactivity per mg metal) and radionuclide purity; (ii) radiation characteristics; and (iii) the half-life. Ensuring low levels of bone marrow toxicity is vital. A radionuclide that could prove promising is radioactive tin-117m (^{117m}Sn). It is particularly novel in that it emits mono-energetic conversion electrons with a discrete range (0.2-0.3mm) in bone tissue, which allows for larger bone radiation doses without excessive radiation to the bone marrow. Radionuclides that have previously been considered [9] include ^{153}Sm and ^{166}Ho with observed ranges of 0.55mm and 2.7mm, respectively. ^{153}Sm and ^{166}Ho emit high energy beta radiation, which do not allow for an increase in the administered radiation dose without posing a threat to bone marrow in terms of its radiotoxicity. Therefore their therapeutic efficacy is compromised due to these dosage limitations. Being an Auger emitting radionuclide, ^{117m}Sn will introduce a highly localized distribution of electrons once inside the cell. Furthermore, ^{117m}Sn possesses a favourable half-life of 13.6 days. Therefore, by virtue of the favourable radiation characteristics that radioactive ^{117m}Sn demonstrates, it would be beneficial to conduct preliminary experiments with stable isotopes of tin (Sn^{II} and Sn^{IV}), in which tin is considered as a component of prospective radio-drugs by studying its interaction with potential bone-seeking ligands. Suffice to note that tin, in itself, is also regarded as bone-seeking [4]. By calculating the relevant equilibrium constants (β) – using potentiometric methods and ESTA computer analysis, it is

possible to predict the speciation of the systems, whereupon the susceptibility of the complex to competition within blood plasma can be tested by ECCLES modelling.

The function of the ligand is to prevent complex dissociation and to facilitate the transfer of the radionuclide to the target site. The complex should exhibit a selective affinity for the tumour tissue, as in the case of secondary bone metastasis requiring it to be bone-seeking. The ligand of choice should selectively accumulate in regions of high Ca^{II} concentration, which is characteristic of areas affected by secondary bone metastasis. Phosphonates are known to have a particular affinity for Ca^{II}. Some (di)phosphonic acid derivatives that have been previously considered include EDTMP (ethylenediamine-tetramethylenephosphonate) and [1-hydroxyethylidene]-disphonic acid (HEDP) [5]; and also diethylenetriamine penta-acetic acid (DTPA) [6]. Others were methylenediphosphonic acid (MDP) [5]; 1-hydroxy-3-amino-propilydenediphosphonic acid (APD) [7]; and more recently N,N-dimethylenephosphonate-1-hydroxy-4-aminopropylidenediphosphonate (APDDMP) [8]. Although some of these ligands showed limited success, ^{153}Sm-EDTMP is commercially used. The characteristics of $^{117m}Sn^{IV}$-DTPA appear to be more optimal [9] despite the fact that DTPA is not a phosphonate ligand and therefore not a bone-seeker per se. The effectiveness is derived from $^{117m}Sn^{IV}$ which has a relatively high affinity for bone [4].

APD had been applied in the inhibition of osteoclast activity by adsorption on the bone surface (hydroxyapatite). In addition to minimizing resorption APD served a complimentary function in regenerating bone tissue [10] in that, due its mobilisation of Ca^{II} and Mg^{II} in blood plasma, whereby they are deposited onto bone. Being such a versatile ligand, attempts were made to capitalize on its capabilities by complexing it to a radioactive metal-ion, and in so doing utilize it as a bone-cancer diagnostic agent; e.g. ^{99m}Tc-APD for bone scintigraphy [11]. However, in studies with trivalent lanthanides such as $^{166}Ho^{III}$ a neutral complex $[MLH]^0$, and hence, a colloid formed at pH 7.4 (where M = Ho^{III}, L = APD, H = proton), which resulted in excessive liver uptake [7, 12]. Furthermore APD exhibited a high affinity for Ca^{II} which impeded the

delivery of the radionuclide $^{166}Ho^{III}$ to bone. In an endeavour to avert the formation of a neutral species, APD was modified by adding two charged methylenephosphonate groups at the primary amine centre, resulting in the synthesis of APDDMP - with a net charge of 7- (*Figure 1.1a*) [13]. APDDMP possesses 8 dissociable protons. However, protonation of the tertiaty amine results in an overall charge of 7- in solution.

***Figure 1.1a**: Molecular structure of the ligand N,N,-dimethylenephosphonate-*

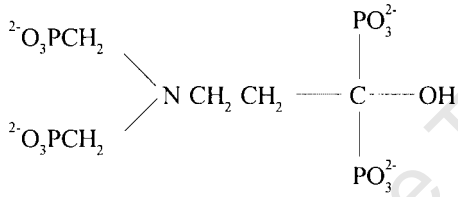

APDDMP

1-hydroxy-4-aminopropylidene-diphosphonate (APDDMP)

A recent approach was to develop/design a water-soluble polymer which is bone-seeking, and in so doing attempt to exploit the 'Enhanced Permeability and Retention Effect' [14] by which these macromolecules passively accumulate in solid tumours. This uses the principle that tumours often have ruptured vasculature, which results in an increase vascular permeability of the tumour tissue. Therefore particles of the right size might escape the vasculature and enter the tumour. The macromolecules are then simply retained within the tumour, especially due to an ailing lymphatic system within tumour tissue. However, it is important to note that size does matter. By virtue of its size, the aim is to avoid uptake by healthy tissue (too small), and accumulation within organs such as kidneys and liver (too large). In this study this was achieved by functionalizing the water-soluble polymer polyethyleneimine (PEI) with methylenephosphonate groups; essentially, the polymerized version of EDTMP, called polyethyleneiminomethyl phosphonic acid (PEI-MP) [6, 15] (*Figure 1.1b*). The optimum fraction of 10 to 30 kDa was determined by Dormehl *et al* [16].

These two 'newer' ligands were considered in the experiments presented in the subsequent chapters 2 to 5, namely APDDMP (N,N-dimethylenephosphonate-1-hydroxy-4-aminopropylidenediphosphonate) (Chapters 2, 3 and 5) and PEI-MP (*N,N',N'-trimethylenephosphonate-polyethyleneimine*) (Chapter 4).

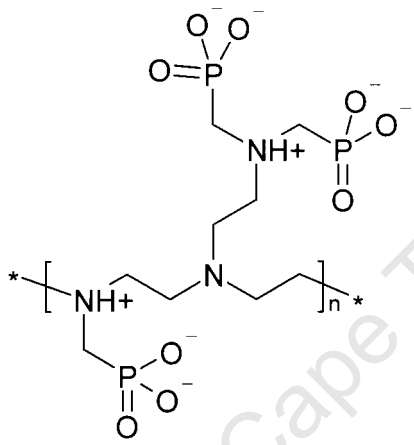

***Figure 1.1b**: Molecular structure of the ligand N,N',N'-trimethylenephosphonate-polyethyleneimine (PEI-MP)*

1.2 Potentiometry

The primary technique adopted during the investigation of prospective radiopharmaceuticals is that of potentiometry. Fundamentally, the method is based on the interpretation of electrode potentials generated by the (electro)chemical interaction between Lewis acids (metal ions) and bases (ligands) – demonstrating, chemically, the tendencies of a given system placed under certain stresses within conditions of interest.

The electrode potentials arise due to the movement of electrons between the two entities comprising what is referred to as half-reactions. During the reaction the rates of the two half-reactions become equal and equilibrium is reached. The individual half-reactions do not stop, but continue reversibly. Each half reaction possesses a standard electrode potential, E^{o}, which is defined as the electrode potential at which the activities of all the reactants and products are unity [17]. Electrode potentials are measured relative to that of the standard hydrogen electrode (SHE), which being reversible, behaves as either an anode or a cathode. This characteristic makes it an ideal reference, and can sensibly assume a potential of 0.000V. Its action as either a cathode or anode is determined by the electrode with which it is coupled. By convention, the SHE acts as the anode, rendering the electrode potential as a reduction potential. The oxidation potential is distinguished by a negative sign. The SHE operates by bubbling hydrogen gas (at constant pressure of 1atm, and hydrogen ion activity of 1*M*) over platinum metal – which serves merely as a site for electron transfer and does not itself participate in the reaction. The reaction is as follows:

$$\mathbf{2H^{+}_{(aq)} + 2e^{-} \leftrightarrows H_{2(g)}} \qquad \textbf{(1.2a)}$$

and schematically represented as

$$\mathbf{Pt,H_2(p = 1.00\ atm)|([H^{+}] = 1M)||} \qquad \textbf{(1.2b)}$$

Essentially, electrode potentials are simply the measure of the extent of reduction; and by virtue of its sign, the ease/readiness of the reaction with relative to the standard hydrogen potential.

The electrode potential of a half-reaction can be calculated from the concentrations of the individual species comprising the process, as well as the conditions such as temperature and, in some instances, pressure. These are substituted into an expression known as the Nernst equation, which for a typical reversible half-reaction

$$\mathbf{aA + bB + \ldots + ne^{-} \leftrightarrows cC + dD} \qquad \textbf{(1.2c)}$$

can be written as

$$E = E^{\circ} - \frac{RT}{nF} \ln \frac{[C]^c[D]^d \ldots}{[A]^a[B]^b \ldots} \quad \textbf{(1.2d)}$$

where A, B, C, D represent molecular formulas of the species, e^- is the electrons, and *a, b, c, d* are the number of moles of the respective species participating in the given half-reaction. E° is the standard electrode potential.

For example, consider the half-reaction of the SHE above (equation 1.2a). The Nernst expression for the electrode potential is given by:

$$E = E^{\circ} - \frac{RT}{nF} \ln \frac{p_{H_2}}{[H^+]^2} \quad \textbf{(1.2e)}$$

Substituting the constants R = 8.314$JK^{-1}mol^{-1}$, T = 298K (25°C), and F = 96485 C, and replacing the natural logarithm with log (base 10), ln = 2.303log, the equation can be re-written:

$$E = E^{\circ} - \frac{0.0592}{2} \log \frac{p_{H_2}}{[H^+]^2} \quad \textbf{(1.2f)}$$

Note that when a species is a gas the activity/concentration is replaced by the partial pressure (atm). Should the reaction have a solid or a pure liquid, the activity assumes the value 1, as its concentration is considered to be constant – as too with the solvent.

The general Nernst equation (1.2d) can thus also be written as

$$E = E^{\circ} - \frac{0.0592}{n} \log \frac{[C]^c[D]^d \ldots}{[A]^a[B]^b \ldots} \quad \textbf{(1.2g)}$$

Being a very versatile analytical tool, potentiometry provides a means whereby the activity of cations and anions in solution can be determined. Its application in this regard has been adapted for the purpose of studying the behaviour of potential radiopharmaceuticals in an intricate system such as blood plasma. The Nernst equation can be derived for calculating the activities of cations or anions.

For anion A^{n-} $$E_{cell} = K + \frac{0.0592}{n} pA \quad \textbf{(1.2h)}$$

and for cation X^{n+} $$E_{cell} = K - \frac{0.0592}{n} pX \quad \textbf{(1.2i)}$$

(where $K = E_j - E_{ref} + L$, $pA = -\log a_A$, and $pX = -\log a_X$.)

E_{cell} is the experimentally determined cell potential. The typical cell being represented as

reference electrode | salt bridge | analyte solution | indicator electrode

Therefore $E_{cell} = E_{ind} - E_{ref} + E_j$, where the reference electrode represents a half-reaction with an accurately known electrode potential E_{ref}, and is independent of the concentration of the analyte or any other spectator ions in solution. The indicator electrode, which, by convention, is treated as the cathode, measures the analyte potential, E_{ind}. Across the salt bridge a potential develops at the liquid junctions, the net potential of which is given by E_j (net junction potential).

With potentiometry, small changes in the analyte concentration can be observed, which makes it a useful tool for more accurate determination of end-points or inflections during titrimetric experiments. The cell potential is measured as a function of the titrant volume. Potentiometric titration data provide sequential "snapshots" of changes, if any, that a given system (analyte) could experience as induced by the gradual addition of a reagent. For example, the stepwise dissociation of a ligand (Lewis base) such as EDTA (ethylenediaminetetraacetic acid) can be elucidated by gradually increasing the pH. The titration data can be analyzed by software programs such as ESTA (Equilibrium Simulation for Titration Analysis) [18, 19] during which relevant changes, if any, in the system can be interpreted.

By introducing a metal (Lewis acid) to the ligand analyte, the formation of various complexes can be observed as the ligand's protons dissociate with increasing pH. These are known as complexiometric or complex-formation titrations. Various equilibrium constants can be calculated from cell potentials. Among others, are dissociation constants and formation constants (β), which are of greater significance for complexation and speciation studies.

1.3 Speciation and Modeling

Radiopharmaceuticals are composed of a radioisotope/radionuclide (radioactive metal ion) moiety which is bound by/to a ligand to form a complex. Essentially, the ligand is responsible for delivering the radionuclide to the target organ where the tumor is present. Ideally the ligand should exhibit a relatively high, and selective, affinity for the tumour tissue, which serves as a key driving force for directing the drug to the target. However, when dealing with intricate physiological/biological systems such as the human body, one has to take into consideration the factors that could affect the stability of a drug. Upon injection into the body, a drug is exposed to a wide variety of other ligands and metal-ions present in blood plasma alone. This could pose a threat to the survival of the radio-drug, before it reaches the target site. The ligands present in blood plasma could have higher affinity for the metal-ion bound within a given complex, or the in vivo metal-ions could easily displace the radioactive metal-ion. A successful radiopharmaceutical is one that accumulates selectively at the tumour site, having effectively overcome competition, and survived the conditions within blood plasma.

The stability of a complex can be considered in two respects; kinetic and thermodynamic. The thermodynamic stability is obtained when the system reaches equilibrium and is represented by an equilibrium constant. The kinetic stability refers to the rate at which the equilibrium was reached. Thermodynamic equilibria provide information about the binding characteristics between metal-ions and ligands, and can assist in understanding the behaviour of a complex under certain conditions. Consider the general reaction (where M = metal-ion, L = ligand, and N = maximum coordination number of the metal-ion for the particular ligand (N is dependent on the ligand):

$$\mathbf{M} + N\mathbf{L} \rightleftharpoons \mathbf{ML}_N \qquad \textbf{(1.3a)}$$

The equilibrium can be represented by the overall formation constant as follows:

$$\beta_N = \frac{[ML_N]}{[M][L]^N} \quad \textbf{(1.3b)}$$

Alternatively, the thermodynamic equilibrium can be expressed in terms of the step-wise stability constants:

$$K_N = \frac{[ML_N]}{[ML_{N-1}][L]} \quad \textbf{(1.3c)}$$

according to the reaction:

$$\mathbf{ML_{N-1} + L \rightleftharpoons ML_N} \quad \textbf{(1.3d)}$$

The overall formation constant can also be described as the product of the step-wise formation constants.

$$\beta_n = K_1 K_2 K_3 ... K_n = \prod_{i=1}^{i=n} K_i \quad \textbf{(1.3e)}$$

For example, a typical reaction $aM + bL + cH \rightleftharpoons M_aL_dH_c$ **(1.3f)**

will produce the following result:

$$\beta_{a,b,c} = \frac{[M_a L_b H_c]}{[M]_a [L]_b [H]_c} \quad \textbf{(1.3g)}$$

(where M = metal-ion, L = ligand, H = hydrogen ions within the complex, and *a, b, c* are the number of moles of the respective participating species).

The same equation can be used to describe the proton dissociation (protonation) of the ligand, when the metal is omitted, i.e. a = 0.

1.3.1 ESTA

The data obtained from potentiometric experiments can be processed by a computer package of programs known as ESTA (Equilibrium Simulation for Titration Analysis). This robust software package provides an effective means for optimizing the data and refining the formation constants, thereby deriving a suitable model that best defines the system (interactions of the ligand and metal) of interest. The program equates the experimental/real concentrations (T_i^r) with the calculated total

concentrations (T_i^C) in the form of a mass-balance equation, which it attempts to solve by Newton-Raphson methods [20].

$$T_i^r = T_i^C \qquad (i = 1, \ldots, NC \qquad \text{for } NC \text{ complexes}) \qquad \textbf{(1.3.1a)}$$

T_i is the sum of the individual concentrations of the species comprising the system;

$$T_i = X_i + \sum_j S_j k(i,j) \qquad \textbf{(1.3.1b)}$$

where S_j is the species concentration, X_i is the free concentration and $k(i,j)$ is the stoichiometric coefficient.

$$S_j = \beta_j \prod_i X_i^{k(i,j)} \qquad (\beta_j = \text{equilibrium constant}) \qquad \textbf{(1.3.1c)}$$

The equations are solved iteratively, by calculating for "*NC-free*" concentrations, whereupon an electrode equation is evaluated so as to obtain the free electrode-ion concentrations, $[X_k]$, as observed by the electrode potential E_k:

$$E_k = E_k^0 + E_k^S + E_k^J \qquad \textbf{(1.3.1d)}$$

(where E_k^0 = electrode response intercept, E_k^S = electrode selectivity, and E_k^J = liquid-junction potential.).

The Henderson equation [21, 22] (*1.3.1e*) is used to correct for changes in the liquid-junction potentials when the glass electrodes are calibrated;

$$E_k^J = -\frac{RT}{F} \ln\left(1 + d\frac{[X_H]}{I}\right) \qquad \textbf{(1.3.1e)}$$

where I = concentration of background univalent electrolyte.

The effects of interfering ions are also accounted for by the Eisenman equation [20];

$$E_k^{IS} = s_k \log\left(\{X_k\}^{1/\alpha} + K_{ki}\{X_i\}^{1/\alpha}\right)^{\alpha} \qquad \textbf{(1.3.1f)}$$

Effectively, the parameters such as thermodynamic formation constants, β, and some unknown free concentrations can be calculated from other *free* concentrations and parameters – or reasonable estimates thereof – that have been experimentally

determined and/or derived from the electrode equations. (The formation constants are dependent on the conditions in which they are determined, particularly the ionic strength (I) of the medium.) The equations – usually of an absolute-value nature, or natural logarithm in the case of $[X_k]$ and β – are soluble by simultaneous back-substitution. The Secant method [23] can also be attempted to solve the equations for free concentrations only, in the event that the Newton-Raphson calculation is unsuccessful.

Gauss-Newton algorithms [24] are used to optimize a calculated model representation of the experimental data. This is achieved by firstly calculating the experimental parameters, such as the initial concentrations of the participating species and formation constants, at the first and second titration points – from experimental values. The free electrode-ion concentration can then be calculated from these initial estimates and their respective electrode potentials. Whereupon, the parameters at each subsequent point can then be estimated by linear extrapolation from the previous two points by considering the change in the electrode potential at each titration point. Essentially, the program simulates the experimental titration data in an attempt to derive a favourable representation of the formation of complexes within the system. This iterative process is then repeated until the fitted model – with the estimated parameters – is sufficiently refined and close to the solution. The extent, to which the calculated parameters fit the experimental data, can be determined by observing the standard deviations of the parameters and the Hamilton R-factor [24, 25], and the Hamilton R-limit [24, 25] – the Hamilton R-factor being a measure of the difference between the objective function (parameters being refined) and experimental data points. The Hamilton R-limit gives the theoretical minimum of the Hamilton R-factor by considering the total number of data points, the number of refined parameters and the standard error in the experimental data. Therefore the goodness of fit of the calculated model is reflected by the difference between the Hamilton R-factor and the R-limit – the smaller the difference the better the fit. This sequential analysis of titration data allows for the calculation and refinement of parameters such as total analytical concentrations, initial vessel and burette concentrations, initial vessel

volume, estimation of formation constants, and even the determination of emf values and electrode slope. A least-squares method is used to calculate the optimum values within groups of identical parameters (same type or value) of a combination of titrations, by treating them as a single parameter. The results are interpreted by the ESTA into the following functions:

- $\overline{Z_H}$ and $\bar{n}$, the protonation function, which is defined as the number of protons bound by the free ligand (in absence of complexation) at respective pH values.
- $\bar{Z}$, the complex-formation function, defined as the number of ligands bound per metal-ion(s) at respective pH values.
- $\overline{Q}$, the deprotonation function which describes the number of protons lost by the ligand during complexation at respective pH – essentially, the displacement of protons by the metal-ion(s) during complex-formation.

These functions can be translated into graphs by plotting the calculated potentials, E_k^{calc}, *i.e.* pH against $\overline{Z_H}$ or $\overline{Q}$ (with $\bar{n}$), and $\bar{Z}$ against pA, whereby the observed (experimental) functions, E_k^{obs} can be compared.

Once an acceptable model of formation constants has been derived, representing the interactions between a ligand and metal-ion of interest, the speciation of the ligand can be determined – i.e. a distribution of the corresponding complexes/species as they form at their relevant pH values.

1.3.2 ECCLES, Blood Plasma Modeling

The potentiometric data and ESTA analysis thereof provides a reasonably good idea of how the system (combination of ligand with metal-ion) will behave in isolation, within simulated physiological conditions. However, in order make more accurate predictions of the performance of the potential radio-drug, it will be beneficial to extend the investigation to compensate for the likelihood (more often than not) of competition by physiological ligands and metal ions within the blood plasma. The

ECCLES computer program and database can aid in this respect (ECCLES = Evaluation of Constituent Concentrations in Large Equilibrium Systems [26]).

In the body, metal-ions can be found as components of proteins, complexed to low-molecular-weight ligands (LWL) that occur naturally in blood plasma, or as the water-solvated aqua-ions. The ECCLES program takes into account the reactions between free metal-ions and LWLs.

The effect of protein binding (irreversibly or reversibly) on metal-ion–LWL equilibria is to buffer the free metal-ion concentration such that it remains fairly constant, considering that the total concentration of proteins present in blood plasma greatly exceeds the total metal-ion concentration, and the free metal-ion concentration is significantly less than that of the protein bound metal-ions. Excessive denaturation of proteins will be necessary to noticeably influence the free metal-ion concentration – the equilibrium of which will, most likely, eventually be restored.

During blood plasma simulations the free metal-ion concentration is fixed, whilst the total metal-ion concentration is allowed to vary, but within blood plasma limits. The percentage distribution of essential transition metal-ions is calculated as they are bound among a host of ligands, forming a vast cocktail of complexes. The calculations allow for the complexation of more than one ligand per metal-ion, i.e. binary and ternary complexes. The free metal-ions include (in order of decreasing concentration in blood plasma): Ca^{2+}, Mg^{2+}, Zn^{2+}, Fe^{2+}, Mn^{2+}, Pb^{2+}, Cu^{+}, Ni^{2+}, Cu^{2+}, and Fe^{3+}.

1.4 Research objectives

This study forms part of the ongoing pursuit for an effective treatment, and pain palliative therapy of metastatic bone cancer. The aim is to develop novel radiopharmaceuticals which are selective for bone tissue, and capable of providing anti-tumour effect with minimal side effects.

The core components of these radiopharmaceuticals include a radio-active metal-ion (radioisotope), which provides the therapeutic effect, and a ligand (Lewis base), which serves mainly as a carrier/transporter medium for the radioisotope. This study is primarily intended towards identifying these moieties in the context of bone cancer, and to elucidate their combined action as potential radio-therapeutic agents. This would entail having to design or select suitable ligand structures that exhibit bone-seeking, as well as tumour accumulation ability. Furthermore, a radioisotope will have to be identified that exhibits favourable radiation characteristics with minimal radiotoxicity. Once these have been established the complexation behaviour of the metal-ion and ligand can be evaluated by potentiometry, and in so doing determine the equilibrium constants of formation for the complexes – hence their speciation. It will also be beneficial to explore the interaction of the selected ligands with major metal-ions constituting blood plasma, namely Ca^{II}, Mg^{II} and Zn^{II}, providing some basic insight into the *in vivo* action of the respective drug. With the aid of computer modelling – incorporating the formation constants mentioned above – it is possible to account for the likelihood of competition for complexation by free metal-ions and ligands typically found in blood plasma. Thereby simulating the binding interactions (speciation) of physiological metal-ions and ligands, whereupon predictions can be made as to the survival/susceptibility of these drugs within the body, elucidating its effectiveness. The blood plasma modelling results could then be used to hopefully verify and explain the observed biodistribution of these, and similar radiopharmaceuticals as studied in animal experiments reported in literature [27, 28].

1.5 Thesis outline

Chapter 1 provides some basic background into the problem that this thesis is intended address, namely bone cancer and metastases and the development of an effective treatment in the form of radiopharmaceuticals. The fundamental aspects of the research methodology is described here, as well as outlining the criteria for the design and/or selection of bone-seeking radio-therapeutic agents. The rationale behind the selection of both the ligands and the radioisotope considered in this study is stipulated. Chapter 2 describes the speciation of Sn^{II} with a phosphonate derived ligand, namely N,N-dimethylenephosphonate-1-hydroxy-4-aminopropylidenediphosphonate (APDDMP) [8]. The subsequent chapter (Chapter 3) describes the measurement of the formation constants of Ca^{II}, Mg^{II} and Zn^{II} with APDDMP. The ECCLES database had been expanded to include the complete blood plasma model for Sn^{II} (for all blood plasma ligands) [13] so as to elucidate the *in vivo* behaviour of Sn^{II}-APDDMP, thereby predicting and interpreting biodistribution studies during animal experiments (Chapter 5) [27]. Chapter 4 discusses an alternative radiopharmaceutical considered for the treatment of metastatic bone cancer, namely Sn^{IV}-PEI-MP (PEI-MP = N,N',N'-trimethylenephosphonate-polyethyleneimine). Sn^{II}-PEI-MP had previously been reported by Zeevaart *et al.* [6]. The final chapter (Chapter 6) serves to draw to conclusion the broader context of this study by putting into perspective the individual components of this thesis; discussing successes, constraints and providing recommendations for future work.

1.6 References

[1] N. Jarvis, J. M. Wagener, G. E. Jackson, *J. Chem. Soc. Dalton Trans.*, 1995, 1411-1415.

[2] G .A. Rodan and T. J. Martin, *Science*, 2000, **289**, 1508-1514.

[3] L. A. Liotta, *Nature*, 2001, **410**, 24-25.

[4] R. A. M. J. Claessens and Z. I. Kolar, *Langmuir,* 2000, **16**, 1360-1367.

[5] J. R. Zeevaart, N. V. Jarvis, I. Cukrowski, G. E. Jackson, *S. Afr. J Chem., 1997,* **50**, 189-194.

[6] J. R. Zeevaart, W. K. A. Louw, Z. I. Kolar, J. M. Wagener, N. V. Jarvis, R. A. M. J. Claessens, *Journal of Radioanalytical and Nuclear Chemistry,* 2003, **257**, 83-91

[7] J. R. Zeevaart, N. V. Jarvis, W. K. A. Louw, G. E. Jackson, I. Cukrowski, C. J. Mouton, *Journal of Inorganic Biochemistry, 1999,* **73**, 265-272.

[8] J. R. Zeevaart, N. V. Jarvis, W. K. A. Louw, G. E. Jackson, *Journal of Inorganic Biochemistry, 2001,* **83**, 57-65.

[9] H. L. Atkins, L. F. Mausner, S. C. Srivastava, G. E. Meinken, R. F. Straub, C. J. Cabahug, D. A. Weber, C. T. C. Wong, D. F. Sacker, S. Madajewicz, T. L. Park, and A. G. Meek, *Radiology*, 1993, 186, 279

[10] B. Thürlimann, R. Morant, W. F. Jungi, and A. Radziwill, *Support Care Cancer,* 1994, **2**, 61.

[11] O. J. Degrossi, P. Oliveri, H. G. Del Rio, R. Labriola, D. Artagaveytia and E. B. Degrossi, *J. Nucl. Med.,* 1985, **26**, 1135.

[12] J. R. Zeevaart, W. K. A. Louw, N. V. Jarvis and J. M. Wagener, *J. Lab. Comp. Radiopharm.,* 2001, **44** suppl 1, S799-S801.

[13] J. R. Zeevaart, N. V. Jarvis, W. K. A. Louw and G. E. Jackson, *J. Inorg. Biochem.,* 2001, **83**, 57-65.

[14] L. W. Seymour, *CRC Crit. Rev. Ther. Drug Carrier Syst.,* 1992, **9**, 249

[15] J. R. Zeevaart, W. K. A. Louw, Z. I. Kolar, E. Kilian, F. E. Jansen van Rensburg and I. C. Dormehl, *Arzneimittel-Forschung Drug Reseach*, 2004, **54**, 340-347.

[16] I. C. Dormehl, W. K. A. Louw, R. J. Milner, E. Kilian and F. H. A. Schneeweiss, *Drug Res.*, 2001, **54**, 258-263.

[17] D. A. Skoog, D. M. West, F. J. Holler, *"Fundamentals of Analytical Chemistry, 7th Edition"*, 1996, Harcourt College Publishers, pp. 297, 386, 423-427.

[18] P. M. May, K. Murray and D. R. Williams, Talanta, 1985, **32**, 483-489.

[19] P. M. May, K. Murray and D. R. Williams, Talanta, 1988, **35**, 823-830, 927-932.

[20] P. M. May, K. Murray and D. R. Williams, *Talanta*, 1985, **32**, 483-489.

[21] P. Henderson, *Z. Phys Chem.*, 1907, **59**, 118; 1908, **63**, 325.

[22] G. Biedermann and L. G. Sillén, *Ark. Kemi*, 1953, **5**, 425.

[23] N. Ingri, W. Kakolowicz, L. G. Sillén and B. Warnqvist, *Talanta*, 1969, **14**, 1261; corrections, 1970, **15**, No. 3, p. xi.

[24] P. M. May, K. Murray and D. R. Williams, *Talanta*, 1988, **35**, 825-830.

[25] A. Vacca in *Proc. Summer School on Stability Constants*, Bivigliano, Florence, June 1974, p.105, Edizioni Scuola Universitaria, Firenze, Italy.

[26] P. M. May, P. W. Linder and D. R. Williams, *J. Chem. Soc. Dalton Trans.*, 1977, 588.

[27] J. R. Zeevaart, D. R. Jansen, M. F. Botelho, A. Abrunhosa, C. Gomes, L. Metello, Z. I. Kolar, G. C. Krijger, W. K. A. Louw, and I. C. Dormehl, *Journal of Inorganic Biochemistry* 2004, **98**, 1521-1530.

[28] S. C. Srivastava, G. E. Meinken, P. Richards, P. Som, Z. H. Oster, H. L. Atkins, A. B. Brill, F. F. Kapp Jr, and T. A. Butler, *Int. J. Nucl. Med. Biol.,* 1985, **12**, 167-174.

[29] D. M. Taylor and D. R. Williams, *Trace Element Medicine and Chelation Therapy,* 1995, The Royal Society of Chemistry, Cambridge.

[30] F. Albert and G. Wilkinson, *Advanced Inorganic Chemistry, 5th Edition,* 1988, Wiley-Interscience, pp. 35-83.

[31] J. R. Duffield and D.R. Williams, *Chem. Br.*, April 1989.

[32] W. A. Volkert, *J. Nucl. Med.,* 1991, **32**, 174.

[33] A. S. Alberts, B. J. Smit, W. K. A. Louw, A. J. van Rensburg, A. van Beek, V. Kritzinger and J. S. Nel, *Radiother. Oncol.,* 1997, **43**, 175-179.

[34] G. Eichhorn, '*Inorganic Biochemistry*', Elsevier, Amsterdam, 1973.

SPECIATION OF APDDMP WITH Sn^{II}

2.1 Introduction

To accurately predict the blood plasma speciation of a potential radiopharmaceutical the formation constants of such a complex need to be measured. This choice of metal ion and ligand were determined by the following considerations.

In finding a cure for metastatic bone cancer, one of the key factors to be addressed is ensuring that the level of toxicity to the target (bone marrow) is favourably reduced – if not eliminated. ^{117m}Sn with its conversion electrons of discrete energies assists in this regard. Exploiting this characteristic allows for an increase in the administered dose. Another factor to be considered would be selective accumulation of the drug in affected areas – with high bone-turnover. This is characteristic of areas affected with secondary bone metastasis. N,N,-dimethylenephosphonate-1-hydroxy-4-aminopropylidene-diphosphonate (APDDMP) (Figure 2.1) is known to have a high affinity for Ca^{II}, and could therefore be suitable to address the problem.

Glass electrode potentiometry was employed in the study of the complexation of APDDMP with Sn^{II}. Five titrations were carried out, with the following metal to ligand ratios; 1:1, 1:2, 1:3, 2:1, 1½:1. These were conducted under conditions which simulated that of blood plasma (*in vivo*), i.e. [NaCl] = 0.15*M*. The titration data were analysed with the aid of the computer programme ESTA, from which it was evident that binuclear complexes (M_2L – type complexes) were most favoured. Potentiometry showed that at the pH of interest for *in vivo* studies, pH 7.4, the complexes $[Sn^{II}_2(APDDMP)OH]^{4-}$ and $[Sn^{II}(APDDMP)^{5-}]$ predominate. The effect that competing ligands and metal ions, found in blood plasma, have on these species will also be shown.

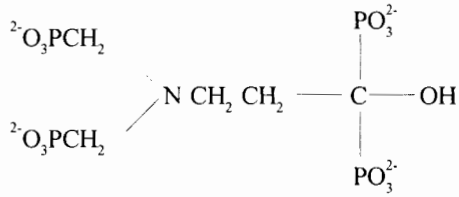

APDDMP

***Figure 2.1**: Molecular structure of the ligand N,N,-dimethylenephosphonate-1-hydroxy-4-aminopropylidene-diphosphonate (APDDMP)*

2.2 Method

Complexation of Sn^{II} with N,N,-dimethylenephosphonate-1-hydroxy-4-aminopropylidene-diphosphonate (APDDMP) was studied. Five potentiometric titrations were conducted with metal to ligand ratios 1:1, 1:2, 1:3, 2:1 and 1½:1. Conditions were chosen to simulate that of blood plasma, i.e. physiological conditions: 25°C, 0.15*M* NaCl.

In each case the initial pH was set to approximately 1.7 using 0.05*M* HCl solution in 0.1*M* NaCl, and was titrated against a 0.05*M* NaOH solution in 0.1*M* NaCl.

To prevent the oxidation of the Sn^{II} to Sn^{IV}, all solutions were prepared with de-aerated water and stored under Argon. The Sn^{II} salt was also weighed under Argon.

2.3 Results and discussion

Data points where precipitation had occurred were excluded from the analysis.
Analysis of the protonation titrations by ESTA rendered the following results for APDDMP and its complexes with Sn^{II}:

Table 2.1. *Protonation and formation constants for APDDMP and Sn^{II} determined at 25°C and I=150 mM NaCl.*

Equilibrium/ Species [#]	*log β*	*Number of data points*	*Hamilton* **R-Factor**	*log β, 37°C* [1]
$H + HL \rightleftharpoons H_2L$	9.79 ± 0.01	700	0.01736	9.82
$H + H_2L \rightleftharpoons H_3L$	16.83 ± 0.02			17.03
$H + H_3L \rightleftharpoons H_4L$	22.74 ± 0.02			23.12
$H + H_4L \rightleftharpoons H_5L$	27.68 ± 0.02			28.01
$H + H_5L \rightleftharpoons H_6L$	30.04 ± 0.04			30.05
$Sn^{II} + OH \rightleftharpoons Sn^{II}OH$	-4.20 *			
$Sn^{II} + 2\ OH \rightleftharpoons Sn^{II}(OH)_2$	-8.01 *			
$Sn^{II} + 3\ OH \rightleftharpoons Sn^{II}(OH)_3$	-17.44 *			
$2\ Sn^{II} + 2\ OH \rightleftharpoons Sn^{II}{}_2(OH)_2$	-4.16 *			
$4\ Sn^{II} + 3\ OH \rightleftharpoons Sn^{II}{}_4(OH)_3$	-9.55 *			
$2Sn^{II} + LH \rightleftharpoons Sn_2LH$	31.10 ± 0.04	974	0.01406	
$2Sn^{II} + L \rightleftharpoons Sn_2L$	26.63 ± 0.03			
$2Sn^{II} + L + OH \rightleftharpoons Sn_2LOH$	34.52 ± 0.03			
$2Sn^{II} + L + 2\ OH \rightleftharpoons Sn_2L(OH)_2$	40.62 ± 0.03			
$2Sn^{II} + L + 3\ OH \rightleftharpoons Sn_2L(OH)_3$	44.82 ± 0.03			
$2Sn^{II} + L + 4\ OH \rightleftharpoons Sn_2L(OH)_4$	48.23 ± 0.05			
$Sn^{II} + L \rightleftharpoons SnL$	15.26 ± 0.02			
$Sn^{II} + L + OH \rightleftharpoons SnL(OH)$	20.30 ± 0.03			

[#] *The charges on the ligands and complexes have been omitted for simplicity.*

* *Hydrolysis constants for Sn^{II} were obtained from literature [2] and included in the model.*

2.3.1 Protonation titrations

Within the pH range of 3 to 10 the experimental data in the $\overline{Z_H}$ curves (*Figure 2.3.1(a)*) agree favourably with the calculated function.

The proton dissociation/stability constants of APDDMP are presented in the Table 2 above. These closely resemble the values reported in literature [1, 3], despite the difference in temperature. The graphical representation of the model (Figure 2.3.1(a))

shows good agreement between the calculated curve and the experimental data. This is substantiated by the relatively low R-factor and standard deviations of the stability constants.

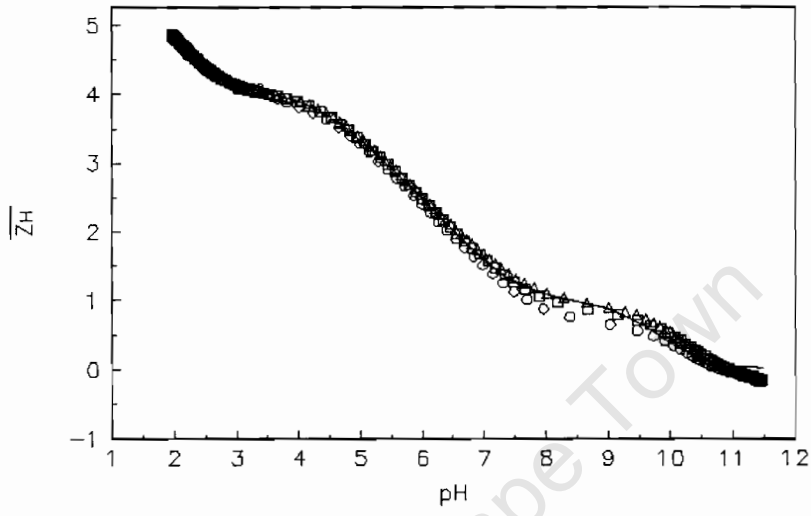

***Figure 2.3.1(a)**. Experimental (points) and modelled (lines) protonation formation curves for APDDMP. Three titrations are represented by (O) 1.02mM APDDMP and 6.56mM HCl;(Δ) 1.49mM APDDMP and 10.68mM HCl and (□) 1.19mM APDDMP and 8.41mM HCl, all titrated against 50.24mM NaOH in 100.30mM NaCl. All solutions were at 25°C and 150mM NaCl or 150mM total ionic strength.*

The proton dissociation constants can be rationalized by comparing them with results obtained in literature for similar ligands, such as APD (1-hydroxy-3-amino-propylidene-diphosphonate) [4] and EDTMP (ethylenediamine-tetramethylenephosphonate) [5]. In solution it is expected that the tertiary amine will be protonated, and the dissociation constant of this centre has been reported as pKa = 11.87 [3]. However, this is not observed (pKa_1), therefore it can be assumed that the amine remains protonated in solution. This can be confirmed in the presence of a metal-ion, whereupon coordinating at the amine site, the proton will be expected to dissociate. Amine proton dissociations are typically reported to be higher the pKa 10, for example APD exhibits a pKa_1 = 10.95 [4], and EDTMP has two amine centres for

dissociation with pKa_1 = 10.67 and pKa_2 = 9.47 [5]. The third and fifth acid dissociation constants observed for APDDMP, pKa_4 5.91 and pKa_2 9.79, are consistent with that of two diphosphonate sites for APD, which are 6.01 and 9.80, respectively [4]. The pKa_3 of 7.04, however, compares best with the protonation constant for the methylene-phosphonate centre of EDTMP (7.63) [5]. pKa_5 and pKa_6 correspond with protonations at the remaining methylene-phosphonate site and a diphosphonate site. For the purpose of this study the deprotonated ligand, usually L, was defined as H-APDDMP – with the APDDMP remaining protonated at the tertiary amine (Figure 2.1). The protonated amine does not dissociate, meaning that the completely deprotonated species is not realized.

The curves tend towards 5 below pH 3, indicating that there are five protonation sites. Below pH 10 the graph levels off at 0, suggesting that no further protons are lost.

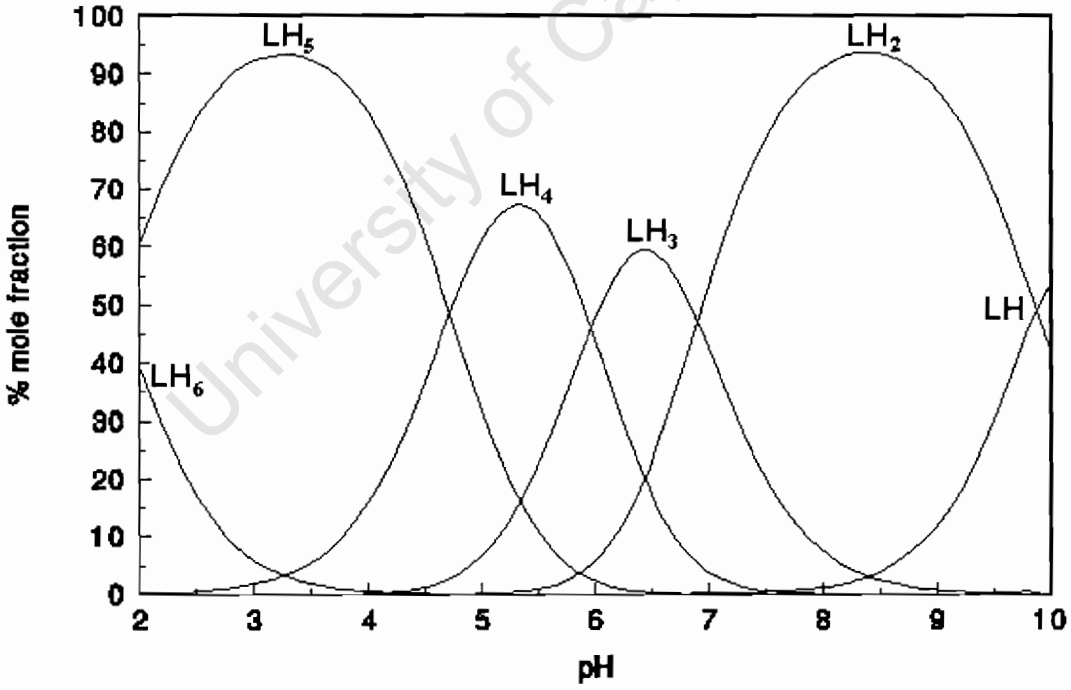

Figure 2.3.1(b). *Species distribution curves for the protonation of APDDMP at 25°C and 0.15M.*

The proposed proton-species distribution of APDDMP can be seen in *Figure 2.3.1(b)*. The inflections viewed in the $\overline{Z_H}$ curve corresponds well with the formation of the various species comprising the model. All protons are lost beyond pH 10, and only the HAPDDMP species remains. At pH 2 the LH_6 species constitutes 40% of the total ligand concentration. This supports the high standard deviation observed for LH_6. The model predicts that a dramatic increase in pH will be needed to exhibit the completely deprotonated ligand APDDMP, especially considering the already high basicity of the LH species, which is only partially formed (~ 45%) at pH 10. At pH 7.4, which is of special interest when considering physiological (in vivo) conditions, the predominant species is LH_2 (75%) with LH_3 being present to lesser degree (25%).

2.3.2. Complexation of APDDMP with Sn^{II}

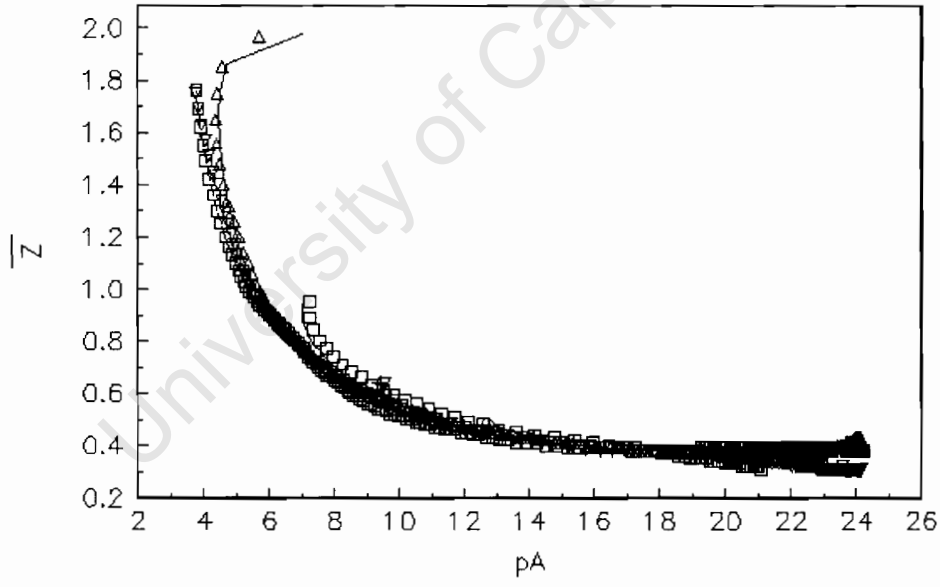

Figure 2.3.2(a). *Experimental (points) and modelled (lines) formation for Sn^{II} complexation by APDDMP. pA is the negative log of the free ligand concentration. The 5 titrations are represented by (O) 3.41mM Sn^{II} and 1.66mM APDDMP; (□)1.67mM Sn^{II} and 1.66mM APDDMP; (Δ)1.69mM Sn^{II} and 3.33mM APDDMP; (▽)1.66mM Sn^{II} and 5.00mM APDDMP and (+)2.53mM Sn^{II} and 1.66mM APDDMP. All solutions were at 25°C and 150mM NaCl.*

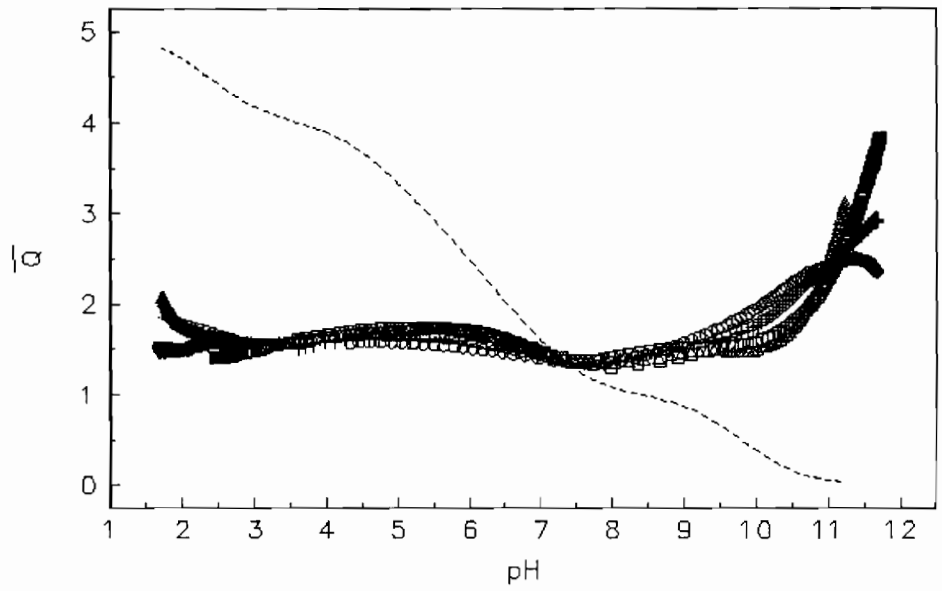

Figure 2.3.2(b). *Experimental (points) and modelled (lines) formation for Sn^{II} complexation by APDDMP. pA is the negative log of the free ligand concentration. The dotted line represents the* $\bar{n}$ curve, which is the protonation state of APDDMP in the absence of metal. *The 5 titrations are represented by (O) 3.41mM Sn^{II} and 1.66mM APDDMP; (□)1.67mM Sn^{II} and 1.66mM APDDMP; (Δ)1.69mM Sn^{II} and 3.33mM APDDMP; (▽)1.66mM Sn^{II} and 5.00mM APDDMP and (+)2.53mM Sn^{II} and 1.66mM APDDMP. All solutions were at 25°C and 150mM NaCl.*

Back-fanning in $\bar{Z}$ curves (*Figure 2.3.2(a)*) at high pH reveals evidence of hydrolysis. The curves tend towards 0.5 at low free ligand concentration (low pH), indicating the presence of binuclear complexes (e.g. M_2L).

Good agreement can be found between the calculated (modelled) $\bar{Z}$ curve (Figure 2.3.2(a)) and the experimental data points, as is true for the $\bar{Q}$ curve (Figure 1.2(b)) as well.

The $\bar{Q}$ curves remain relatively constant at 1.5 below pH of 9, after which they rise to about 4. At pH beyond 7.5 the $\bar{Q}$ curves cross the $\bar{n}$ curve, confirming the presence of (OH) containing species. The tendency of the $\bar{Q}$ curves toward 4, at high pH, can be interpreted as the species $M(OH)_4$ being present. The behaviour of the curves about 1.5 implies that three protons are released on complexation per two metal ions – i.e. $2M - 3H^+$ - verifying the presence of binuclear species (M_2L – type complexes).

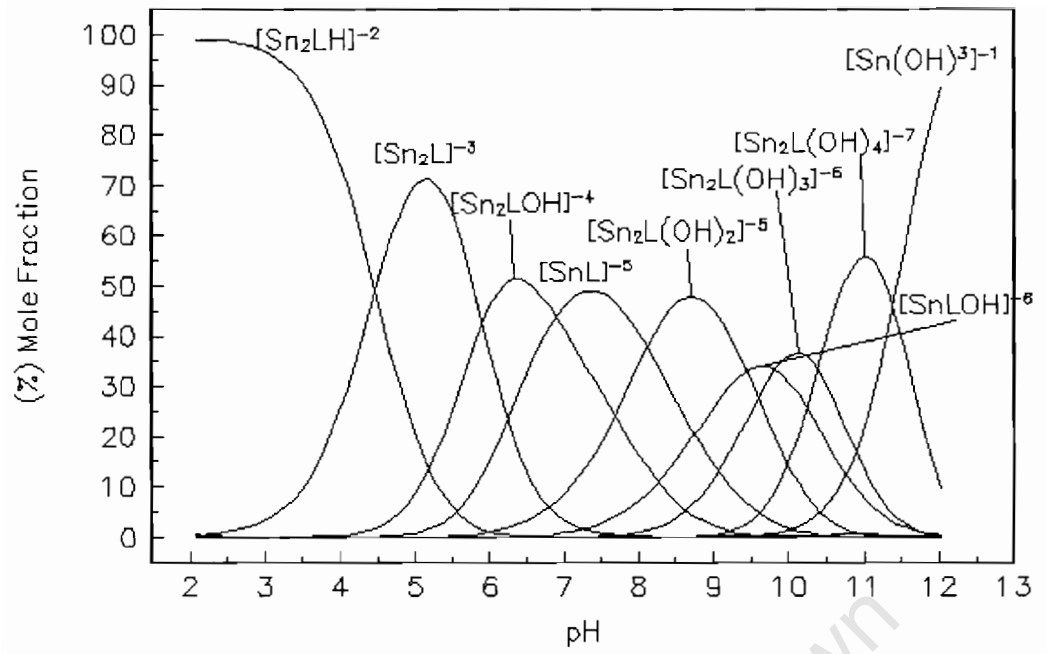

Figure 2.3.2(c). *Speciation distribution for the complexation of Sn^{II} with APDDMP.*

The experimental curves deviated from the calculated curves at pH 10-11.

In an attempt to improve on the model, the titrations were separated into two groups; one containing those titrations with high ligand content, and the other with the high Sn^{II} content – 1:1 formed part of the latter. Each set of titrations was modelled separately and then recombined to obtain a new model, which was a reasonable representation of the two. This, however, proved unsuccessful.

The speciation for the Sn^{II} complexes with APDDMP can be seen in the *Figure 2.3.2(c).* This clearly shows the relative distribution of the Sn^{II}-APDDMP complexes as they are formed in tandem. A definite presence of hydroxide complexes is evident from pH 5 and beyond, as was expected upon studying the $\overline{Z}$ and $\overline{Q}$ curves. At the pH7.4 (physiological pH) five complexes are formed: $[Sn^{II}\text{-APDDMP}]^{5-}$, $[Sn^{II}_2\text{-APDDMP(OH)}]^{4-}$, $[Sn^{II}_2\text{-APDDMP(OH)}_2]^{5-}$, $[Sn^{II}\text{-APDDMP(OH)}]^{6-}$, and $[Sn^{II}_2\text{-APDDMP}]^{3-}$. Their respective percentage mole fractions being: 48%, 32%,16%, 3% and 1%.

For the species SnLOH and Sn_2LOH the loss of a proton could be due to hydrolysis of water or by dissociation from the ligand (which would be better defined as $SnLH_{-1}$). This is distinguishable by the step-wise formation constant log K_{11-1} = 5.04 (SnL + OH ⇆ SnLOH), which is greater than that for the hydrolysis of Sn^{II}, log K_{10-1} = -4.20. This suggests that, upon coordinating with the metal, the ligand loses a proton rather than that of a Sn-bound water molecule. The most likely site for deprotonation would be the tertiary amine, thereby freeing the nitrogen lone-pair to bind with Sn^{II}(*Figure 2.3.2(d)*). This serves to further support the protonation model as evidence of the existence of the protonated amine site. Similarly for log K_{21-2} = 6.10 (Sn_2L + OH ⇆ $Sn_2L(OH)_2$), which is much greater than the hydrolysis constant of the binuclear Sn^{II}-ion (log K_{20-2} = -4.16).

Interesting to consider are the various possibilities for coordination of the Sn^{II}-ion(s). The possible structures can be deduced – APDDMP being a rather flexible polydentate ligand, Sn-APDDMP complexes could take on various forms. The ligand could chelate the tin-ion(s) forming rather stable cyclic structures, as illustrated in *Figure 2.3.2(d)* and *Figure 2.3.2(e)*. With the aid of NMR spectroscopy – i.e. NMR titrations, which was outside of the scope of this study – more accurate predictions can be made.

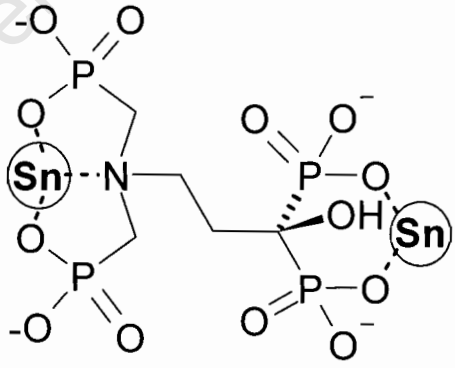

Figure 2.3.2(d). *Proposed structure for binuclear Sn^{II}_2-APDDMP(OH) complex. Showing two sites for coordination of Sn^{II}: (i) an amine and methylene-phosphonate site (bicyclo[3,3,0]), and (ii) a diphosphonate site (6-membered ring).*

The coordination of the Sn^{II}-ion at the amine centre could lead to the formation of two stable 5-membered rings (a biclyclo[3,3,0]-species) – with additional interactions of the methylenephosphonate groups (*Figure 2.3.2(d)*). This type of chelation is possible for both the binuclear and mononuclear species (Sn_2LOH and SnLOH). By taking into consideration one further interaction at the diphosphonate binding site, to include coordination at the alcohol, this could afford the formation of another bicyclic system (bicylco[2,2,1]-species) as illustrated in *Figure 2.3.2(e)*.

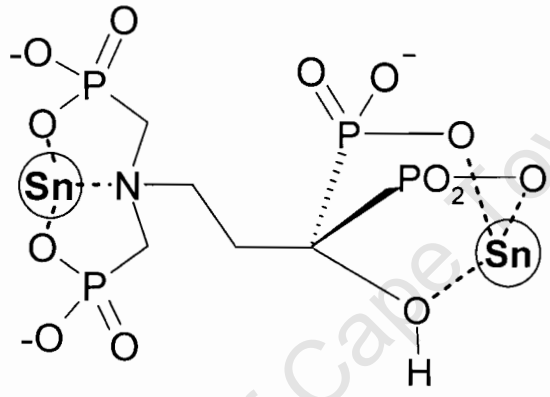

Figure 2.3.2(e). *Proposed structure for binuclear Sn^{II}_2-APDDMP(OH) complex. Showing two sites for coordination of Sn^{II}: (i) an amine and methylene-phosphonate site (bicyclo[3,3,0]), and (ii) a diphosphonate site including coordination at the alcohol (bicyclo[2,2,1]).*

In order to distinguish between the methylenephosphonate and diphosphonate interactions to distinguish the formation constants of Sn^{II}-APDDMP can be compared with that of another ligand comprising only the diphosphonate functionality, namely HEDP (1-hydroxyethylene-diphosphonate) [6]. The complexation of HEDP with Sn^{II}, to form Sn^{II}-HEPD, results in the formation constant of $\log\beta_{110}$ = 14.76 [6]. This closely resembles the same species obtained for APDDMP, i.e. $\log\beta_{110}$ = 15.26. Therefore it is safe to assume that the Sn^{II}-ion would initially coordinate at the diphoshonate site forming Sn^{II}-APDDMP (*Figure 2.3.2(f)*), and would migrate to the

methylenephosphonate region upon deprotonation of the amine, to form Sn^{II}-APDDMP(OH) as explained above and illustrated in *Figure 2.3.2(f)*.

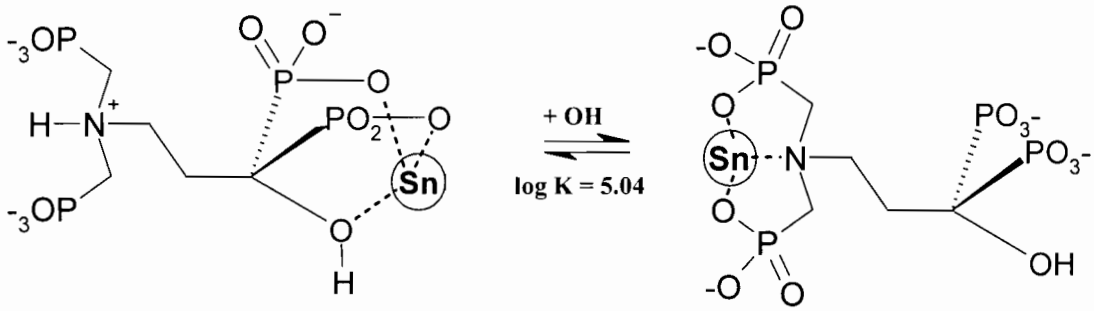

Sn^{II}-APDDMP **Sn^{II}-APDDMP(OH)**

Figure 2.3.2(f). *Proposed structure for Sn^{II}-APDDMP species. Showing the initial coordination of Sn^{II} at the diphosphonate site, and the subsequent coordination at the methylenephosphonate site following the deprotonation of the tertiary amine.*

The same comparison cannot be made for the binuclear species Sn^{II}_2L of HEDP, since the value reported by Claessens *et al* [7] $\log\beta_{210}$ = 25.3 was measured using $(CH_3)_4NNO_3$ as background electrolyte with *I = 0.1M*. However, this does reveal that it is possible for two metal-ions to bind at the diphosphonate site to form Sn^{II}_2-APDDMP. It can be postulated that upon deprotonation of the amine that at least one of the metal-ions could migrate towards the methylenephosphonate site to form Sn^{II}_2-APDDMP(OH). Furthermore, the formation constant for that of Sn^{II} with PEI-MP (N,N',N'-trimethylenephosphonate-polyethyleneimine) [6] can be considered, which consists purely of methylenephosphonate groups. The value of the equilibrium constant obtained for the formation of Sn^{II}_2-APDDMP exactly matches that of Sn^{II}_2-PEI-MP as reported by Zeevaart *et al* [6]. This clearly indicates the preference for the Sn^{II}-coordination at the methylenephosphonate site for the Sn^{II}_2-L complex of APDDMP. Therefore, both the diphosphonate and the methylenephosphonate sites

will most likely be occupied by Sn^{II}-ions initially (for Sn^{II}_2-APDDMP) with the amine remaining protonated. Deprotonation of the amine would then result in the additional coordination of the nitrogen lone-pair to form the type of species depicted in *Figure 2.3.2(e),* Sn^{II}_2-APDDMP(OH). The step-wise hydrolysis of the Sn^{II}_2-APDDMP complexes, and their formation equilibria, coincide with that of the Sn^{II}_2-PEI-MP [6], with the exception of the $M_2L(OH)_4$ species, which is unique to APDDMP (*Table 2.2*). Also common to both APDDMP and PEI-MP is the formation (and magnitude of the equilibrium constant) of the M_2LH species.

Table 2.2. *Comparison of the step-wise formation constants for complexation of Sn^{II} with APDDMP and PEI-MP[6], as determined at 25°C and I=150 mM NaCl.*

Equilibrium/ Species	***APDDMP log K [this work]***	***PEI-MP log K*** [6]
$2Sn^{II}_2L + H \leftrightarrows Sn_2LH$	4.47 *± 0.04*	4.15 ± 0.04
$2Sn^{II} + L \leftrightarrows Sn_2L$	26.63 *± 0.03*	26.62 ± 0.04
$Sn^{II}_2L + OH \leftrightarrows Sn_2LOH$	7.89 *± 0.03*	8.46 ± 0.03
$Sn^{II}_2LOH + OH \leftrightarrows Sn_2L(OH)_2$	6.10 *± 0.03*	6.05 ± 0.03
$Sn^{II}_2L(OH)_2 + OH \leftrightarrows Sn_2L(OH)_3$	4.20 *± 0.03*	3.75 ± 0.03
$Sn^{II}_2L(OH)_3 + OH \leftrightarrows Sn_2L(OH)_4$	3.41 *± 0.05*	
$Sn^{II} + L \leftrightarrows SnL$	15.26 *± 0.02*	
$Sn^{II}L + OH \leftrightarrows SnL(OH)$	*5.04 ± 0.03*	

2.4 Conclusion

In the protonation and the Sn^{II} complexation curves for APDDMP (i.e. $\overline{Z_H}$, $\overline{Z}$ and $\overline{Q}$ curves), the calculated function follows the experimental data very closely (Figures 2.3.1(a), 2.3.2(a), 2.3.2(b)). It can be deduced that no further protons are lost before pH 12 as the curves level off at zero towards the higher pH region. At low free-ligand concentrations, the $\overline{Z}$ curves (Figure 2.3.2(a)) shows an inflexion at 0.5, suggesting the existence of binuclear (M_2L) complexes. Furthermore, the $\overline{Z}$ curves exhibit back-

fanning, which is indicative of hydroxy-species being formed. The $\overline{Q}$ curves (Figure 2.3.2(b) remain constant at 1.5 from pH 2 to 9, implying that 3 protons are lost for every 2 metal ions; confirming the presence of binuclear species. Beyond pH 7.5 the $\overline{Q}$ curve rises above the $\overline{n}$ curve, confirming the existence of hydroxy-species (MLOH – species).

It is clear that APPDMP favours the formation of binuclear complexes with Sn^{II}. At the pH of interest for potential in vivo studies (pH 7.4) three complexes are observed: $[Sn^{II}\text{-APDDMP}]^{5-}$ (47%), $[Sn^{II}_2\text{-APDDMP(OH)}]^{4-}$(32%), and $[Sn^{II}_2\text{-APDDMP(OH)}_2]^{5-}$(18%). In the model presented above, there is a discrepancy as to whether the SnL(OH) species should be included. Excluding the SnL(OH) complex results in only a slight increase in the Hamilton R-Factor (0.015). Its presence also only slightly improves the $\overline{Q}$ curves at pH 10-11. Hydrolysis of Sn^{II} occurs at high pH, as can be evident in the species distribution diagram – *Figure 2.3.2(c).* The presence of the Sn(OH) results in the 'distortion' of the data in the high pH region, accounting for the deviations observed in the $\overline{Q}$ curves at pH 10-11.

We've also managed to show similarity in the binding characteristics of APDDMP and PEI-MP [6] when forming M_2L -type (binuclear) complexes.

2.5 References

[1] J. R. Zeevaart, N. V. Jarvis, W. K. A. Louw and G. E. Jackson, *J. Inorg. Biochem.,* 2001, **83**, 57-65.

[2] J. R. Duffield, D. R. Williams, and I. Kron, *Polyhedron,* 1991, **10**, 377-387.

[3] B. K. Shcherbakov, F. I. Bel'skii, M. P. Komarova, Y. M. Polikarpov, T. Y. Medved, M. I. Kabachnik, Izv. Akad. Nauk. SSSR Ser. Khim. 1982, **3**, 560-564.

[4] J. R. Zeevaart, N. V. Jarvis, W. K. A. Louw, G. E. Jackson, I. Cukrowski, C. J. Mouton, *J. Inorg. Biochem.* 1999, **73**, 265-272.

[5] N. V. Jarvis, J. M. Wagener, G. E. Jackson, *J. Chem. Soc. Dalton Trans.,* 1995, 1411-1415.

[6] J. R. Zeevaart, W. K. A. Louw, Z. I. Kolar, J. M. Wagener, N. V. Jarvis, R. A. M. J. Claessens, *Journal of Radioanalytical and Nuclear Chemistry,* 2003, **257**, 83-91.

[7] R. A. M. J. Claessens and J. G. M. van der Linden, *J. Inorg. Biochem.,* 1984, **21**, 73-82.

[8] J. R. Zeevaart, PhD Thesis, *'Metal ion speciation in Blood Plasma as a Tool in Predicting the in vivo Behaviour of Potential Bone-Seeking Radiopharmaceuticals', Delft University of Technology,* 2001, Delft University Press, The Netherlands, pp. 127-144.

SPECIATION OF APDDMP WITH MAJOR METAL-ION COMPONENTS IN BLOOD PLASMA – Ca^{II}, Mg^{II} AND Zn^{II}

3.1 Introduction

To effectively understand the behaviour of the ligand within the blood plasma, the factors affecting its action have to be taken into consideration. Rationalising the affinity of the ligand for the target material, and the stability of a given metal-ligand complex when introduced into a complex system such as the blood plasma are key aspects of the development of a potential radiopharmaceutical.

The ligand, whose function is to carry the radionuclide to the target site, should exhibit an affinity for the tumour tissue, essentially making it bone-seeking. The ligand of choice should selectively accumulate in regions of high Ca^{II} concentration, which is characteristic of areas affected by secondary bone metastasis. Phosphonates are known to have a particular affinity for Ca^{II}. Some (di)phosphonic acid derivatives that had been previously considered include ethylenediamine-tetramethylenephosphonate (EDTMP) and [1-hydroxyethylidene]-disphonic acid (HEDP) [1]. Less successful were phosphonate ligands methylenediphosphonic acid (MDP) [1]; and 1-hydroxy-3-amino-propilydenediphosphonic acid (APD) [2]. Studies had also been performed on EDTA-type (ethylenediaminetetra-acetic acid) derivatives, such as diethylenetriamine-penta-acetic acid (DTPA) [3], and proved not to be as effective a bone-seeking agent [4, 5].

The first step to elucidating the complete behaviour of a radiopharmaceutical would be to conduct speciation experiments. These experiments aid in understanding the function of the ligand or metal-ion in blood plasma. Blood plasma modelling is of interest as it serves as an effective tool for predicting the *in vivo* behaviour of the complex, before pursuing clinical trials. One such success story was ^{153}Sm-EDTMP; the blood plasma model closely matched the clinical observations [7]. Establishing a similar model for APDDMP would entail having to measure the formation constants of the ligand with the major

metal ion constituents found in blood plasma, such as Ca^{II}, Mg^{II}, and Zn^{II}. To a large extent, these constants can be obtained from literature, and at different ionic strengths and temperatures.

The technique employed is that of glass electrode potentiometry. Titrations were conducted in a manner so as to closely simulate physiological conditions, i.e. an ionic strength (I) of $0.15 mol.dm^{-3}$ NaCl – all solutions were prepared isotonic to blood plasma. In so doing the ionic strength could effectively be maintained throughout the experiments. Titration data were refined with the aid of a software programme ESTA, from whence the formation constants were calculated. However, a temperature of 25°C was deemed appropriate, as opposed to 37°C (physiological conditions) - since the results for the protonation of APDDMP as observed at both temperatures were in good agreement (see paragraph 3.2 below).

3.2 Results

The following models were obtained in the study of the complexation of APDDMP with Ca^{II}, Mg^{II} and Zn^{II}. Attempts to reproduce the exact models previously reported were unsuccessful.

The results (*Table 3*) differ from those reported by Zeevaart *et al.* [3] as the titration conditions differ. For the purpose of these experiments it was considered suitable to conduct experiments at 25°C so as to be consistent with the majority of formation constants reported in literature and in the ECCLES database. Furthermore, the lower temperature of 25°C was easier to maintain, minimizing evaporation and condensation within the vessel, which could affect the reproducability of the results. There was very little or no difference in results obtained for the protonation constants of the ligand, for experiments conducted at 25°C as compared to literature data (37°C), hence justifying the use of the lower temperature.

Table 3. *Protonation and formation constants for complexes of APDDMP with Ca^{II}, Mg^{II} and Zn^{II}, determined at 25°C and I=150 mM NaCl.*

Equilibrium/ Species [#]	***log β [This work]***	***Number of data points***	***Hamilton R-Factor***	***log β, 37°C Zeevaart[3]***
$H + HL \rightleftharpoons H_2L$	9.79 ± 0.01	700	0.01736	9.82
$H + H_2L \rightleftharpoons H_3L$	16.83 ± 0.02			17.03
$H + H_3L \rightleftharpoons H_4L$	22.74 ± 0.02			23.12
$H + H_4L \rightleftharpoons H_5L$	27.68 ± 0.02			28.01
$H + H_5L \rightleftharpoons H_6L$	30.04 ± 0.04			30.05
$2Ca^{II} + LH_3 \rightleftharpoons Ca_2LH_3$	30.89 ± 0.03	600	0.00637	
$2Ca^{II} + LH_2 \rightleftharpoons Ca_2LH_2$	25.74 ± 0.03			24.20
$2Ca^{II} + LH \rightleftharpoons Ca_2LH$	20.54 ± 0.03			18.29
$2Ca^{II} + L \rightleftharpoons Ca_2L$	14.34 ± 0.03			10.99
$2Ca^{II} + L + OH \rightleftharpoons Ca_2LOH$	20.29 ± 0.03			
$Ca^{II} + L + H \rightleftharpoons CaLH$	Not observed			13.87
$Ca^{II} + L + OH \rightleftharpoons CaLOH$	Not observed			8.60
$Ca^{II} + L + 2OH \rightleftharpoons CaL(OH)_2$	14.68 ± 0.02			11.61
$2Mg^{II} + LH_3 \rightleftharpoons Mg_2LH_3$	30.46 ± 0.03	750	0.00918	
$2Mg^{II} + LH_2 \rightleftharpoons Mg_2LH_2$	25.41± 0.04			24.16
$2Mg^{II} + LH \rightleftharpoons Mg_2LH$	20.26 ± 0.03			18.44
$2Mg^{II} + L \rightleftharpoons Mg_2L$	13.48 ± 0.04			11.10
$2Mg^{II} + L + OH \rightleftharpoons Mg_2LOH$	19.93 ± 0.04			4.47
$2Mg^{II} + L + 2OH \rightleftharpoons Mg_2L(OH)_2$	24.51± 0.04			
$Mg^{II} + L + 2OH \rightleftharpoons MgL(OH)_2$	Not observed			12.19
$2Zn^{II} + LH_3 \rightleftharpoons Zn_2LH_3$	31.19 ± 0.03	727	0.00496	
$2Zn^{II} + LH \rightleftharpoons Zn_2LH$	23.36 ± 0.02			
$2Zn^{II} + L \rightleftharpoons Zn_2L$	18.23 ± 0.03			
$2Zn^{II} + L + OH \rightleftharpoons Zn_2LOH$	26.31 ± 0.03			
$2Zn^{II} + L + 2OH \rightleftharpoons Zn_2L(OH)_2$	32.53 ± 0.03			
$Zn^{II} + L + OH \rightleftharpoons ZnLOH$	16.36± 0.02			13.46
$Zn^{II} + L + 2OH \rightleftharpoons ZnL(OH)_2$	Not observed			15.49
$Zn^{II} + L \rightleftharpoons ZnL$	Not observed			9.53
$Zn^{II} + L + H \rightleftharpoons ZnLH$	Not observed			16.72
$Zn^{II} + L + 2H \rightleftharpoons ZnLH_2$	Not observed			22.75
$Zn^{II} + L + 3H \rightleftharpoons ZnLH_3$	Not observed			27.01

[#] *The charges on the ligands and complexes have been omitted for simplicity.*

3.2.1 Ca-Apddmp model

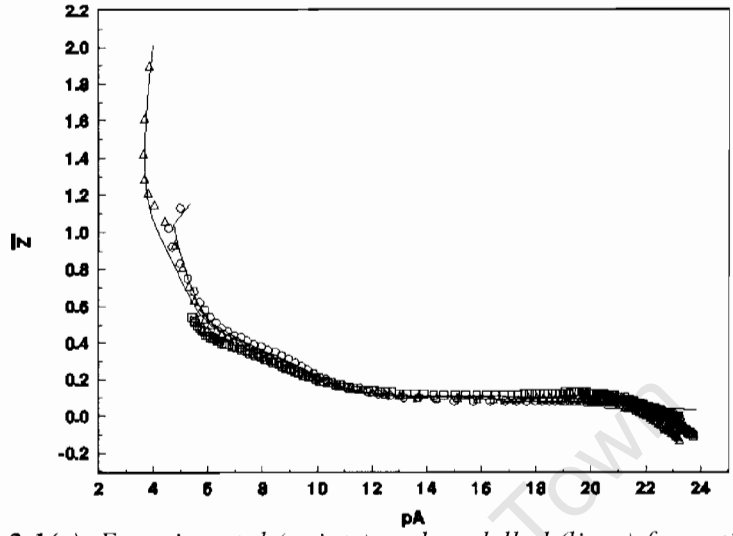

Figure 3.2.1(a). *Experimental (points) and modelled (lines) formation for Ca^{II} complexation by APDDMP. pA is the negative log of the free ligand concentration. The 3 titrations are represented by (O) 1.38mM Ca^{II} and 1.61mM APDDMP; (Δ) 0.70mM Ca^{II} and 1.63mM APDDMP; (□) 1.48mM Ca^{II} and 4.47mM APDDMP. All solutions were at 25°C and 150mM NaCl.*

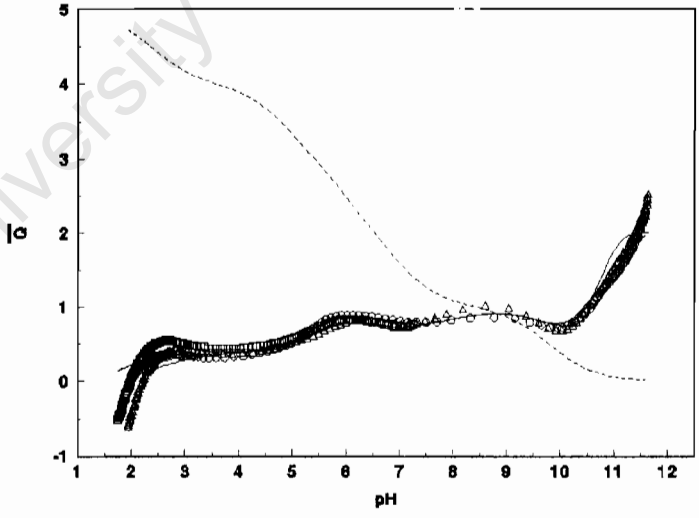

Figure 3.2.1(b). *Experimental (points) and modelled (lines) formation for Ca^{II} complexation by APDDMP. The dotted line represents the* $\bar{n}$ curve, which is the protonation state of APDDMP in the absence of metal. *The 3 titrations are represented by (O) 1.38mM Ca^{II} and 1.61mM APDDMP; (Δ) 0.70mM Ca^{II} and 1.63mM APDDMP; (□) 1.48mM Ca^{II} and 4.47mM APDDMP. All solutions were at 25°C and 150mM NaCl.*

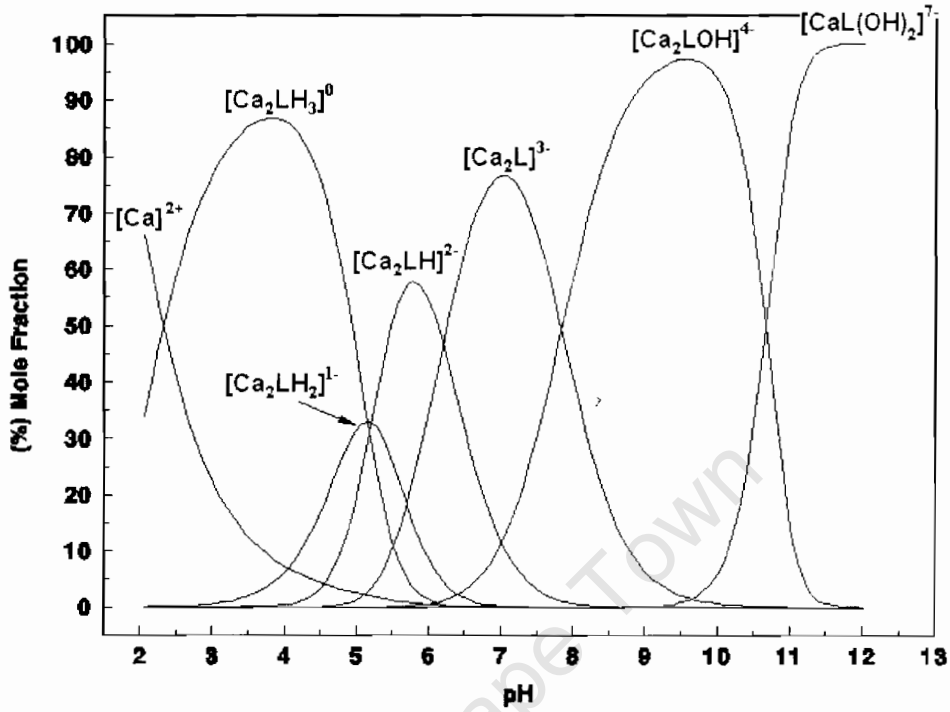

Figure 3.2.1(c). *Species distribution for the complexation of Ca^{II} with APDDMP.*

3.2.2 Mg-Apddmp model

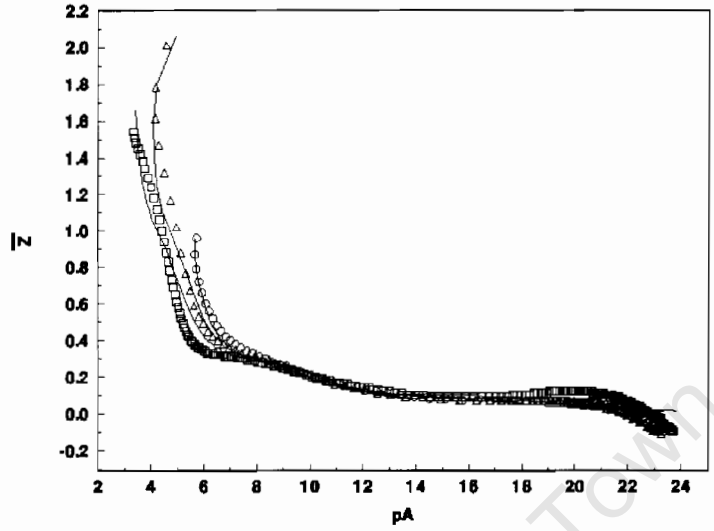

Figure 3.2.2(a). *Experimental (points) and modelled (lines) formation for Mg^{II} complexation by APDDMP. pA is the negative log of the free ligand concentration. The 3 titrations are represented by (O) 1.54mM Mg^{II} and 1.61mM APDDMP; (Δ) 0.78mM Mg^{II} and 1.65mM APDDMP; (□) 1.55mM Mg^{II} and 4.87mM APDDMP. All solutions were at 25°C and 150mM NaCl.*

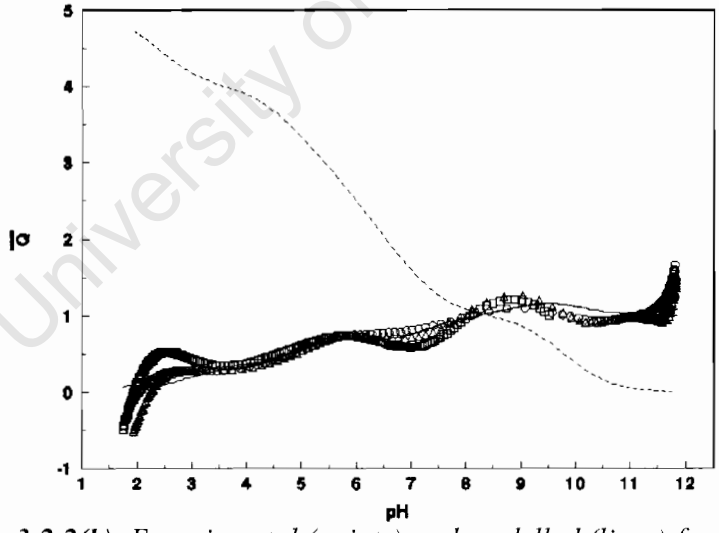

Figure 3.2.2(b). *Experimental (points) and modelled (lines) formation for Mg^{II} complexation by APDDMP. The dotted line represents the* $\bar{n}$ curve, which is the protonation state of APDDMP in the absence of metal. *The 3 titrations are represented by (O) 1.54mM Mg^{II} and 1.61mM APDDMP; (Δ) 0.78mM Mg^{II} and 1.65mM APDDMP; (□) 1.55mM Mg^{II} and 4.87mM APDDMP. All solutions were at 25°C and 150mM NaCl.*

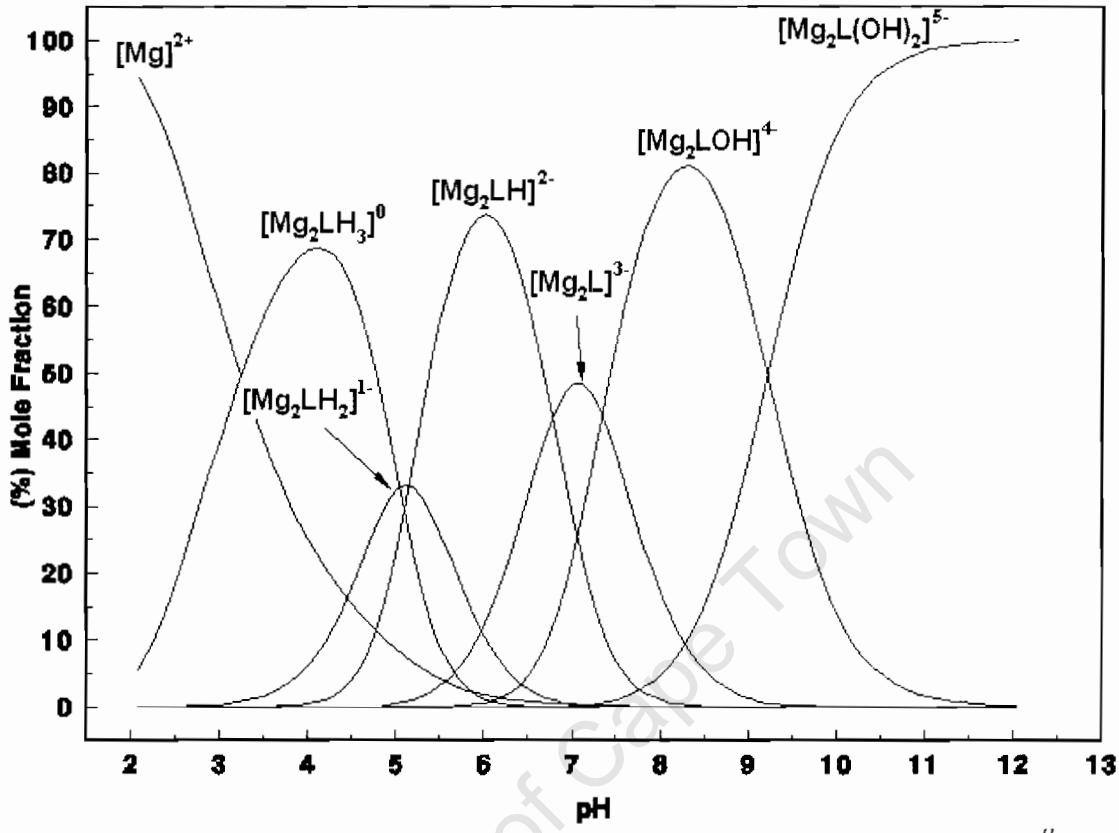

Figure 3.2.2(c). *Species distribution for the complexation of Mg^{II} with APDDMP.*

3.2.3 Zn-Apddmp model

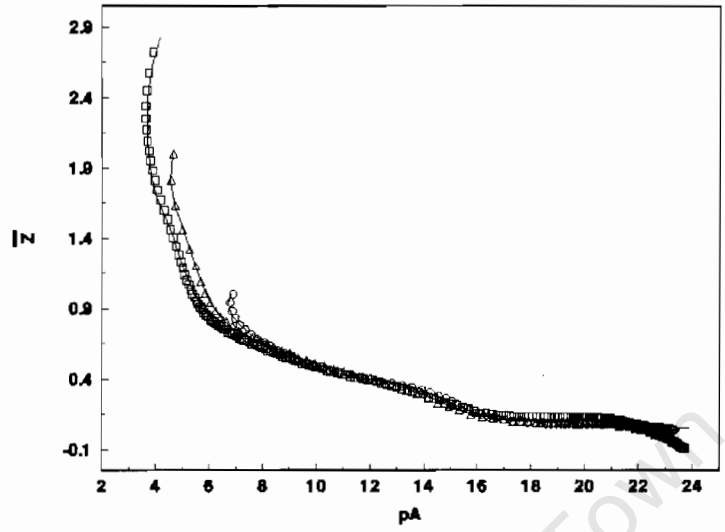

Figure 3.2.3(a). *Experimental (points) and modelled (lines) formation for Sn^{II} complexation by APDDMP. pA is the negative log of the free ligand concentration. The 3 titrations are represented by (O) 1.51mM Zn^{II} and 1.61mM APDDMP; (Δ) 0.76mM Zn^{II} and 1.66mM APDDMP; (□) 1.57mM Zn^{II} and 4.65mM APDDMP. All solutions were at 25°C and 150mM NaCl.*

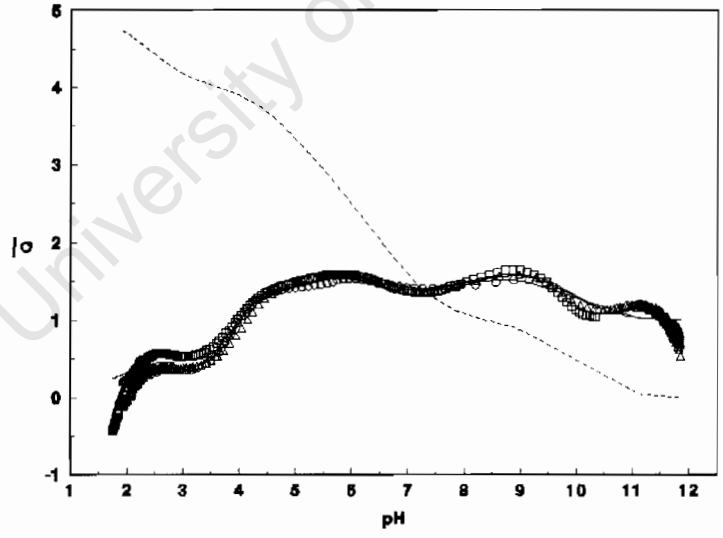

Figure 3.2.3(b). *Experimental (points) and modelled (lines) formation for Sn^{II} complexation by APDDMP. The dotted line represents the $\bar{n}$ curve, which is the protonation state of APDDMP in the absence of metal. The 3 titrations are represented by (O) 1.51mM Zn^{II} and 1.61mM APDDMP; (Δ) 0.76mM Zn^{II} and 1.66mM APDDMP; (□) 1.57mM Zn^{II} and 4.65mM APDDMP. All solutions were at 25°C and 150mM NaCl.*

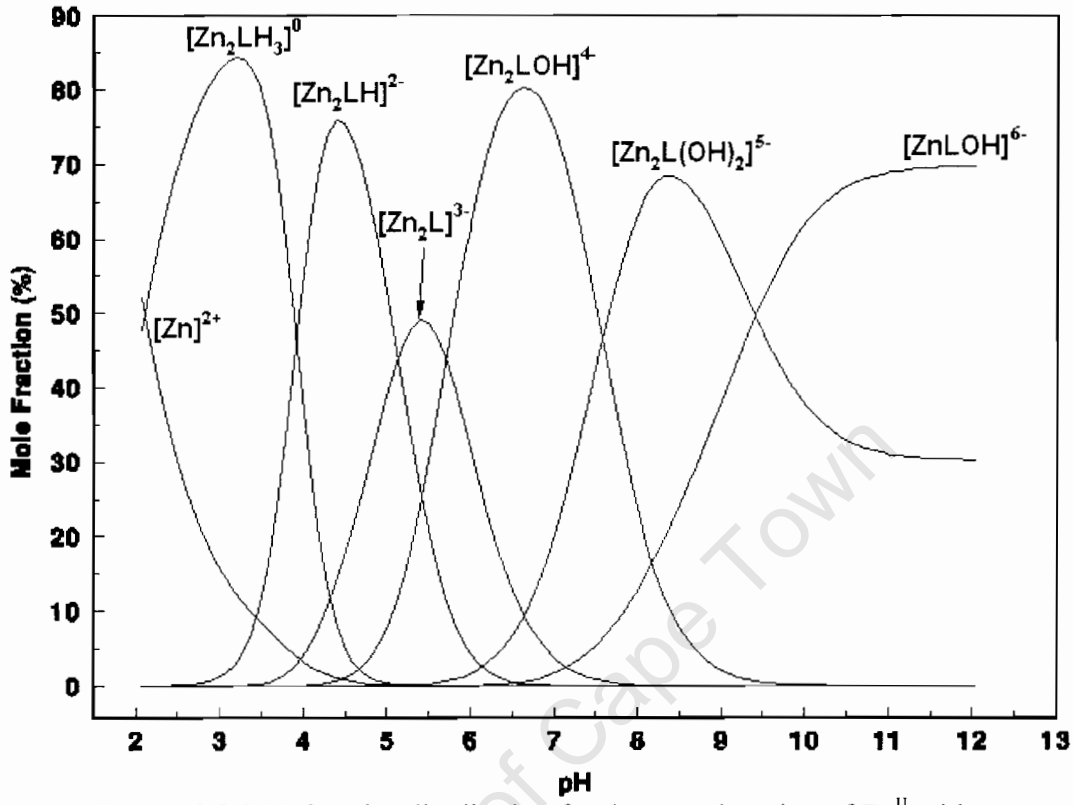

Figure 3.2.3(c). Species distribution for the complexation of Zn^{II} with APDDMP.

3.3 Discussion

The Mg-Apddmp model was the most troublesome, and as a result a good fit could not be obtained with the experimental and calculated data – as is evident in the $\overline{Q}$ and $\overline{Z}$ curves. However, the model presented above proved to be the most sensible.

As observed in the $\overline{Z}$ curves for all three systems – APDDMP with Ca^{II}, Mg^{II} and Zn^{II} – the calculated models (lines) follow the experimental data points. At high free ligand concentration the curves exhibit back-fanning, indicating that the APDDMP form hydrolysed complexes with the metal ions.

The modelled $\overline{Q}$ curves (lines) show a relatively good fit with the experimental data (points). For the Ca^{II} and Mg^{II} systems the $\overline{Q}$ curves average at 0.5 between pHs 3 and 7.

Hence the formation of binuclear complexes can be expected (i.e. two metal centres per one ligand unit, M_2L). Beyond pH 8 the graphs gradually rise above the $\bar{n}$ curve, indicating that more protons are dissociated than are available from the ligand. This supports earlier observations of the $\bar{Z}$ curves, from which the formation of hydroxy-complexes was anticipated. The Zn^{II}-APDDMP system differs from the rest slightly in that the $\bar{Q}$ curves flatten at 0.5 below pH 3 only, whereupon it rises to 1.5 where it stays relatively constant. In both cases the species that form may still be binuclear (of the type M_2L), but they differ in the number of protons that dissociate per metal ion that the ligand complexes with. For example, should a single proton dissociate for every two metal ions that complexes with APDDMP, the result will be a $\bar{Q}$ of 0.5. The $\bar{Q}$ curves remaining constant at 1.5 could be the result of three protons dissociating per every two metal ions that form a complex with APDDMP. At approximately pH 7.5 the $\bar{Q}$ curves rise above the $\bar{n}$ curve to substantiate the existence of hydrolysed Zn^{II} complexes.

The following complexes were most prominent at pH 7.4 (physiological conditions), as extrapolated from the speciation curves (where L = H-APDDMP with a net charge of 7-):

- *Ca-APDDMP* $[Ca^{II}_2L]^{3-}$ 69.0%
  $[Ca^{II}_2L(OH)]^{4-}$ 27.5%
  $[Ca^{II}_2LH]^{2-}$ 3.5%

- *Mg-APDDMP* $[Mg^{II}_2L(OH)]^{4-}$ 52.0%
  $[Mg^{II}_2L]^{3-}$ 39.0%
  $[Mg^{II}_2LH]^{2-}$ 7.5%
  $[Mg^{II}_2L(OH)_2]^{5-}$ 1.5%

- *Zn-APDDMP* $[Zn^{II}_2L(OH)]^{4-}$ 54.0%
  $[Zn^{II}_2L(OH)_2]^{5-}$ 40.0%
  $[Zn^{II}L(OH)]^{6-}$ 5.0%
  $[Zn^{II}_2L]^{3-}$ 1.0%

The ligand protonation constants can be interpreted in terms of the chemical environment in which they occur. An effective technique for investigating the proton dissociations would be by NMR-spectroscopic titrations. However, in the absence of this technique it is possible, by making use of the wealth of formation constants that are available in literature, to compare for the individual components constituting the ligand, which in the case of APDDMP are diphosphonates, methylene-phosphonates and a tertiary amine. Two phosphonate derived ligands that exhibit identical functionalities to that of APDDMP are APD (1-hydroxy-3-amino-propylidene-diphophosphonate) [2] and EDTMP (ethylenediamine-tetramethylenephosphonate) [6]. When in solution the ligand will instantly assume a proton at the tertiary amine centre. With a dissociation constant as high as $pK_a = 11.87$ [8], the species is fairly stable and hence the ligand remains protonated in this region. When evaluating the proton dissociation of the ligand it is evident that the amine proton does not appear within the model, and therefore it is necessary to redefine the ligand APDDMP as LH. By comparison to APD ($pKa_1 = 10.95$) [2] and EDTMP ($pKa_1 = 10.67$ and $pKa_2 = 9.47$) [6], the dissociation of the amine proton usually exceeds $pK_a = 10$. This existence of APDDMP in the protonated form can be further substantiated when coordinating with a metal-ion, whereupon the dissociation of the amine proton would be realised, and can then be evaluated in terms of the first hydrolysis equilibrium constant of the complex against that of the metal-ion. Observed acid dissociation constants of APDDMP, $pKa_2 = 9.79$ and $pKa_4 = 5.91$, correspond well with that of two diphosphonate sites of APD, i.e. 9.80 and 6.01. The dissociation represented by $pKa_3 = 7.04$ agrees best with the methylene-phosphonate site of EDTMP, which is 7.63. The remaining protonation sites – methylene-phosphonate and diphosphonate – are represented pKa_5 and pKa_6.

The complexiometric models for Ca^{II}, Mg^{II} and Zn^{II} with APDDMP could not reproduce literature speciation models [3]. Furthermore, the results obtained could also not be matched with similar systems of ligands comprised of the individual components of APDDMP, i.e. diphosphonate and methylenephosphonate functional groups. Ligands such as [1-hydroxyethylidene]-disphonic acid (HEDP) [1], methylenediphosphonic acid

(MDP) [1], 1-hydroxy-3-amino-propilydenediphosphonic acid (APD) [2], and N,N',N'-trimethylenephosphonate-polyethyleneimine (PEI-MP) [9].

3.4 Conclusion

The protonation speciation model for APDDMP compared very well with the literature data considering the difference in temperature, although the complexation models were not reproducible at 25°C.

The proposed models calculated for the three systems studied here – namely APDDMP with Ca^{II}, Mg^{II} and Zn^{II}- were in good agreement with the experimental/observed data. Binuclear complexes (M_2L – type species) are formed with each of the three metals. The complexes that were most dominant within the region of interest (physiological pH 7.4) were M_2L for Ca^{II}, and M_2LH_{-1} for Mg^{II} and Zn^{II}.

3.5 References

[1] J. R. Zeevaart, N. V. Jarvis, I. Cukrowski, G. E. Jackson, *S. Afr. J Chem., 1997,* **50**, 189-194.

[2] J. R. Zeevaart, N. V. Jarvis, W. K. A. Louw, G. E. Jackson, I. Cukrowski, C. J. Mouton, *Journal of Inorganic Biochemistry, 1999,* **73**, 265-272.

[3] J. R. Zeevaart, N. V. Jarvis, W. K. A. Louw and G. E. Jackson, *J. Inorg. Biochem.,* 2001, **83**, 57-65.

[4] J. R. Zeevaart, W. K. A. Louw, Z. I. Kolar, J. M. Wagener, N. V. Jarvis, R. A. M. J. Claessens, *Journal of Radioanalytical and Nuclear Chemistry,* 2003, **257**, 83-91.

[5] R. A. M. J. Claessens, Z. I. Kolar, *Langmuir,* 2000, **16**, 1360.

[6] W. K. A. Louw, I. C. Dormehl, A. Jansen van Rensburg, N. Hugo, A. S. Alberts, O. E. Forsyth, G. Beverly, M. A. Sweetlove, J. Marais, and A van Aswegen, *Nucl. Med. Biol.,* 1996, **23**, 935.

[7] H. L. Atkins, L. F. Mausner, S. C. Srivastava, G. E. Meinken, R. F. Straub, C. J. Cabahug, D. A. Weber, C. T. C. Wong, D. F. Sacker, S. Madajewicz, T. L. Park, and A. G. Meek, *Radiology,* 1993, **186**, 279.

[8] B. K. Shcherbakov, F. I. Bel'skii, M. P. Komarova, Y. M. Polikarpov, T. Y. Medved, M. I. Kabachnik, Izv. Akad. Nauk. SSSR Ser. Khim. 1982, **3,** 560-564.

[9] N. V. Jarvis, J. R. Zeevaart, J M. Wagener, W. K. A. Louw, I. C. Dormehl, R. J. Milner and E. Killian, *Radiochim. Acta* 2002, **90**, 237-246.

DETERMINATION OF THE FORMATION CONSTANTS FOR THE COMPLEXATION OF PEI-MP WITH Sn^{IV} BY GLASS ELECTRODE POTENTIOMETRY

4.1 Introduction

In the pursuit for a cure for metastatic bone cancer the complexation of N,N',N'-trimethylenephosphonate-polyethyleneimine (PEI-MP) – *Figure 4.1* – with Sn^{IV} was considered. PEI-MP is known for its high affinity for Ca^{II}, and is therefore an ideal ligand for selective accumulation in affected bone.

A successful radiopharmaceutical is one that selectively accumulates at the target tumor without posing any threat to healthy, non-cancerous tissue. In developing palliative and therapeutic agents for metastatic bone cancer, two criteria have to be met. Firstly, the ligand should be selective for calcium and accumulate especially in regions of high Ca^{II} concentration - as is typical of bone tumors. Secondly, the metal of choice should render minimal toxicity to the sensitive bone marrow.

The metal-ligand system considered here is that of Sn^{IV} and a methylenephosphonate-functionalised polyethyleneimine, namely PEI-MP. $^{117m}Sn^{IV}$ is proposed, as it emits low energy electrons, which will comply favourably with minimizing the toxicity to the bone marrow. Furthermore, lower levels of toxicity would make it possible to administer larger doses, thereby ensuring the effectiveness of the pharmaceutical. The high calcium affinity of PEI-MP will aid in delivering and accumulating the radioactive ^{117m}Sn at the target site.

To gain some understanding into the behaviour of $^{117m}Sn^{IV}$-PEI-MP complexes in blood plasma, the formation constants were measured using glass electrode potentiometry. Titrations were carried out with an ionic strength of 0.15*M* NaCl to simulate blood plasma, and at 25°C. The challenge was to avoid the hydrolysis of the Sn^{IV}, and hence precipitation. Several attempts at different titration techniques were fruitless. One such

experiment involved titrating the PEI-MP with an acidified solution of Sn^{IV}, while maintaining a constant pH – using 0.05M NaOH. In so doing observe the changes in complexation as the concentration of Sn is increased relative to the PEI-MP. A series of titrations were conducted at various pHs, and the data were analyzed using the ESTA modeling program. The data would not refine, and hence the model was insoluble. However, the method presented here is that of typical complexiometric titrations whereby the ligand-metal interactions were monitored by potentiometry, whilst varying the pH – titrating with an isotonic solution of 0.05M NaOH.

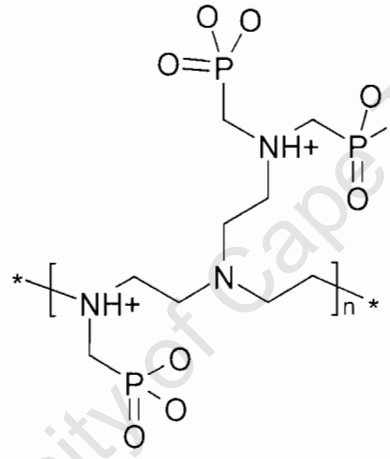

PEI-MP

***Figure 4.1**: Molecular structure of the ligand N,N',N'-trimethylenephosphonate-polyethyleneimine (PEI-MP)*

4.2 Method

The formation constants for the complexes that PEI-MP forms with Sn^{IV} were obtained by glass electrode potentiometry. Three titrations were conducted, of which the data were analysed using ESTA. The metal-to-ligand ratios for the titrations were: 1:2, 2:1 and 1½:1; these were performed with I = 0.15M NaCl (simulating blood plasma conditions). The challenge, however, was the unavoidable hydrolysis of Sn^{IV}, which resulted in the formation of precipitate during the course of the experiment.

The data points corresponding to the formation of precipitate (visible) were omitted from the ESTA modelling.

4.3 Results and discussion

Table 1. *Protonation and formation constants for PEI-MP and Sn^{IV}-PEI-MP as determined at 25 °C (I = 0.15M NaCl).*

Equilibrium/ Species [#]	***log β***	***Number of data points***	***Hamilton R-Factor***	***Log β [1]***
$H + L \rightleftharpoons HL$	9.683 ± 0.007	750	0.01207	9.341
$H + HL \rightleftharpoons H_2L$	17.461 ± 0.009			16.882
$H + H_2L \rightleftharpoons H_3L$	23.788 ± 0 .010			22.833
$H + H_3L \rightleftharpoons H_4L$	27.780 ± 0.012			26.095
$Sn^{IV} + OH \rightleftharpoons SnOH$	-1.94 *			
$Sn^{IV} + 6\ OH \rightleftharpoons Sn(OH)_6$	-24.11 *			
$2Sn^{IV} + L - 3H \rightleftharpoons Sn^{IV}_2L(OH)_3$	39.971 ± 0.100	357	0.01729	
$2Sn^{IV} + L - 4H \rightleftharpoons Sn^{IV}_2L(OH)_4$	36.658 ± 0.021			
$2Sn^{IV} + L - 5H \rightleftharpoons Sn^{IV}_2L(OH)_5$	27.402 ± 0.032			
$2Sn^{IV} + L - 6H \rightleftharpoons Sn^{IV}_2L(OH)_6$	18.637 ± 0.059			
$2Sn^{IV} + L - 7H \rightleftharpoons Sn^{IV}_2L(OH)_7$	9.634 ± 0.053			

[#] *The charges on the ligands and complexes have been omitted for simplicity.*

* *Hydrolysis constants for Sn^{IV} were obtained from literature [2] and included in the model.*

4.3.1 Proton dissociation constants

In the protonation curve for PEI-MP, $\overline{Z_H}$, the calculated function follows the experimental data very closely (*Figure 4.3.1(a)*).It can be deduced that no further protons are lost beyond pH 10 as the curves level off at zero towards the higher pH region. The analysis reveals that there are four sites of protonation (proton dissociation). The $pK_1 = 9.683$ would be due to dissociation at an amine centre, and

the remaining three stability constants corresponds with the methylenephosphonated functional groups. A fifth stability constant with a value greater than pK_1 above can be expected [3] – at an amine site, but would require excessively basic conditions to achieve dissociation. Note that the $\overline{Z_H}$ tends toward 5, indicating the propensity for further protonation. A fifth protonation constant was excluded from this model, as it was only allowed at the expense of pKa_4 (3.992), which resulted in a large Hamilton R-factor and standard deviations of all species, and furthermore, compromising the fit between the experimental data (points) and the calculated $\overline{Z_H}$ curve (line) that could best be achieved in the region pH 2 to 4 (*Figure 4.3.1(a)*). *Figure 4.3.1(b)* shows the distribution of the protonated ligand (PEI-MP) species at the respective pHs. The proposed model shows the consecutive dissociation of the ligand's protons as the pH is gradually increased.

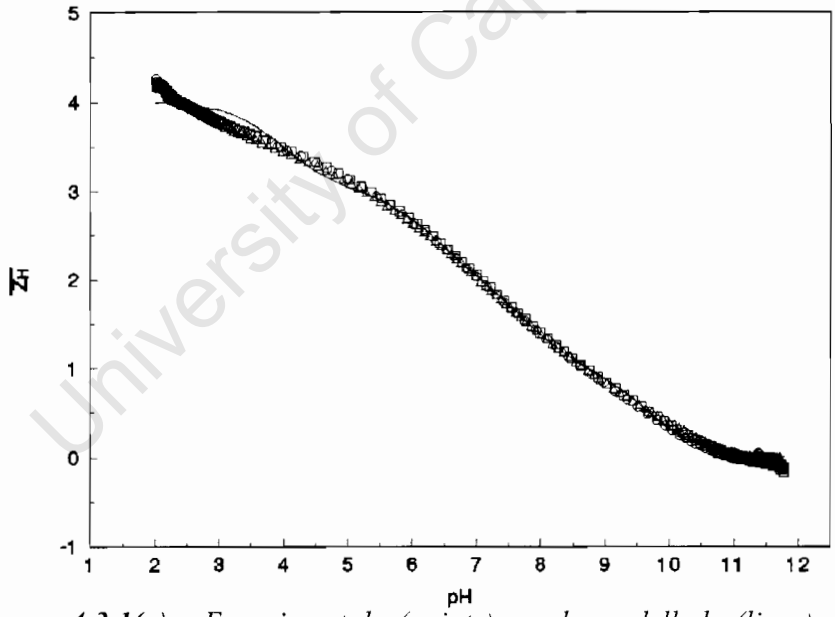

Figure 4.3.1(a). *Experimental (points) and modelled (lines) protonation formation curves for PEI-MP. Three titrations are represented by (O) 1.25mM PEI-MP and 12.5mM HCl;(□) 1.89mM PEI-MP and 13.66mM HCl and (Δ) 2.49mM PEI-MP and 12.59mM HCl, all titration against 50.24mM NaOH in 100.3mM NaCl. All solutions were at 25°C and 150mM NaCl or 150mM total ionic strength.*

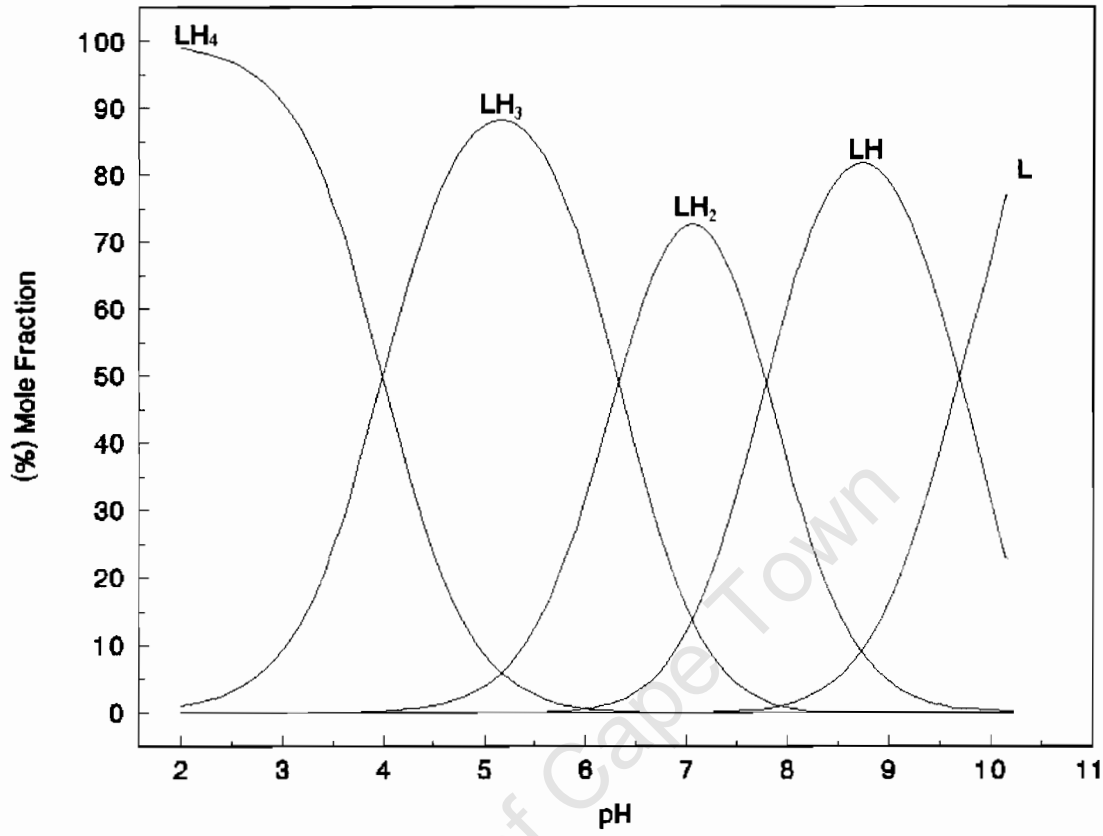

Figure 4.3.1(b). *Species distribution curves for the protonation of PEI-MP at 25°C and 0.15M NaCl.*

4.3.2 Sn^{IV}-(PEI-MP) formation constants

For the titrations of PEI-MP with Sn^{IV} the $\bar{Z}$ curves (*Figure 4.2.2(a)*) exhibit back-fanning at high pH (and high free ligand concentration), which is indicative of the presence of hydroxide containing species. This can be further supported when studying the $\bar{Q}$ curves (*Figure 4.3.2(b)*) generated from PEI-MP- Sn^{IV} titration data, in which the experimental curves lie predominantly above the $\bar{n}$ line beyond pH 4. Furthermore, the speciation distribution analysis results show that all complexes formed were, in fact, hydroxyl species, including the region below pH 4, with $[Sn_2L(OH)_3]^0$ being very prominent. This could be due to the hydrolysis of the Sn^{IV}, which is typically unavoidable in water, and especially at higher pH, rendering the

ESTA analysis results rather distorted. Contrary to what would typically be expected – that due to presence of binuclear species (M_2L), the $\overline{Z}$ curve should be seen to level off at 0.5 – but instead stops at 1, which is more consistent with ML type complexes. However, the existence of the binuclear complexes can be rationalized from the $\overline{Q}$ curves.

The speciation model, at pH 7.4 – which is of special interest when considering *in vivo* (physiological conditions), shows the complex $[Sn^{IV}_2L(OH)_5]^{1-}$ to be dominant (60%), where L = PEI-MP. Two other species are also present, namely $[Sn^{IV}_2L(OH)_4]^0$ (37%), and $[Sn^{IV}_2L(OH)_3]^{1+}$ (3%). Note that the formal charge of the ligand is negative 4, i.e. $[L]^{4-}$. Because of the instant formation of the hydrolysed species – $[Sn^{IV}_2 L(OH)_3]^{1+}$ – at the start of the titrations, comprising close to 100% (*Figure 4.3.2(c)*), little or no free metal was available for an equilibrium to exist. Hence the equilibrium constant for this species is inaccurate and practically unresolved within this experiment – as is evident from the high standard deviation. The model was refined as best possible including the $M_2L(OH)_3$ species – ignoring all significant correlations – after which the formation constant for this species was kept fixed for further analysis of the other constants.

Upon coordinating with the Sn^{IV}-ion(s), PEI-MP exhibits the loss of one more proton than expected. This could be due to deprotonation at an amine centre, or from a metal-coordinated water molecule – in which case we'd expect the formation constant of the MLOH species to be of similar magnitude than that of the first hydrolysis constant of Sn^{IV} ($\log K_{10\text{-}1} = -1.94$). This is not immediately evident from the model. However, having observed the dissociation constant for an amine site in the ligand-protonation model (*Table 1*), $pKa_1 = 9.68$, it is evident that upon interacting with the Sn^{IV}-ion(s) the formation constants $\log K_{21\text{-}5} = -9.25$ and $\log K_{21\text{-}7} = -9.00$, are close enough to assume that the metal-ion(s) coordinate at an amine centre resulting in the dissociation of a proton.

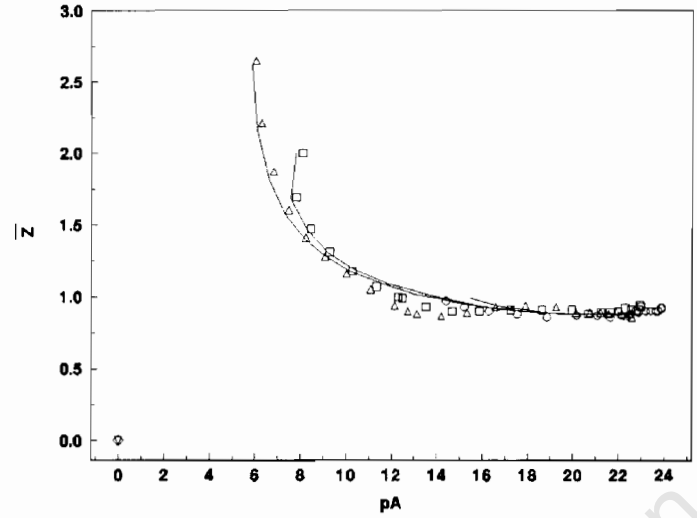

Figure 4.3.2(a). *Experimental (points) and modelled (lines) for* $\bar{Z}$ *curves for PEI-MP complexation with* Sn^{IV}. *Five titrations are represented by (**O**) 0.30mM* Sn^{IV}, *0.30mM PEI-MP and 7.28mM HCl; (□) 0.14mM* Sn^{IV}, *0.29mM PEI-MP and 7.08mM HCl; (**Δ**)0.14mM* Sn^{IV}, *0.43mM PEI-MP and 6.97mM HCl; (◊)0.43mM* Sn^{IV}, *0.29mM PEI-MP and 9.92mM HCl and (▽)0.56mM* Sn^{IV}, *0.28m5M PEI-MP and 12.38mM HCl, all titration against 50.02m1M NaOH in 100mM NaCl. All solutions were at 25°C and 150mM NaCl or 150mM total ionic strength.*

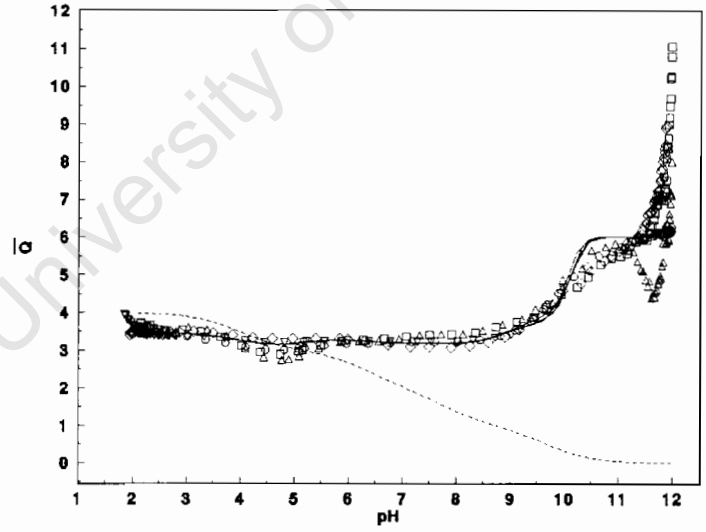

Figure 4.3.2(b). *Experimental (points) and modelled (lines) for* $\bar{Q}$ *curves for PEI-MP complexation with* Sn^{IV}. *The dotted line represents the* $\bar{n}$ curve, which is the protonation state of APDDMP in the absence of metal. *Five titrations are represented by (**O**) 0.30mM* Sn^{IV}, *0.30mM PEI-MP and 7.28mM HCl; (□)0.14mM* Sn^{IV}, *0.29mM PEI-MP and 7.08mM HCl; (**Δ**)0.14mM* Sn^{IV}, *0.43mM PEI-MP and 6.97mM HCl; (◊)0.43mM* Sn^{IV}, *0.29mM PEI-MP and 9.92mM HCl and (▽)0.56mM* Sn^{IV}, *0.28mM PEI-MP and 12.38mM HCl, all titration against 50.02mM NaOH in 100mM NaCl. All solutions were at 25°C and 150mM NaCl or 150mM total ionic strength.*

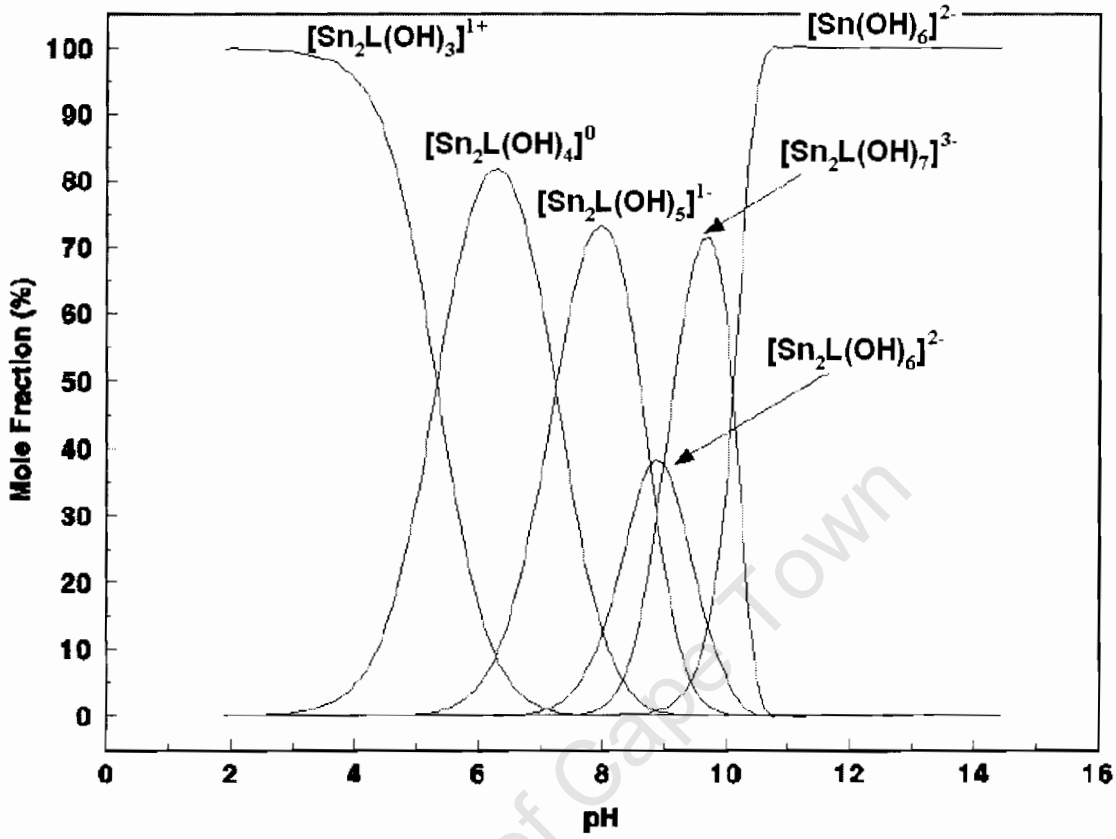

Figure 4.3.2(c). *Species distribution curves for the complexation of PEI-MP with Sn^{IV} at 25°C and 0.15M NaCl.*

Due to its nature as a polymer, some steric constraints can be anticipated when considering the possible binding sites for metal-ions in solution. Upon coordination the ligand can be expected to wrap around the Sn^{IV}-ion(s) effectively shielding the metal-ion(s) from the aqueous environment, thereby limiting hydrolysis. There are essentially two methylene-phosphonate sites for metal coordination per PEI-MP sub-unit, with the likelihood of amine interactions at each. Various possible structures exist for Sn^{IV}-PEI-MP complexes. PEI-MP has the potential to form multiple cyclic structures, which would contribute to the stability of these species. Examples of these are illustrated in *Figures 4.3.2 (d), (e)* and *(f)*. A common feature in all three structures proposed here is the chelation at the amine centres in conjunction with the neighbouring methylenephosphonate functional groups – resulting in the formation of stable 5-membered rings. At one of the coordination sites a bicyclo[3,3,0]-structure could exist

(*Figure 4.3.2(d)*). A third ring is possible in this region, as the ligand wraps around the metal-ion to form a bicyclo[3,3,3]-species, as depicted in *Figure 4.3.2(e)*.

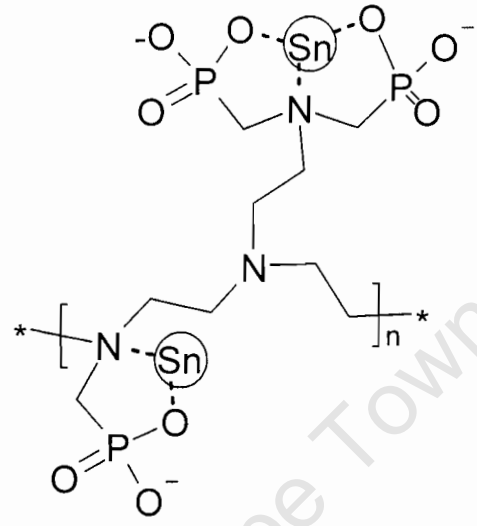

Figure 4.3.2(d). *Proposed structure for a typical Sn_2PEIMP complex. Illustrating two possible metal-binding sites.*

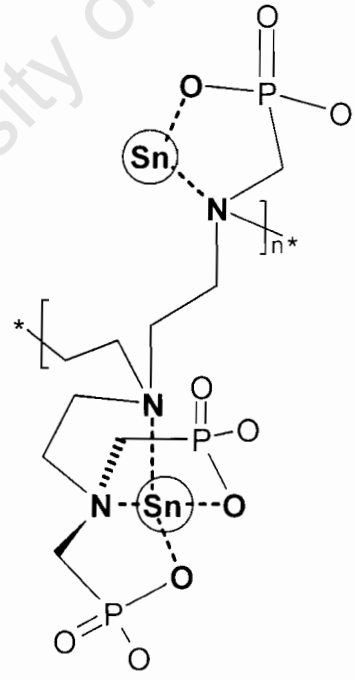

Figure 4.3.2(e). *Proposed structure for a Sn_2PEIMP species. Illustrating the ability of the PEI-MP ligand to wrap around the metal-ion forming a bicyclo[3,3,3]-structure.*

The wrapping action of the ligand includes the possible coordination at the amine centre present in main chain of the polymer. An alternative structure – also considering the possible wrapping around and coordination of the same amine centre – could be to form two bicyclo[3,3,0] entities at the opposite ends of the polymer sub-unit (*Figure 4.3.2(f)*).

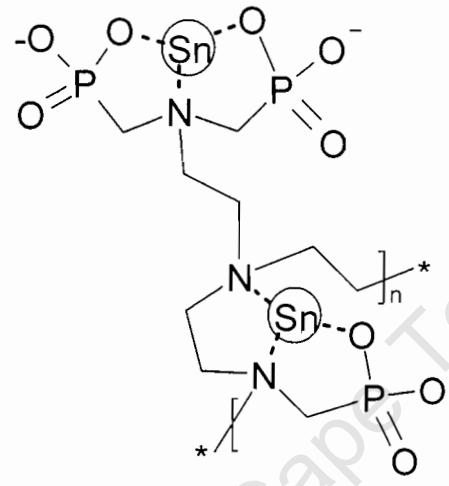

Figure 4.3.2(f). *Proposed structure for a Sn_2PEI-MP species. Illustrating the ability of the PEI-MP ligand to wrap around the metal-ion forming two bicyclo[3,3,0] moieties.*

PEI-MP has the ability to form reasonably stable complexes, with some interesting coordination possibilities. NMR-spectroscopic techniques, such as NMR-titrimetry, will render more accurate predictions of these structures, and could lead to the enhanced understanding of their possible action within biological systems. However, this was outside the scope of these experiments, but could form the bases of future work.

4.4 Conclusion

The analyses of titration data for the protonation experiments reveal that PEI-MP possesses four dissociable protons, with successive protonation at the methylenephosphonate sites, followed by the amine. Further dissociation would be possible at another amine site, should higher pH's be obtainable, or observable. The titrations conducted with Sn^{IV} revealed the exclusive formation of hydrolysed complexes,

as confirmed in the $\overline{Z}$ and $\overline{Q}$ curves. The Sn^{IV} complexes were binuclear i.e. of the type M_2L (two metal centres were present). The Sn^{IV}-PEI-MP species distribution was as follows: $[Sn^{IV}_2L(OH)_x]^{y-}$ (x = 3, 4, 5, 6, 7; and y = –1, 0, 1, 2, 3 respectively, and L = PEI-MP). The anticipated hydrolysis of Sn^{IV} also featured strongly at pH beyond 10, with $[Sn^{IV}(OH)_6]^{2-}$ being observed. At pH 7.4, which is of physiological significance, the following complexes occur (with their respective percentage mole fraction composition in parenthesis):

- $[Sn^{IV}_2L(OH)_5]^{1-}$ (60%),
- $[Sn^{IV}_2L(OH)_4]^{0}$ (37%),
- $[Sn^{IV}_2L(OH)_6]^{2-}$ (3%).

Various attempts at different models were fruitless in lowering the uncertainties of the individual species, as well as the Hamilton R-factor. The model presented above was the most sensible that could be derived and refined. The species distribution at pH 7.4 shows that 60% of the metal is in the, $[Sn^{IV}_2L(OH)_5]^{1-}$ complex. Hence, under physiological conditions within blood plasma, Sn^{IV}-PEI-MP complexes are more likely to exist in the form $M_2L(OH)_5$. This could prove beneficial as a more directed action could be expected of the radiopharmaceutical when administered intravenously, reducing unwanted side-effects.

Sn^{IV} is readily hydrolysed in solution and forms a precipitate, making glass electrode potentiometric analysis and evaluation by ESTA rather challenging. The method can be modified to counteract the precipitation by conducting titrations at static pH whilst titrating with an aqueous solution of Sn^{IV} (0.005M $SnCl_4$ in 0.1M HCl). This can be achieved by incorporating a second burette (0.05M NaOH in 0.1M NaCl) for maintaining the pH. This method was attempted with the Sn^{IV}-PEI-MP experiments, but with no success. The technique will have to be fine-tuned and could prove beneficial for use with other experiments or systems with similar complications such as precipitation. PEI-MP forms very stable complexes with Sn^{IV} such that at at low pH the complex was almost 100% formed.. Better data could possibly be obtained by using a second ligand, which

could compete with PEI-MP. In this case the stability of the PEI-MP complexes would be determined relative to the new ligand.. For example, EDTA (ethylenediamintetraacetic acid) could be a likely candidate.

4.5 References

[1] N. V. Jarvis, J. R. Zeevaart, J. M. Wagener, W. K. A. Louw, I.C. Dormehl, R. J. Milner and E. Killian; *Radio Chimica Acta*, 2002, **90**, 237-246

[2] J. R. Duffield, D. R. Williams, and I. Kron, *Polyhedron,* 1991, **10**, 377-387.

[3] Martell, A.E., Smith R. M.; Critical Stability Constants, Vols 3 and 6, Plenum, New York, 1977 and 1989.

[4] J. R. Zeevaart, W. K. A. Louw, Z. I. Kolar, J. M. Wagener, N. V. Jarvis, R. A. M. J. Claessens; *Journal of Radioanalytical and Nuclear Chemistry*, 2003, **257**, 2003, 83-91.

[5] J. R. Zeevaart, W. K. A. Louw, Z. I. Kolar, E. Killian, F. E. Jansen van Rensburg and I. C. Dormehl; *Arzneim.-Forsch/Drug Res.*, 2004, **54**, 340-347.

RATIONALISING THE HIGH KIDNEY UPTAKE OF $^{117m}Sn^{II}$-APDDMP IN RATS BY BLOOD PLASMA MODELLING USING ECCLES

5.1 Introduction

As part of a study to understand the bio-distribution of $^{117m}Sn^{II}$-APDDMP in the body, tests were conducted on rats [1]. With a potential application in the diagnosis and treatment of metastatic bone cancer, the extent to which APDDMP localizes in bone relative to the rest of the body tissue was the objective of the study. In principle the radioactive $^{117m}Sn^{II}$ is released at the point of uptake of APDDMP by bone, exchanging the Sn^{II} for Ca^{II} (in bone tissue). Effectively, γ-Ray images taken of the subject will make it possible to locate regions of high Ca^{II} concentration, which is typical of bone tumours.

However, images obtained of the rats revealed that most of the $^{117m}Sn^{II}$ was located in the kidneys [1] for the 4 hour duration of the experiment. This was consistent with earlier studies found in literature [2], of tin-based radiopharmaceuticals (including Sn-chlorides for both oxidation state: 2+ and 4+), which exhibited rapid initial clearance of $^{117m}Sn^{II}$ within the first 3 hours after injection. In order to unravel this phenomenon three hypotheses were presented:

(i) The *first* of which was to assume that APDDMP clears faster with respect to $^{117m}Sn^{II}$, i.e. competition for APDDMP by other metal ions in blood plasma is greater.

(ii) The *second* assumption was that the $^{117m}Sn^{II}$ clears faster with respect to APDDMP, meaning that the body flushes out the $^{117m}Sn^{II}$ faster than the $^{117m}Sn^{II}$-APDDMP complex can reach the bone tissue – i.e. competition for tin by other ligands in the blood plasma is too great.

(iii) *Thirdly* it was assumed that the entire $^{117m}Sn^{II}$-APDDMP complex clears too rapidly for the APDDMP to reach the bone tissue. This would be typically expected of highly charged complexes, as those formed by APDDMP and Sn^{II} (Chapter 2).

These postulates were investigated using the blood plasma modelling programme ECCLES.

5.2 Procedure

The ECCLES programme was used to model the behaviour of Sn^{II} (M) and APDDMP (L) respectively in blood plasma relative to changes made to their concentrations.

The three hypotheses were studied as follows:

(i) By keeping the concentration of Sn^{II} constant the ratio of APDDMP to Sn^{II} was gradually reduced by lowering the APDDMP concentration,

(ii) maintaining a constant concentration of APDDMP the L:M ratio was increased by changing the Sn^{II} concentration,

(iii) fixing the L:M ratio, the concentrations of both the APDDMP and Sn^{II} were lowered gradually.

The ECCLES database had been updated to include formation constants measured for all species that Sn^{II} formed with ligands (low molecular weight ligands, LWL) occurring in blood plasma [3], including Sn^{II} hydrolysis constants [4].

5.3 Results

5.3.1 First hypothesis

Table 5.3.1: *Hypothesis One; APDDMP clears rapidly relative to Sn^{II}. Representing the percentages of the total Sn^{II} and APDDMP concentrations that are bound according to the Sn^{II}-APDDMP species.*

MODEL:	Keep Sn(II) constant, decreasing the APDDMP								
	Decreasing the L:M ratio								
(L/M)	10	7.5	5	2.5	1	0.75	0.5	0.25	0.1
MLH / MLOH	1 M : 10 L	1 M : 7.5 L	1 M : 5.0 L	1 M : 2.5 L	1 M : 1.0 L	1 M : 0.75 L	1 M : 0.5 L	1 M : 0.25 L	1 M : 0.1 L
Sn(II)	***2.65E-05***	***2.65E-05***	***2.65E-05***	***2.65E-05***	***2.65E-05***	***2.65E-05***	***2.65E-05***	***2.65E-05***	***2.65E-05***
21-1	35.3%	32.9%	29.2%	22.2%	13.4%	11.0%	8.2%	4.6%	2.0%
21-2	18.0%	16.8%	14.9%	11.3%	6.8%	5.6%	4.2%	2.4%	1.0%
110	4.7%	4.0%	3.0%	1.8%	0.9%	0.7%	0.5%	0.3%	0.1%
210	1.1%	1.0%	0.9%	0.7%	0.4%	0.4%	0.3%	0.1%	0.1%
11-1	0.2%	0.2%	0.1%	0.1%	0.0%	0.0%	0.0%	0.0%	0.0%
21-3	0.1%	0.1%	0.1%	0.1%	0.0%	0.0%	0.0%	0.0%	0.0%
Total %	59.4%	55.0%	48.2%	36.2%	21.5%	17.7%	13.2%	7.4%	3.2%
APDDMP	***2.65E-04***	***1.99E-04***	***1.33E-04***	***6.63E-05***	***2.65E-05***	***1.99E-05***	***1.33E-05***	***6.63E-06***	***2.65E-06***
21-1	1.8%	2.2%	2.9%	4.4%	6.7%	7.3%	8.2%	9.2%	10.0%
21-2	0.9%	1.1%	1.5%	2.3%	3.4%	3.7%	4.2%	4.7%	5.1%
110	0.5%	0.5%	0.6%	0.7%	0.9%	0.9%	1.0%	1.0%	1.1%
210	0.1%	0.1%	0.1%	0.1%	0.2%	0.2%	0.3%	0.3%	0.3%
11-1	0.0%	0.0%	0.0%	0.0%	0.0%	0.0%	0.0%	0.0%	0.0%
21-3	0.0%	0.0%	0.0%	0.0%	0.0%	0.0%	0.0%	0.0%	0.0%
211	0.0%	0.0%	0.0%	0.0%	0.0%	0.0%	0.0%	0.0%	0.0%
21-4	0.0%	0.0%	0.0%	0.0%	0.0%	0.0%	0.0%	0.0%	0.0%
Total %	3.3%	3.9%	5.1%	7.5%	11.2%	12.1%	13.7%	15.2%	16.5%
Total Concetrations complexed									
[Sn(II)]	1.57E-05	1.46E-05	1.28E-05	9.59E-06	5.70E-06	4.69E-06	3.50E-06	1.96E-06	8.48E-07
[APDDMP]	8.75E-06	7.75E-06	6.76E-06	4.97E-06	2.97E-06	2.40E-06	1.82E-06	1.01E-06	4.37E-07
(L/M)	0.56	0.53	0.53	0.52	0.52	0.51	0.52	0.51	0.52

By gradually decreasing the ratio of APDDMP:Sn^{II} in ECCLES the species distribution of both the metal and ligand can be monitored according to their individual complexes, as depicted in Table 5.3.1 above. This serves mainly to monitor any changes in the species composition with respect to ligand concentration. By lowering the concentration of

APDDMP in blood, the percentage of the total Sn^{II} that binds with the ligand also decreases (Figure 5.3.1c). For the individual species the same trend can be observed (Figure 5.3.1a). However, the extent/rate of decrease in the amount of Sn^{II} that occurs within the complexes is greater for the more dominant species. The minor species exhibit a rather steady decline in their composition of Sn^{II} as the APDDMP concentration is lowered.

The relative affinity for complexation between APDDMP and Sn^{II} (considered in terms of the ratio of complexation, Figure 5.3.1e) remains unchanged as the ligand concentration decreases, i.e. for every mole of APDDMP there are approximately 2 moles of Sn^{II} that readily interact to form complexes, and as the total concentration of APDDMP is lowered the amount of Sn^{II} that will complex also decreases accordingly (Figure 5.3.1d). This is observed when APDDMP is administered in excess as well as when the concentration is below that of Sn^{II}. Essentially, this means that any excess APDDMP is taken up by *in vivo* metal-ions, and hence decreasing the adiministered concentration would mean that the only alternative source of APDDMP is from Sn^{II}-APDDMP complexes. Therefore, for any decrease in APDDMP, a relative amount of Sn^{II} will be released so as to maintain the ratio (L:M) of complexation. Should the lowering of the amount APDDMP in blood plasma have not affected the Sn^{II}-APDDMP complexes, the amounts (concentrations) of complexed metal and ligand would have remained the same throughout. However, still resulting in a constant ratio of complexation, but only until the excess has been depleted, whereupon the results will resemble the above experiment (Table 5.3.1). Figure 5.3.1b shows that APDDMP complexation with Sn^{II} is constant, and changes in the available ligand concentration (total) has little or no effect – the influence is mathematical, increasing the percentage of APDDMP that is bound to Sn^{II} mainly due to lowering of the total concentration. In order to prove that renal clearance is mainly due to the ligand, the expected result should've been a decrease in the ratio of complexation by infinitesimally decrementing the APDDMP concentration.

In reality, this scenario would describe the removal of APDDMP by possible competition of physiological metal-ions with the tendency to form more favourable/stable complexes.

It would be expected that the least stable Sn^{II}-APDDMP complexes would be influenced to a larger extent. However, what is observed is a faster decrease within the dominant species, which comprises a larger proportion of the Sn^{II}-ion content.

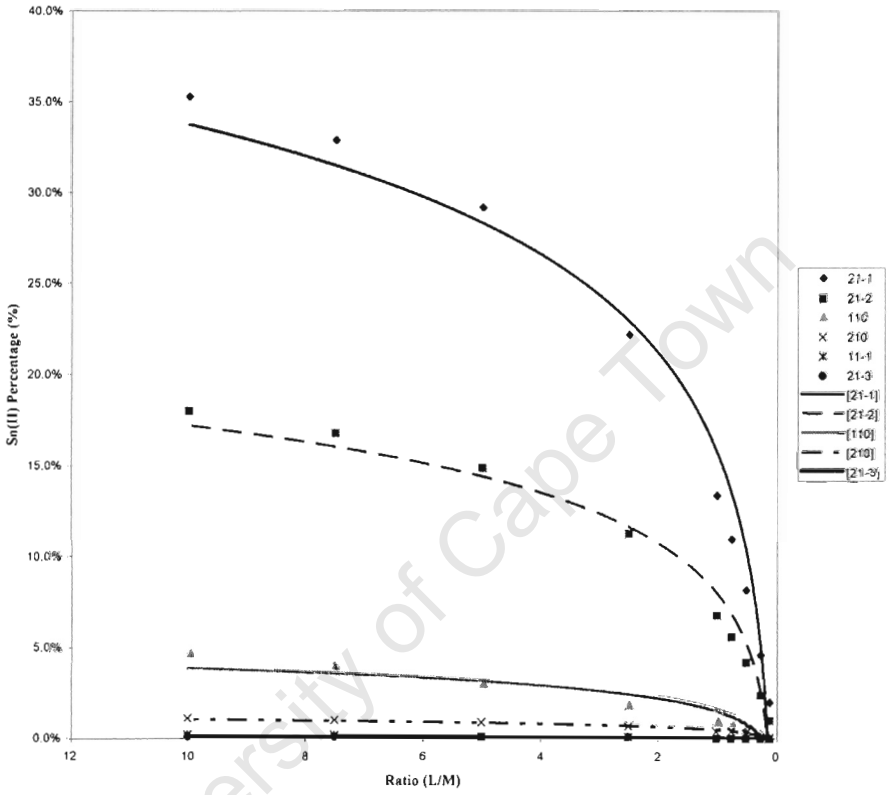

Figure 5.3.1(a): *Model ONE: APDDMP clears rapidly w.r.t. Sn^{II}. Percentage Sn^{II} that complexed with APDDMP verses Ratio administered. Lines represent the best-fit trend curves/functions.*

It would be expected that the least stable Sn^{II}-APDDMP complexes would be influenced to a larger extent. However, what is observed is a faster decrease within the dominant species, which comprises a larger proportion of the Sn^{II}-ion content.

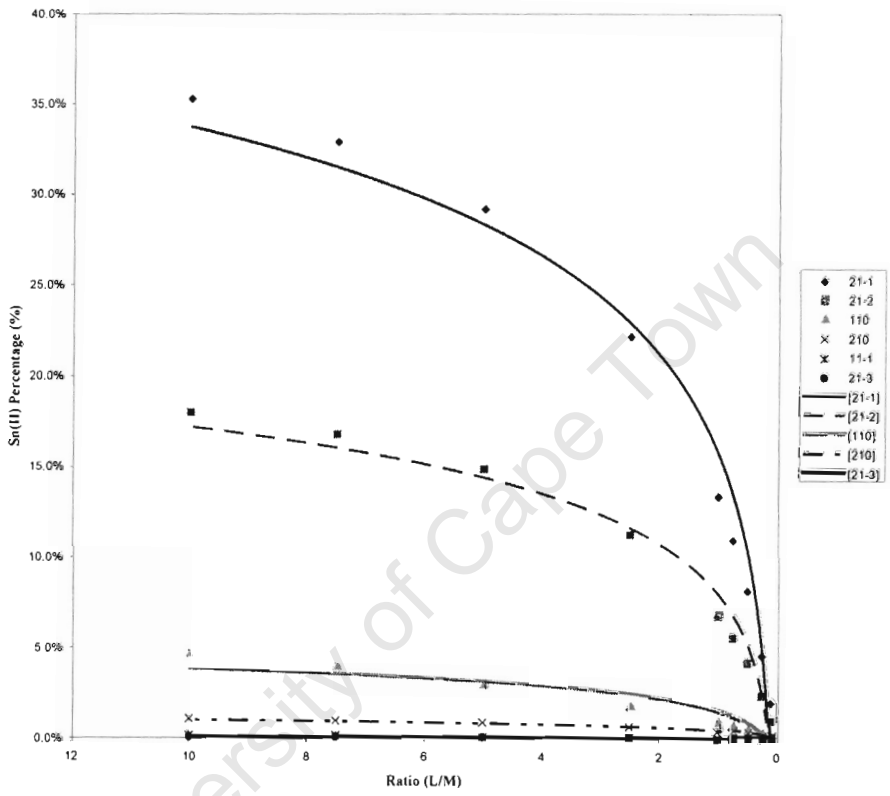

Figure 5.3.1(a): *Model ONE: APDDMP clears rapidly w.r.t. Sn^{II}. Percentage Sn^{II} that complexed with APDDMP verses Ratio administered. Lines represent the best-fit trend curves/functions.*

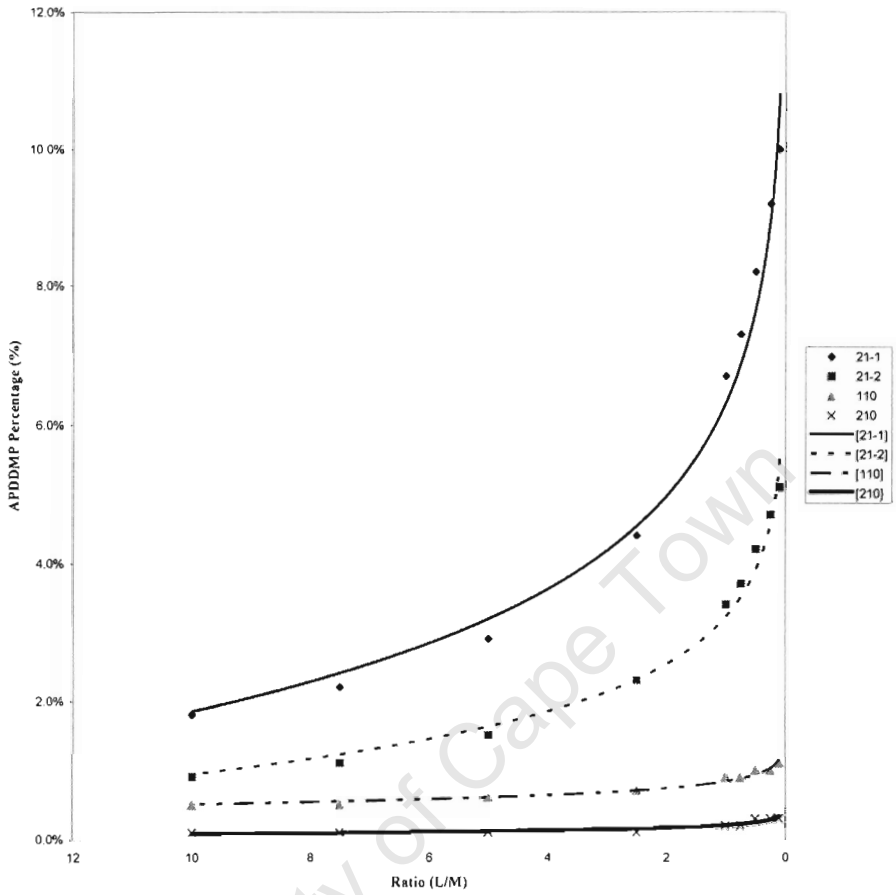

Figure 5.3.1(b): *Model ONE: APDDMP clears rapidly w.r.t. Sn^{II}. Percentage APDDMP that complexed with Sn^{II} verses Ratio administered. Lines represent the best-fit trend curves/functions.*

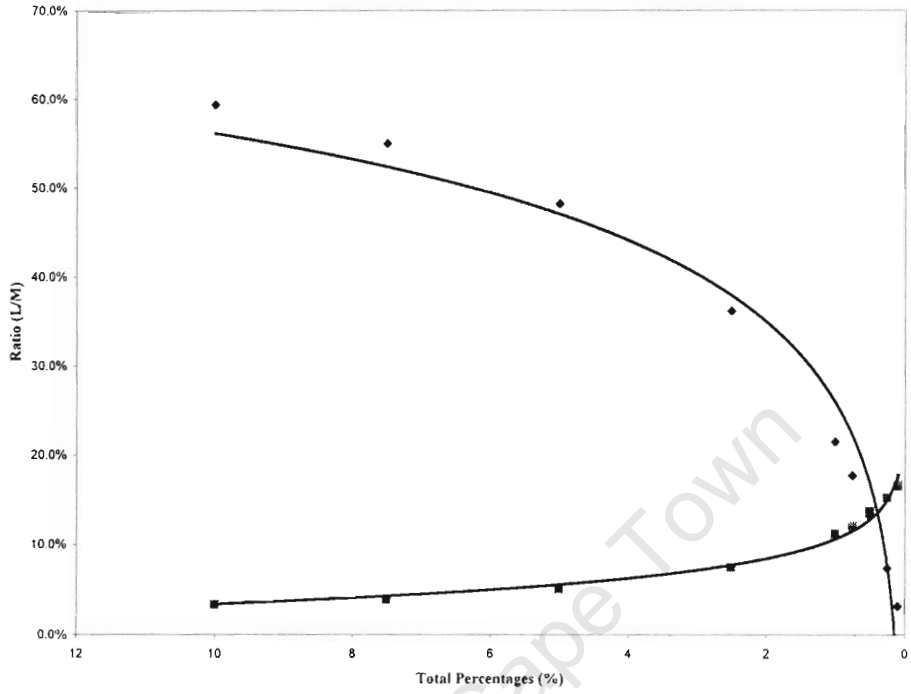

Figure 5.3.1(c): *Changes observed in the amounts (%) of Sn^{II} and APDDMP that remain complexed in vivo, as the administered ratio L:M is decreased (i.e. by gradually lowering the amount of APDDMP administered relative to Sn^{II}).* ♦*Percentage of Sn^{II} that remains complexed;* ■ *percentage of APDDMP that remains complexed. Lines represent the best-fit trend curves/functions.*

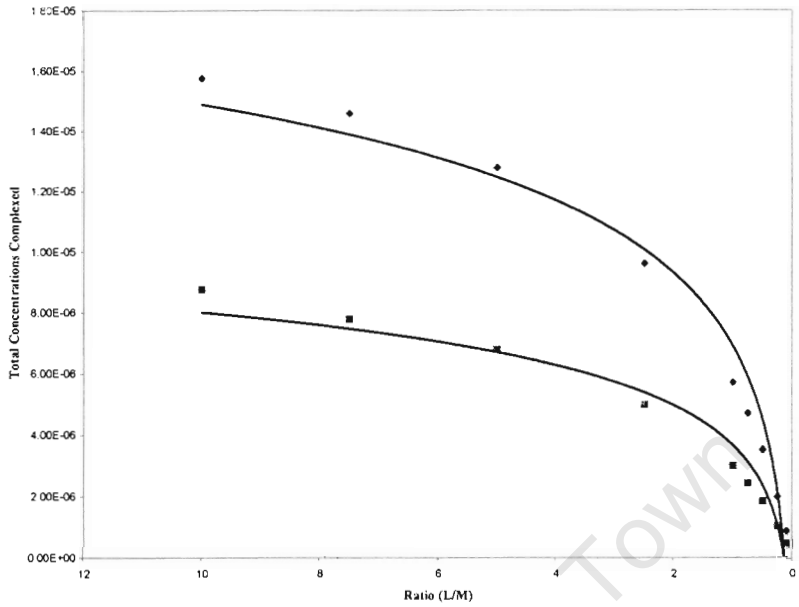

Figure 5.3.1(d): *Change in total concentrations that are complexed as the administered ratio L:M is decreased (i.e. by gradually lowering the amount of APDDMP administered relative to Sn^{II}).* ♦*Total concentration of Sn^{II} that remains complexed;* ■ *total concentration of APDDMP that remains complexed. Lines represent the best-fit trend curves/functions.*

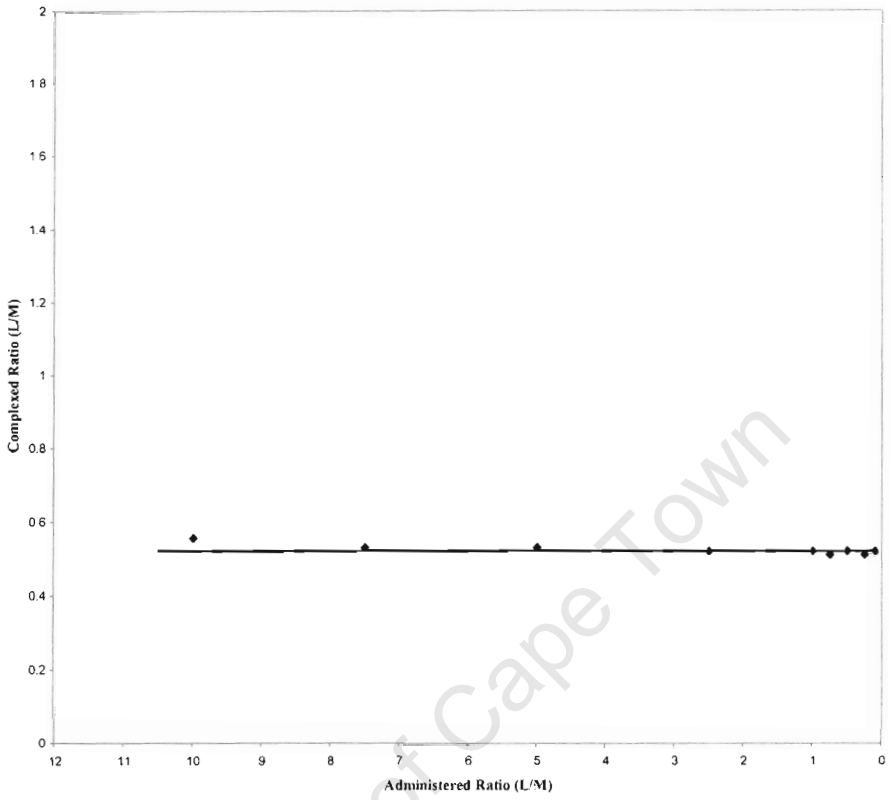

Figure 5.3.1(e): *Changes in (L/M) ratio of complexed APDDMP and SN^{II} as the administered (L/M) ratio is lowered. Trend in the ratio of APDDMP:Sn^{II} that remains complexed in the blood plasma as the ratio that is administered is decreased. ♦ Ratio of in vivo complexation. Lines represent the best-fit trend curves/functions.*

5.3.2 Second hypothesis

Table 5.3.2: *Hypothesis 2; Sn^{II} clears rapidly relative to APDDMP. Representing the percentages of the total Sn^{II} and APDDMP concentrations that are bound according to the Sn^{II}-APDDMP species.*

MODEL:	Keep APDDMP constant, decreasing Sn(II)								
	Increasing the L:M ratio								
(L/M)	10	15	20	25	30	35	40	45	50
MLH / MLOH	1 M : 10 L	1 M : 15 L	1 M : 20 L	1 M : 25 L	1 M : 30 L	1 M : 35 L	1 M : 40 L	1 M : 45 L	1 M : 50 L
Sn(II)	*2.65E-05*	*1.77E-05*	*1.33E-05*	*1.06E-05*	*8.83E-06*	*7.57E-06*	*6.63E-06*	*5.89E-06*	*5.30E-06*
21-1	35.3%	30.8%	27.6%	25.0%	22.9%	21.2%	19.8%	18.5%	17.4%
21-2	18.0%	15.7%	14.1%	12.8%	11.7%	10.8%	10.1%	9.5%	8.9%
110	4.7%	5.5%	6.0%	6.4%	6.7%	7.0%	7.2%	7.4%	7.6%
210	1.1%	1.0%	0.9%	0.8%	0.7%	0.7%	0.6%	0.6%	0.6%
11-1	0.2%	0.2%	0.3%	0.3%	0.3%	0.3%	0.3%	0.3%	0.3%
21-3	0.1%	0.1%	0.1%	0.1%	0.1%	0.1%	0.1%	0.1%	0.1%
Total %	59.4%	53.3%	49.0%	45.4%	42.4%	40.1%	38.1%	36.4%	34.9%
APDDMP	*2.65E-04*	*2.65E-04*	*2.65E-04*	*2.65E-04*	*2.65E-04*	*2.65E-04*	*2.65E-04*	*2.65E-04*	*2.65E-04*
21-1	1.8%	1.0%	0.7%	0.5%	0.4%	0.3%	0.2%	0.2%	0.2%
21-2	0.9%	0.5%	0.4%	0.3%	0.2%	0.2%	0.1%	0.1%	0.1%
110	0.5%	0.4%	0.3%	0.3%	0.2%	0.2%	0.2%	0.2%	0.2%
210	0.1%	0.0%	0.0%	0.0%	0.0%	0.0%	0.0%	0.0%	0.0%
11-1	0.0%	0.0%	0.0%	0.0%	0.0%	0.0%	0.0%	0.0%	0.0%
21-3	0.0%	0.0%	0.0%	0.0%	0.0%	0.0%	0.0%	0.0%	0.0%
211	0.0%	0.0%	0.0%	0.0%	0.0%	0.0%	0.0%	0.0%	0.0%
21-4	0.0%	0.0%	0.0%	0.0%	0.0%	0.0%	0.0%	0.0%	0.0%
Total %	3.3%	1.9%	1.4%	1.1%	0.8%	0.7%	0.5%	0.5%	0.5%
Total Concetrations complexed									
[Sn(II)]	1.57E-05	9.42E-06	6.49E-06	4.81E-06	3.75E-06	3.04E-06	2.52E-06	2.14E-06	1.85E-06
[APDDMP]	8.75E-06	5.04E-06	3.71E-06	2.92E-06	2.12E-06	1.86E-06	1.33E-06	1.33E-06	1.33E-06
(L/M)	0.56	0.53	0.57	0.61	0.57	0.61	0.52	0.62	0.72

In order to elucidate whether the main cause for renal clearance is due to dissociation of the metal-ion from the complex is, the Sn^{II} concentration can be varied to study the trends in the complexation behaviour of the individual species (Table 5.3.1). The amount of Sn^{II} introduced was gradually decreased to eventually allow for a large excess of the ligand. Initially there is a sharp decrease in the amount of APDDMP that binds with Sn^{II}, but beyond the L:M excess of 35 the percentage of the total ligand concentration that forms complexes with tin remains constant (Figure 5.3.2c) – as is also observed for the

individual Sn^{II}-APDDMP species (Figure 5.3.2b). When considering the changes in the amount of Sn^{II} that occur in the individual Sn^{II}-APDDMP complexes, only the prominent species are affected. In the composition of the hydrolysed complexes a decline in the percentage of the total Sn^{II} concentration is evident, whereas for the non-hydrolysed species the inverse is observed – indicating an increased preference for their formation as the amount of Sn^{II} that is administered is lowered (Figure 5.3.2a).

The total amounts of both the metal and ligand that form Sn^{II}-APDDMP complexes decrease rapidly as the concentration of Sn^{II} in blood plasma in lowered (Figure 5.3.2d). If renal clearance was not caused by rapid removal of Sn^{II} from Sn^{II}-APDDMP complexes, then any change in the metal concentration would keep the amount of ligand that complexes per Sn^{II}-ions (ratio of complexation, L:M) constant – i.e. observing a stoichiometric decrease in the percentage of APDDMP that bind with tin. However, Figure 5.3.2e indicates that the complexation ratio increases as the tin concentration decreases, implying that the survival of the Sn^{II}-APDDMP complexes within blood plasma is dependent on Sn^{II} affinity for APDDMP.

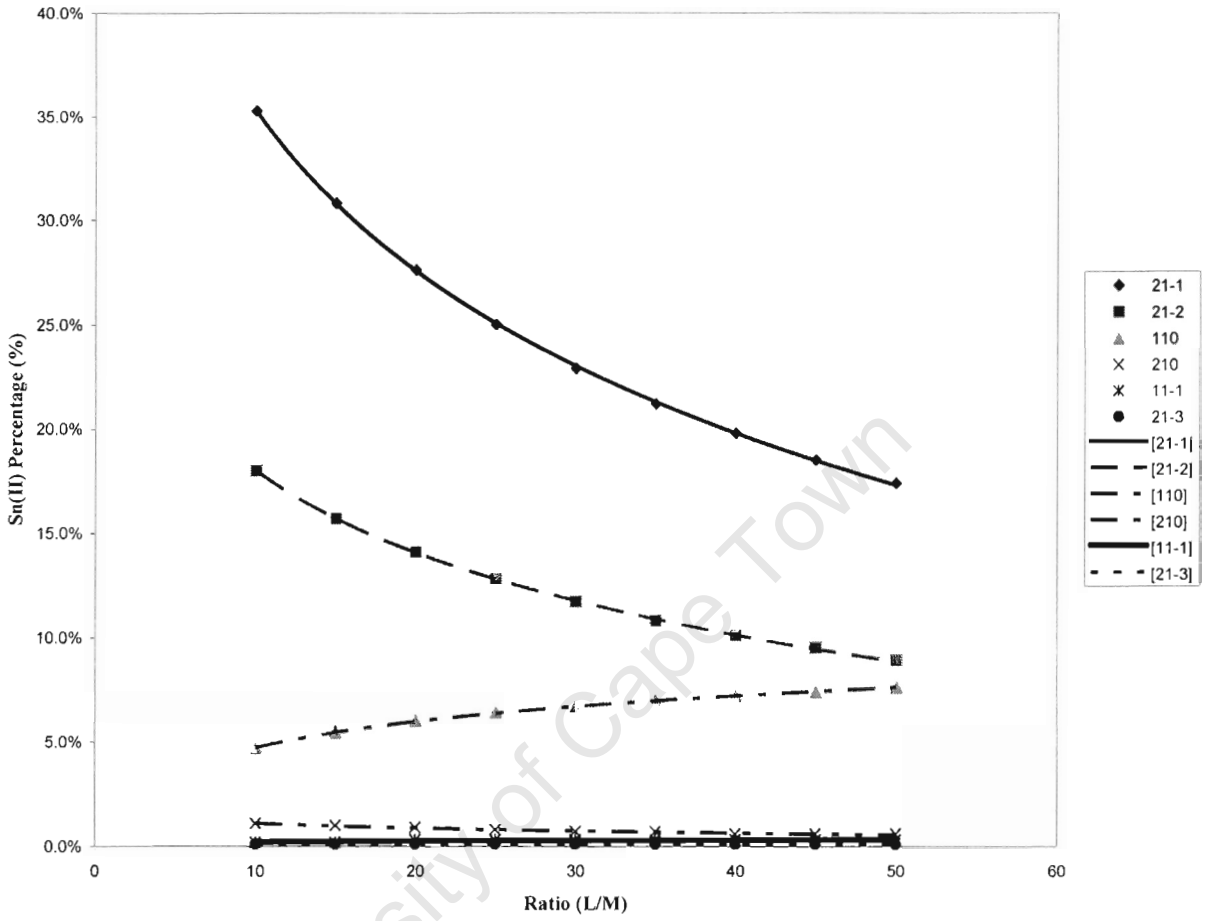

Figure 5.32(a): *Model TWO: Sn^{II} clears rapidly w.r.t. APDDMP. Percentage Sn^{II} that complexed with APDDMP verses Ratio administered. Lines represent the best-fit trend curves/functions.*

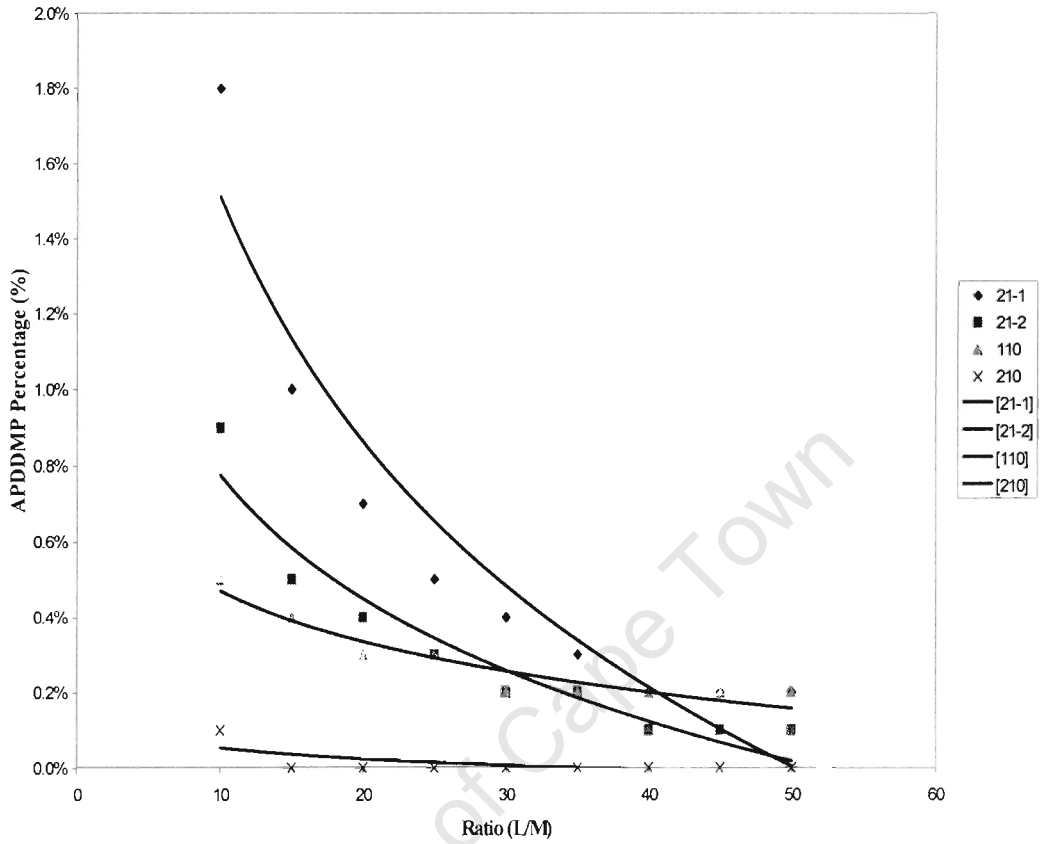

Figure 5.3.2(b): *Model TWO: Sn^{II} clears rapidly w.r.t. APDDMP. Percentage APDDMP that complexed with Sn^{II} verses Ratio administered. Lines represent the best-fit trend curves/functions.*

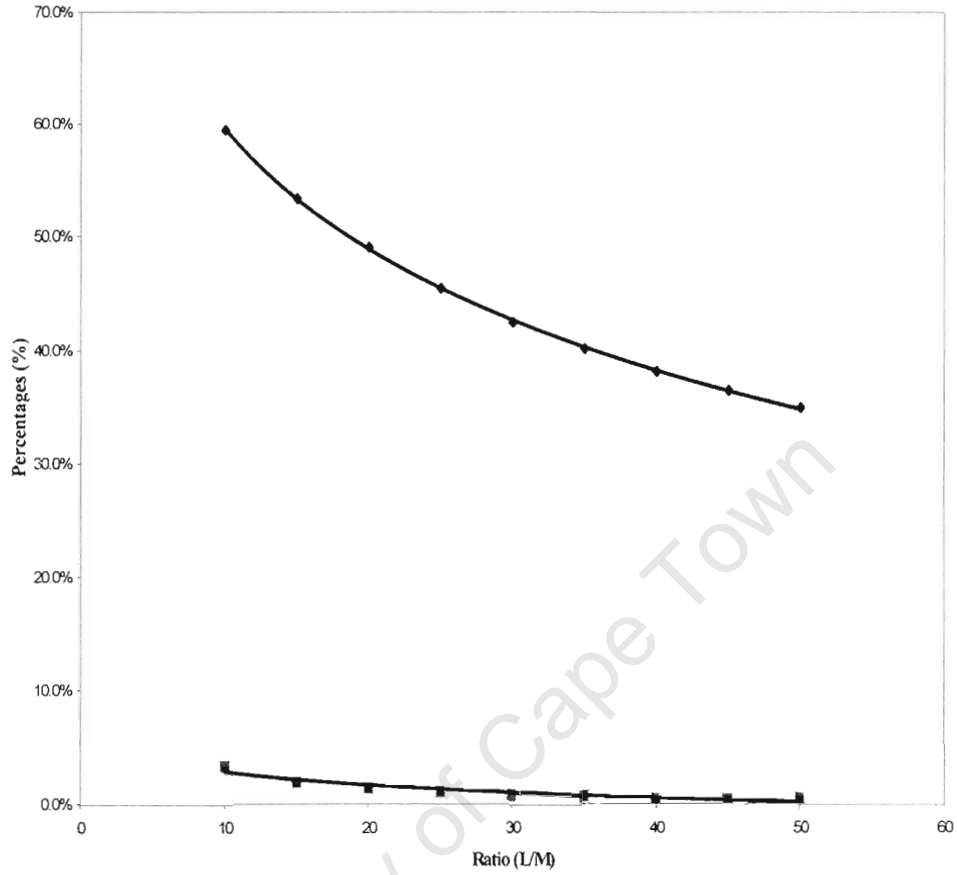

***Figure 5.3.2(c)**: Changes in the percentages of Sn^{II} and APDDMP that are complexed in the blood plasma as the administered ratio APDDMP:Sn^{II} in increased by gradually lowering the Sn^{II} concentration. ♦Percentage of Sn^{II} that remains complexed; ■ percentage of APDDMP that remains complexed. Lines represent the best-fit trend curves/functions.*

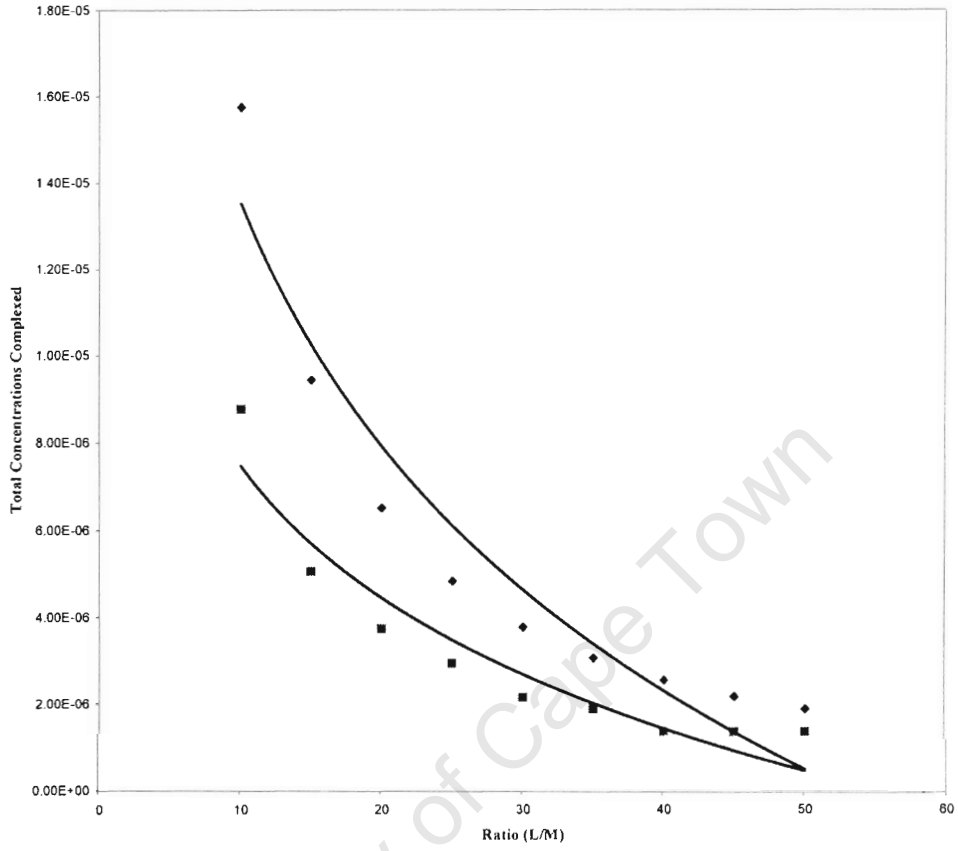

Figure 5.3.2(d): *Changes in the total concentrations that are complexed in the blood plasma as the administered ratio APDDMP:Sn^{II} in increased by gradually lowering the Sn^{II} concentration. ♦Total concentration of Sn^{II} that remains complexed; ■ total concentration of APDDMP that remains complexed. Lines represent the best-fit trend curves/functions.*

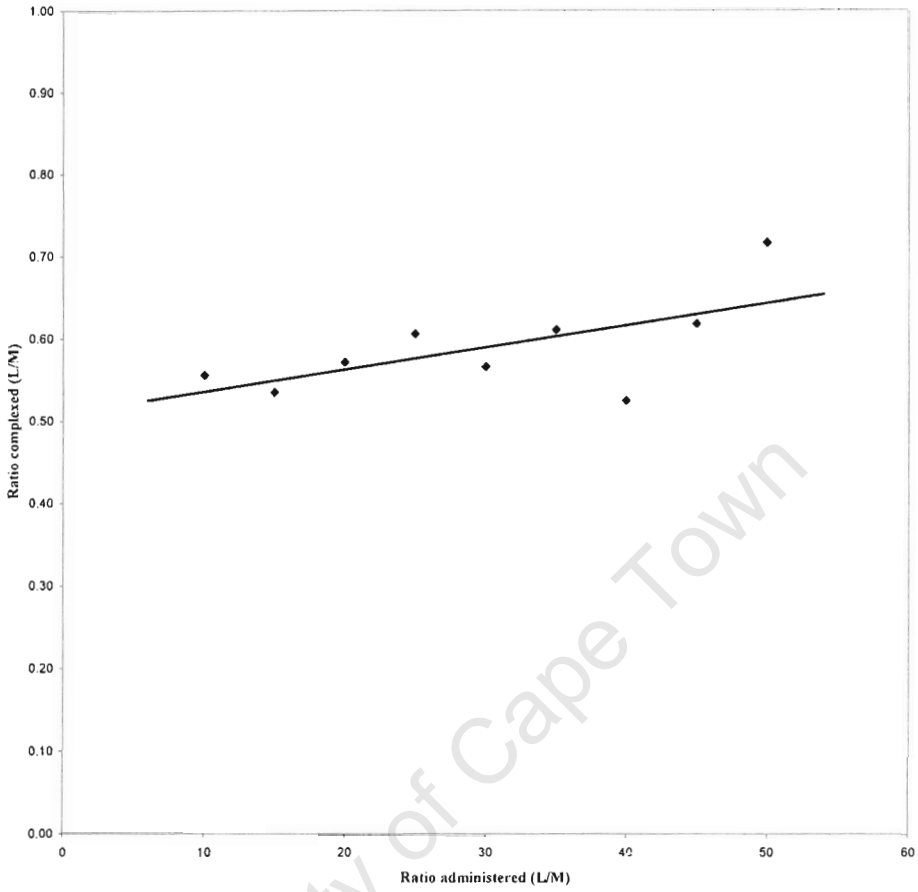

Figure 5.3.2(e): *Changes in the ratio (L/M) for complexed Sn^{II} and APDDMP, as the administered ratio is increased (Sn^{II}). Trend in the ratio of APDDMP:Sn^{II} that is complexed in the blood plasma as observed when the administered ratio is increased.* ♦*Ratio of in vivo complexation. Lines represent the best-fit trend curves/functions.*

5.3.3 Third hypothesis

Table 5.3.3: *Hypothesis 3; Sn^{II}-APDDMP complexes clear rapidly. Representing the percentages of the total Sn^{II} and APDDMP concentrations that are bound according to the Sn^{II}-APDDMP species.*

MODEL:	Keep L:M ratio constant, decreasing the Sn(II) and APDDMP concentrations								
MLH / MLOH	**1 M : 10 L**	**1 M : 10 L**	**1 M : 10 L**	**1 M : 10 L**	**1 M : 10 L**	**1 M : 10 L**	**1 M : 10 L**	**1 M : 10 L**	**1 M : 10 L**
Sn(II)	***2.65E-05***	***1.99E-05***	***1.33E-05***	***6.63E-06***	***2.65E-06***	***1.99E-06***	***1.33E-06***	***6.63E-07***	***2.65E-07***
21-1	35.3%	29.7%	21.3%	9.1%	1.9%	1.1%	0.5%	0.1%	0.0%
21-2	18.0%	15.1%	10.9%	4.6%	1.0%	0.6%	0.3%	0.1%	0.0%
110	4.7%	4.4%	3.7%	2.4%	1.1%	0.8%	0.6%	0.3%	0.1%
210	1.1%	0.9%	0.7%	0.3%	0.1%	0.0%	0.0%	0.0%	0.0%
11-1	0.2%	0.2%	0.2%	0.1%	0.0%	0.0%	0.0%	0.0%	0.0%
21-3	0.1%	0.1%	0.1%	0.0%	0.0%	0.0%	0.0%	0.0%	0.0%
Total %	59.4%	50.4%	36.9%	16.5%	4.1%	2.5%	1.4%	0.5%	0.1%
APDDMP	***2.65E-04***	***1.99E-04***	***1.33E-04***	***6.63E-05***	***2.65E-05***	***1.99E-05***	***1.33E-05***	***6.63E-06***	***2.65E-06***
21-1	1.8%	1.5%	1.1%	0.5%	0.1%	0.1%	0.0%	0.0%	0.0%
21-2	0.9%	0.8%	0.5%	0.2%	0.0%	0.0%	0.0%	0.0%	0.0%
110	0.5%	0.4%	0.4%	0.2%	0.1%	0.1%	0.1%	0.0%	0.0%
210	0.1%	0.0%	0.0%	0.0%	0.0%	0.0%	0.0%	0.0%	0.0%
11-1	0.0%	0.0%	0.0%	0.0%	0.0%	0.0%	0.0%	0.0%	0.0%
21-3	0.0%	0.0%	0.0%	0.0%	0.0%	0.0%	0.0%	0.0%	0.0%
211	0.0%	0.0%	0.0%	0.0%	0.0%	0.0%	0.0%	0.0%	0.0%
21-4	0.0%	0.0%	0.0%	0.0%	0.0%	0.0%	0.0%	0.0%	0.0%
Total %	3.3%	2.7%	2.0%	0.9%	0.2%	0.2%	0.1%	0.0%	0.0%
Total Concetrations complexed									
[Sn(II)]	1.57E-05	1.00E-05	4.91E-06	1.09E-06	1.09E-07	4.98E-08	1.86E-08	3.32E-09	2.65E-10
[APDDMP]	8.75E-06	5.37E-06	2.66E-06	5.97E-07	5.30E-08	3.98E-08	1.33E-08	0.00E+00	0.00E+00
(L/M)	0.56	0.54	0.54	0.55	0.49	0.80	0.71	0.00	0.00

Provided that the ratio of ligand to metal that is introduced into blood plasma is maintained, the extent of complexation between the Sn^{II} and APDDMP should effectively remain constant for any variation in their administered concentrations. Similarly, should there be rapid clearance of the entire Sn^{II}-APDDMP from the body the ratio of complexation should remain unchanged. This was tested by slowly decreasing both the Sn^{II} and APDDMP concentrations within blood plasma, whilst keeping the ligand to

metal ratio fixed (Table 5.3.3). The ratio of the amounts of APDDMP to Sn^{II} that formed complexes varied, with a general trend to increase as the concentrations were decreased (Figure 5.3.3e). Figures 5.3.3c and 5.3.3d reveal that the amount/percentage of Sn^{II}-ions that remains complexed to APDDMP decreases more rapidly than that of the ligand, which could serve to confirm the second postulate which states that the renal clearance is mainly due to dissociation of Sn^{II}.

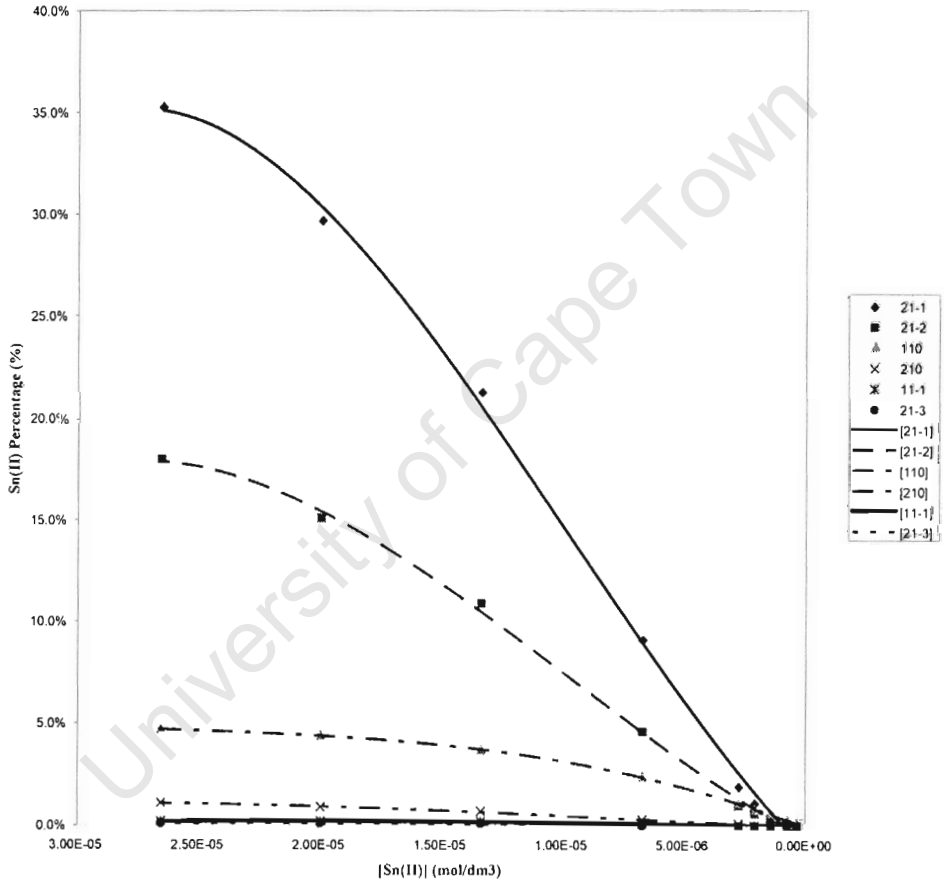

Figure 5.3.3(a): *Model THREE: Sn^{II}-APDDMP clears rapidly. Percentage Sn^{II} that complexed with APDDMP verses concentration administered. Lines represent the best-fit trend curves/functions.*

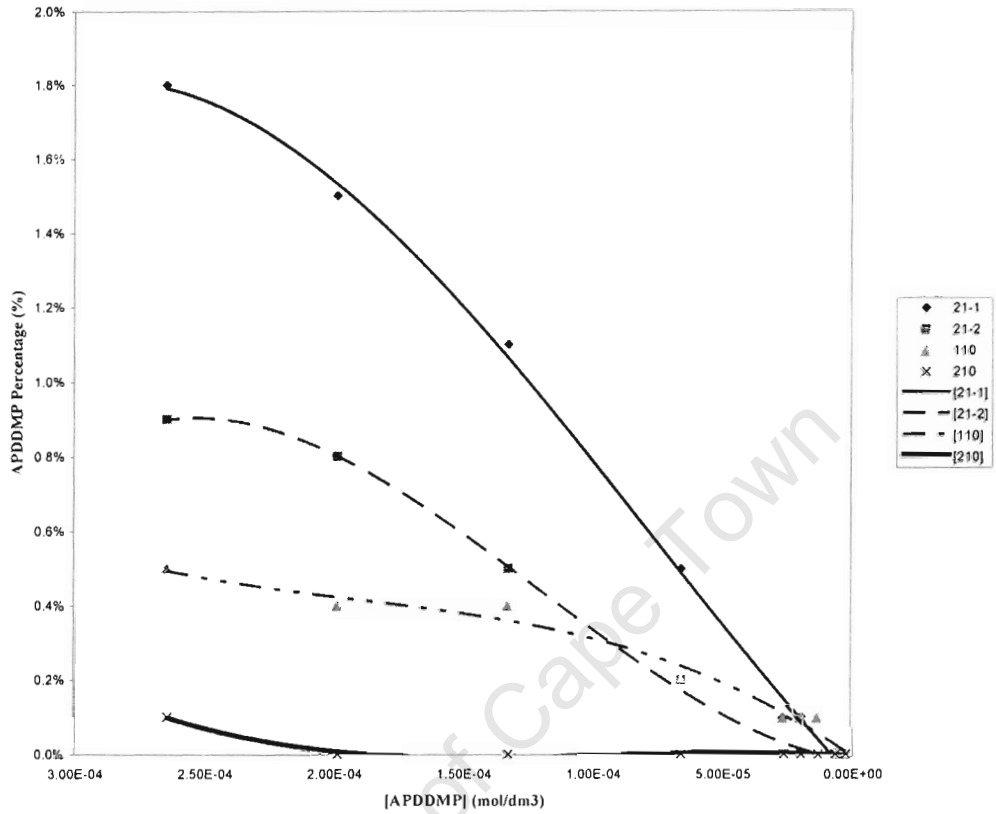

Figure 5.3.3(b): *Model THREE: Sn^{II}-APDDMP clears rapidly. Percentage APDDMP that complexed with Sn^{II} verses concentration administered. Lines represent the best-fit trend curves/functions.*

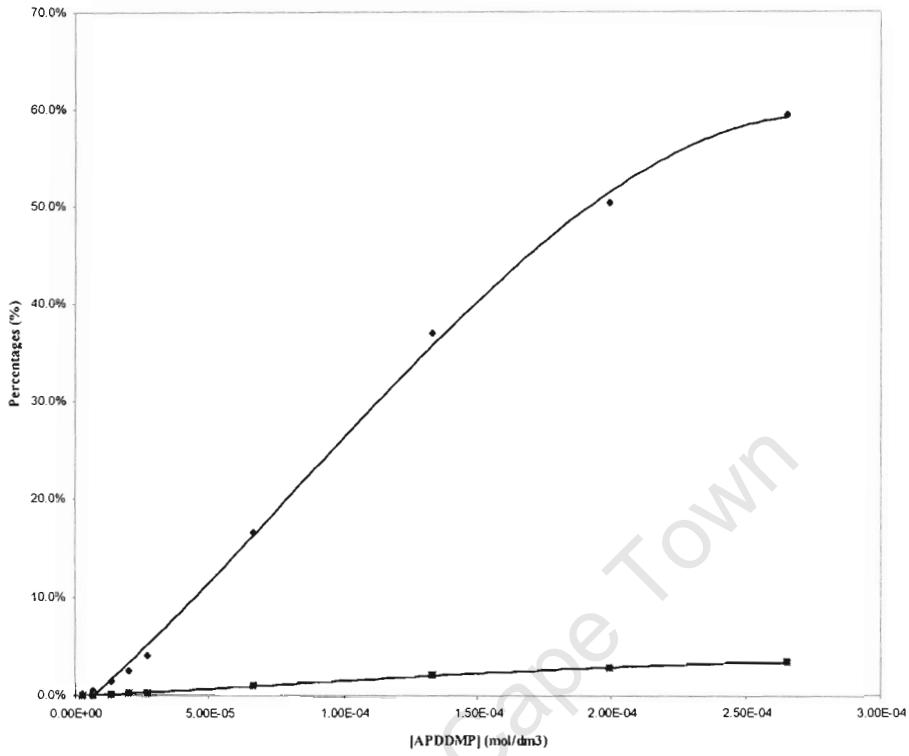

Figure 5.3.3(c): *Changes observed in the amounts (%) of Sn^{II} and APDDMP that remain complexed in vivo, as the concentrations of each is gradually lowered (maintaining a fixed administered ratio L:M)).* ◆ *Percentage of Sn^{II} that remains complexed;* ■ *percentage of APDDMP that remains complexed. Lines represent the best-fit trend curves/functions.*

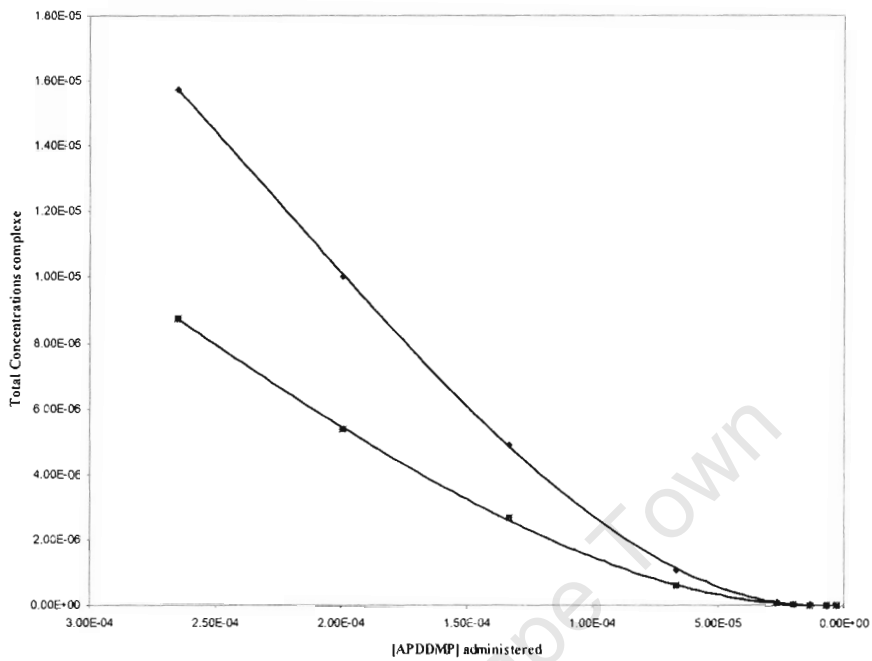

Figure 5.3.3(d): *Changes observed in the total concentrations of Sn^{II} and APDDMP that remain complexed in vivo, as the concentrations of each is gradually lowered (maintaining a fixed administered ratio L:M)).* ♦ *Total concentration of Sn^{II} that remains complexed;* ■ *total concentration of APDDMP that remains complexed. Lines represent the best-fit trend curves/functions.*

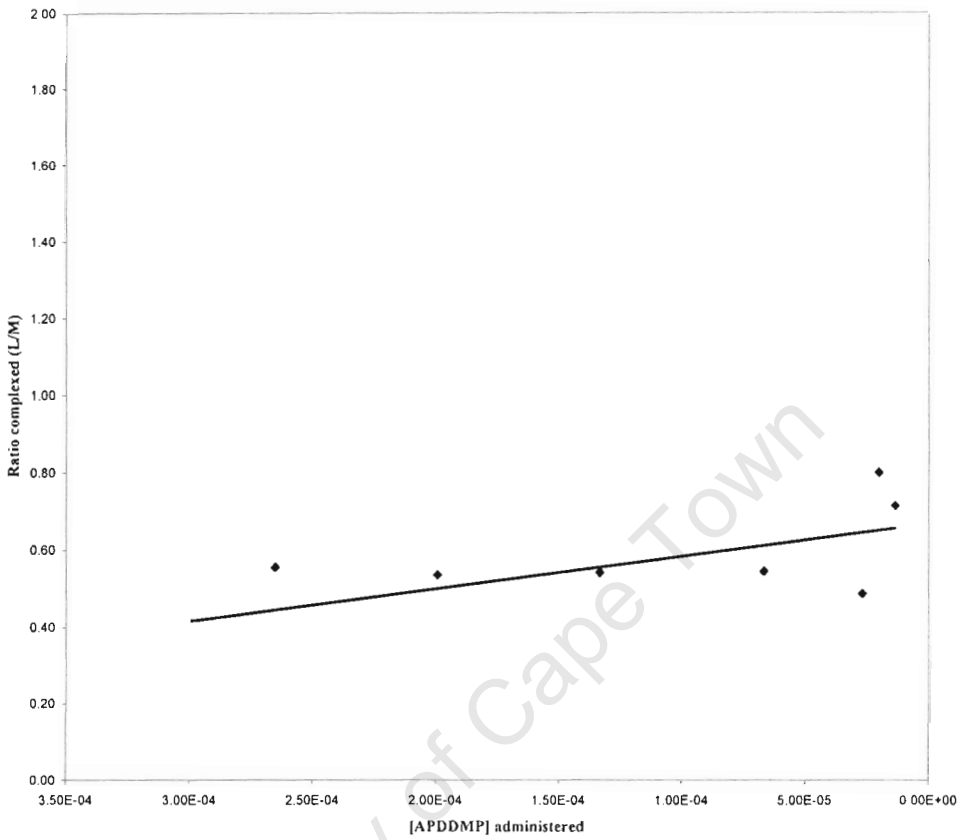

Figure 5.3.3(e): *Changes in ratio (L/M) for complexed Sn^{II} and APDDMP, as the administered concentrations of both Sn and APDDMP decreases. Trend in the ratio of APDDMP:Sn^{II} that is complexed in the blood plasma as observed when the administered concentrations of both Sn^{II} and APDDMP are decreased simultaneously. ♦Ratio of in vivo complexation. Lines represent the best-fit trend curves/functions.*

5.4 Discussion

5.4.1 Blood plasma modeling of Sn^{II}-APDDMP at clinical concentrations

Radiopharmaceuticals are usually administered intravenously, with the ligand (L) in large excess, typically in order of 10:1 (L:M). During animal trials the concentrations of the drug depend on the type of animal being used. The radiopharmaceutical is injected into larger animals such as baboons (primates) with a metal (M) concentration of $8.5\times10^{-6}\,mol.dm^{-3}$ and a ligand concentration of $8.5\times10^{-5}\,mol.dm^{-3}$. In studies with rats (rodents) concentrations of [M] = $2.65\times10^{-5}\,mol.dm^{-3}$ and [L] = $2.65\times10^{-4}\,mol.dm^{-3}$ were used [1]. These concentrations were adopted in the investigation of the rodent blood plasma model using ECCLES. The preferred clinical doses for injecting the radiopharmaceutical $^{117m}Sn^{II}$-APDDMP in patients (human) is similar to that of primate studies, with [M] = $8.5\times10^{-5}\,mol.dm^{-3}$, and [L] = $8.5\times10^{-4}\,mol.dm^{-3}$. Blood plasma was modelled with these concentrations for Sn^{II} and Apddmp and their speciation observed (*Figures 5.4.1a* and *5.4.1b*).

Calcium (Ca^{II}) forms very stable complexes with APDDMP, readily displacing the Sn^{II} into the blood plasma where it reacts with physiologically occurring ligands. This is evident in the speciation diagrams. Almost all (95.1%) of the APDDMP is taken up by Ca^{II} (*Figure 5.4.1b*): Ca_2(APDDMP) (66.8%), Ca_2(APDDMP)OH (24.1%), and Ca_2(APDDMP)H (4.2%). Only 0.1% of the total APDDMP concentration in blood plasma is bound to Sn^{II}, with a remaining 4.7% being attributed to complexation with Mg^{II}: Mg_2(APDDMP)OH (2.2%), Mg_2(APDDMP) (2.0%), and Mg_2(APDDMP)H (0.5%).

A considerable proportion of the Sn^{II} undergoes hydrolysis, $Sn(OH)_2$ (37.9%) and $Sn(OH)_3$ (0.4%), whilst most of the remaining tin binds with the ligands found in blood plasma upon dissociation from the complex(es). The most prominent species being that of

histinidinate, (Sn(His)OH) 35.5% and Sn(His) 2.8%, and cysteinate (Sn(Cys)) 11.7%. The distribution of Sn^{II} is rather extensive (*Figure 5.4.1a*), with interactions of 17 blood plasma ligands, and a considerable amount of these being binary complexes. In total, only about 2.8% of Sn^{II} remains bound by Apddmp: Sn_2(Apddmp)OH (1.8%), Sn_2(Apddmp)$(OH)_2$ (0.9%), and Sn_2(Apddmp) (0.1%). The vast distribution of Sn^{II} can be mainly attributed to the high affinity of the ligand (APDDMP) for Ca^{II}.

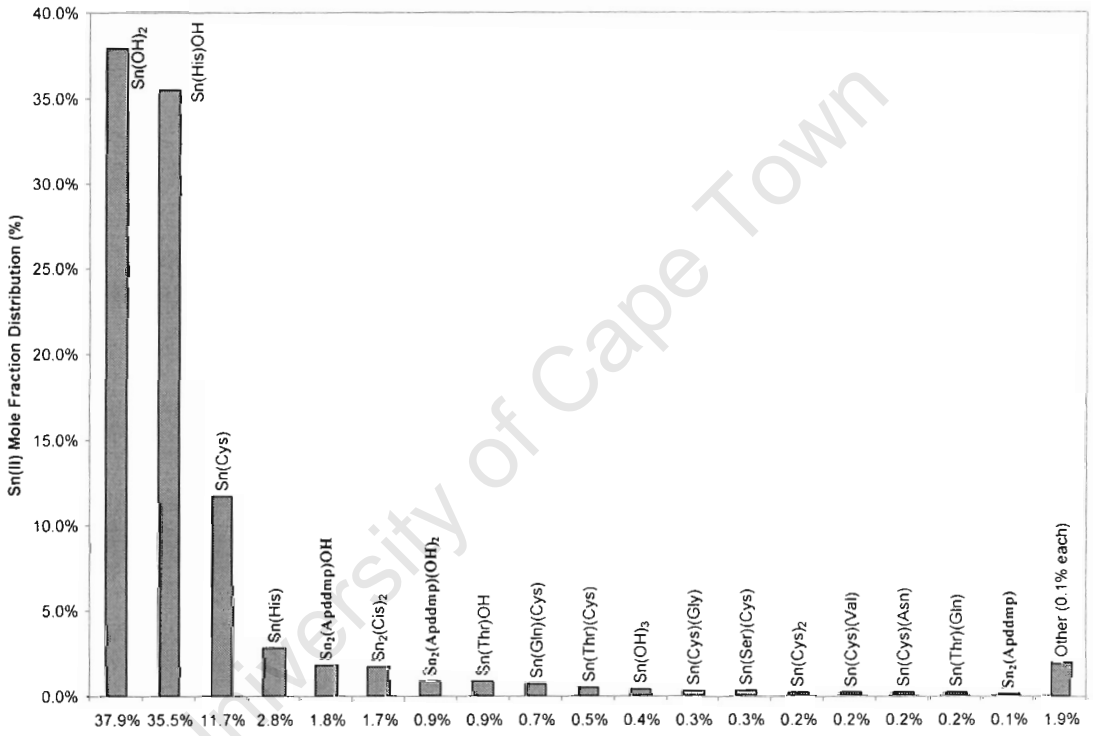

Figure 5.4.1a: *Speciation of Sn^{II} in normal blood plasma at preferred clinical doses, [M] = $8.5\times10^{-5}\,mol.dm^{-3}$ and [L] = $8.5\times10^{-4}\,mol.dm^{-3}$.*

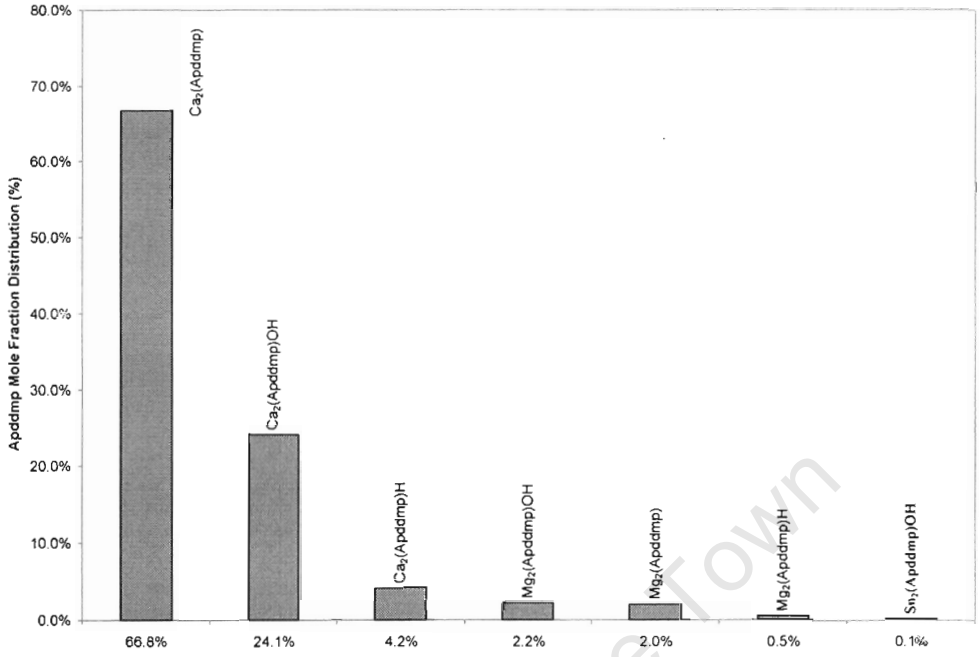

Figure 5.4.1b: *Speciation of Apddmp in normal blood plasma at preferred clinical doses, [M]* $= 8.5\times10^{-5}\,mol.dm^{-3}$ *and [L]* $= 8.5\times10^{-4}\,mol.dm^{-3}$.

In *Figure 5.4.1a* the species defined as "other" are comprised of all complexes which individually account for 0.1% of Sn^{II} within blood plasma. These include: Sn(Cys)(Phe); Sn(Cys)(Leu); Sn(Cys)(Asp); Sn(Cys)(Arg); Sn(Cys)(Pro); Sn(Gln)(Gly); Sn(Gln)(Ser); Sn(Cys)(Cta); Sn(Gly); Sn(Gln)OH; Sn(Gly)(Thr); Sn(Asn)OH; Sn(Ser)(Thr); Sn(Val)(Gln); Sn(Asn)(Gln); Sn(CO3)H; Sn(Cys)(Mla); Sn(Thr)(Val); Sn(Thr)(Asn).

- Abbreviations for *Figures 5.4.1a* and *5.4.1b*:

Arg:	Arginine;	Asn:	Asparaginate;	Asp:	Aspartate;
Cys:	Cysteinate;	Cis:	Cystinate;	Gln:	Glutaminate;
Gly:	Glycinate;	His:	Histidinate;	Leu:	Leucinate;
Phe:	Phenylalanate;	Pro:	Prolinate;	Ser:	Serinate;
Thr:	Threoninate;	Val:	Valinate;	CO3:	Carbonate;
Cta:	Citrate;	Mla:	Malate.		

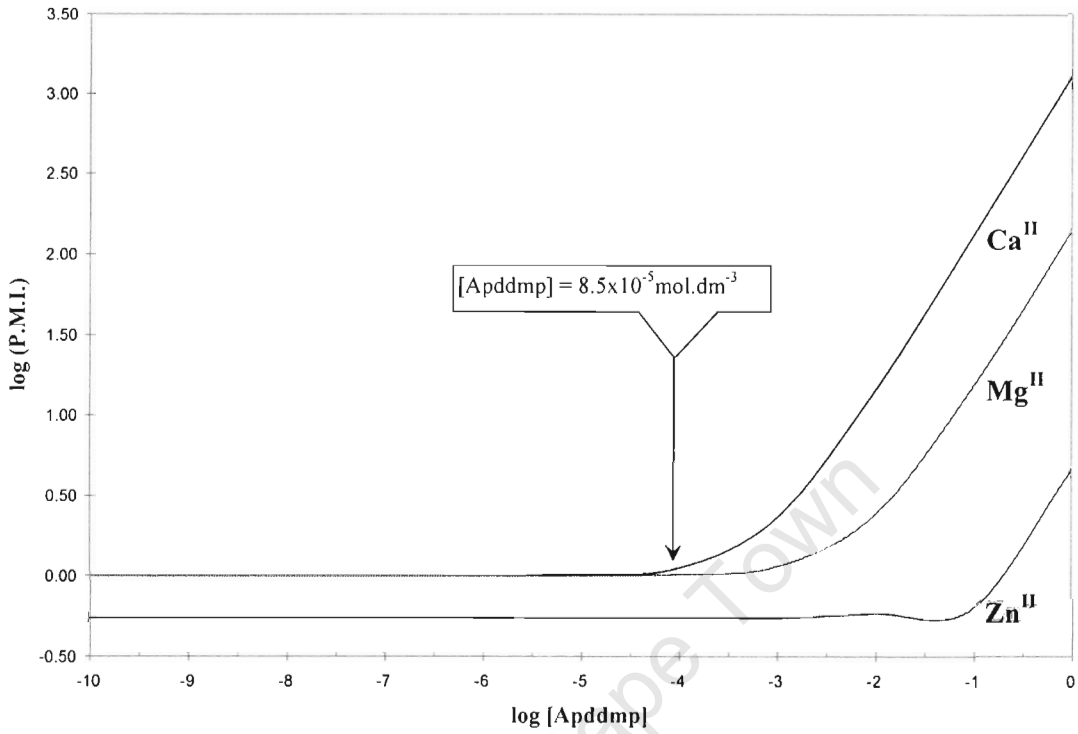

Figure 5.4.1c: *Plasma mobilisation index curves for Apddmp. The arrow represents a probable ligand concentration used for administering the drug in patients: [L]* $= 8.5\times10^{-5} mol.dm^{-3}$.

The blood plasma mobilisation index (P.M.I.) curves (*Figure 5.4.1c*) illustrate the extent to which the ligand, APDDMP, influences the natural balance of particular metal-ions within the blood plasma. The P.M.I. curves give an indication as to whether it would be necessary to provide the patient with mineral supplements so as to compensate for the mobilisation effect of the ligand (APDDMP). The arrow denotes the ligand concentration which would be used in the clinical administration of the radiopharmaceutical. Only Ca^{II}-ions are mobilised by APDDMP at a concentration of $8.5\times10^{-5} mol.dm^{-3}$. Due to the abundance of Ca^{II} within the body, the overall effect is buffered. Hence the observed mobilisation appears to be minor.

5.4.2 Rationalisation of hypotheses

If APDDMP clears faster with respect to Sn^{II} (according to the first postulate) the ratio of APDDMP to Sn^{II} that remains (complexed) in the blood plasma would decrease as the amount of APDDMP is lowered. Therefore, by decreasing the ratio of the "administered dose", the *in vivo* ratio of Sn^{II} and APDDMP that remains complexed would also decrease. A constant "*complexation ratio*" would indicate an independence of APDDMP concentration solely. Meaning that only a limited amount of Sn^{II} readily form complexes with APDDMP in blood plasma. The remaining tin was either substituted by other metal ions upon which it was flushed out via the kidneys, or the Sn^{II} was "hijacked" by other ligands in the blood plasma and then flushed out.

Faster clearance of the Sn^{II} relative to APDDMP would result in an increase in the APDDMP:Sn^{II} ratio of *complexation*. An increase in the ratio that is administered – by gradually decreasing the concentration of Sn^{II} – should then result in an increase in the ratio of APDDMP and Sn^{II} that stays complexed in the blood plasma. As above, a constant *complexation ratio* could mean that Sn^{II} is the limiting component and as a result no more APDDMP will complex with tin than the tin will allow.

Should the Sn^{II}-APDDMP complexes, as a whole, clear too rapidly for any worthwhile interaction with bone tissue to occur, the *ratio of complexation* would then remain constant irrespective of any changes in the concentrations of either Sn^{II} or APDDMP, or both. For a constant ratio of the Sn^{II} and APDDMP administered, a gradual decrease in the concentrations of APDDMP and Sn^{II} respectively, would result in the *ratio of complexation* being maintained.

From *Figure 5.3.1(c)* it is evident that for a fixed amount Sn^{II} the percentage that complexes with APDDMP decreases as the amount of APDDMP decreases. This could be mainly due to other metal ions present in blood plasma competing for APDDMP, and forming more stable complexes than that of Sn^{II}. By decreasing the APDDMP concentration its ability to compensate for competition of the metal ions in reduced. The

percentage APDDMP that form complexes with Sn^{II} increases. This indicates that a fixed amount of APDDMP is available for complexation with Sn^{II} and that a change in the amount of APDDMP in the blood plasma has little effect, if any, on the extent of complexation. The L:M ratio of complexation remains constant ($y = 1\times10^{-16}x + 0.52$, $R^2 = 0.96$, where y is the complexed ratio and x the administered ratio) as the amount of APDDMP is lowered relative to Sn^{II} (*Figure 5.3.1(e)*). Thereby, disproving the first hypothesis that APDDMP clears rapidly with respect to Sn^{II}.

Maintaining a fixed amount of APDDMP while gradually decreasing the Sn^{II} concentration resulted in a drop in the percentage of both Sn^{II} and APDDMP that were complexed – *Figure 5.3.2(c)*. The 'ratio of complexation' increased as the 'administered ratio' was increased ($y = 0.0034x + 0.50$, $R^2 = 0.73$, where y is the ratio of complexation and x the administered ratio) *(Figure 5.3.2(e))*, indicating the likelihood that Sn^{II} clears rapidly relative to APDDMP in blood plasma.

As can be seen in *Figure 5.3.3(c)*, there is an increase in the percentage of both Sn^{II} and APDDMP that are complexed as their concentrations are lowered while maintaining the 'administered' ratio of 1:10. The complexation ratio increases ($y = -0.79x + 0.7$, $R^2 = 0.62$, where y is the complexed ratio and x the administered ratio), rendering the third hypothesis false (*Figure 5.3.3(e)*). The increase in the ratio of complexation could be attributed to the change in the concentration of Sn^{II}, thereby verifying the assumption that Sn^{II} clears rapidly with respect to APDDMP.

The bone seeking ability of phosphonates is well known as is their fast renal clearance. In order to evaluate this for APDDMP a study in a baboon was undertaken [5]. This non-terminal experiment was carried out under protocol and due care was taken to ensure the well-being of the animal at all stages. One can monitor the biodistribution of the ligand by injecting ^{99m}Tc-labeled APDDMP, as conducted by *Zeevaart et al* [5]. Because no uptake of ^{99m}Tc in the thyroid was recorded (indications of free pertechnetate) it was assumed that the ^{99m}Tc stays bound to the polymer presenting an accurate biodistribution of APDDMP. The results, as presented in Figure 5.4.2(a), were corrected to the time of

injection for the radioactive decay of the ^{99m}Tc. From these experiments the rate of renal clearance of the ligand can be compared with that of its distribution in bone. There is a rapid accumulation of ^{99m}Tc-APDDMP in the kidneys within 4 minutes after injection, where the maximum renal concentration is reached (Figure 5.4.2(b)). The spine uptake shows that within 2 minutes of injection the bone receives its maximum dose, after which slow and steady clearance is observed.

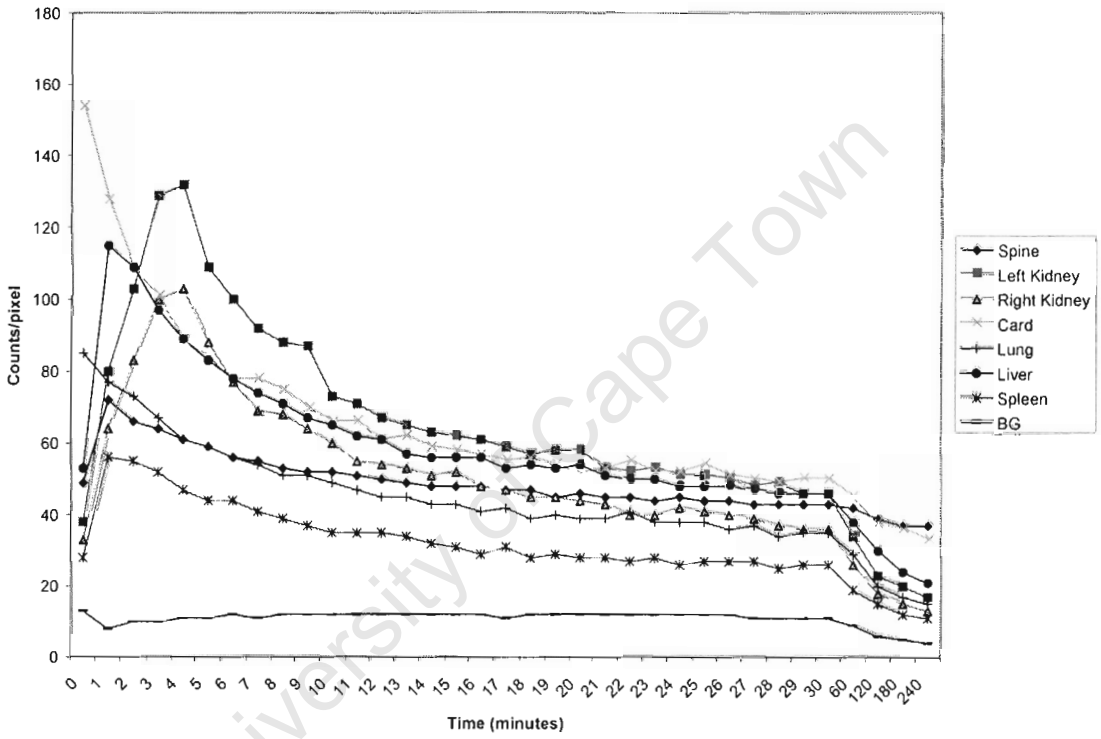

Figure 5.4.2(a). *Biodistribution of ^{99m}Tc-APDDMP as observed in animal experiments [5]. Monitored as count per pixel for a duration of 4 hours, which included a 30 minute dynamic study followed by a static study up to 4 hours. (Where Card = cardiac blood pool; BG = backbround.)*

The rate of clearance can be defined as the time taken for the ligand concentration to be halved ($t_{\frac{1}{2}}$), which in the case of the kidneys was $t_{\frac{1}{2}}$ = 10 minutes. Within the spine the concentration reached after 3 hours (which is the same as observed at 4 hours) is close to the expected half-concentration, therefore $t_{\frac{1}{2}} \geq$ 3 hours for bone. Hence, by comparison, it is clear that the ligand is present at the target (bone) long after the initial rapid renal

clearance. Despite the relatively large amount of APDDMP that is passed via the kidneys there is still an acceptable accumulation of the ligand within bone. From the slow spinal clearance rate ($t_{\frac{1}{2}} \geq 3$ hours) it is also safe to assume that, upon uptake at the bone interface, most of the APDDMP remains favourably bound.

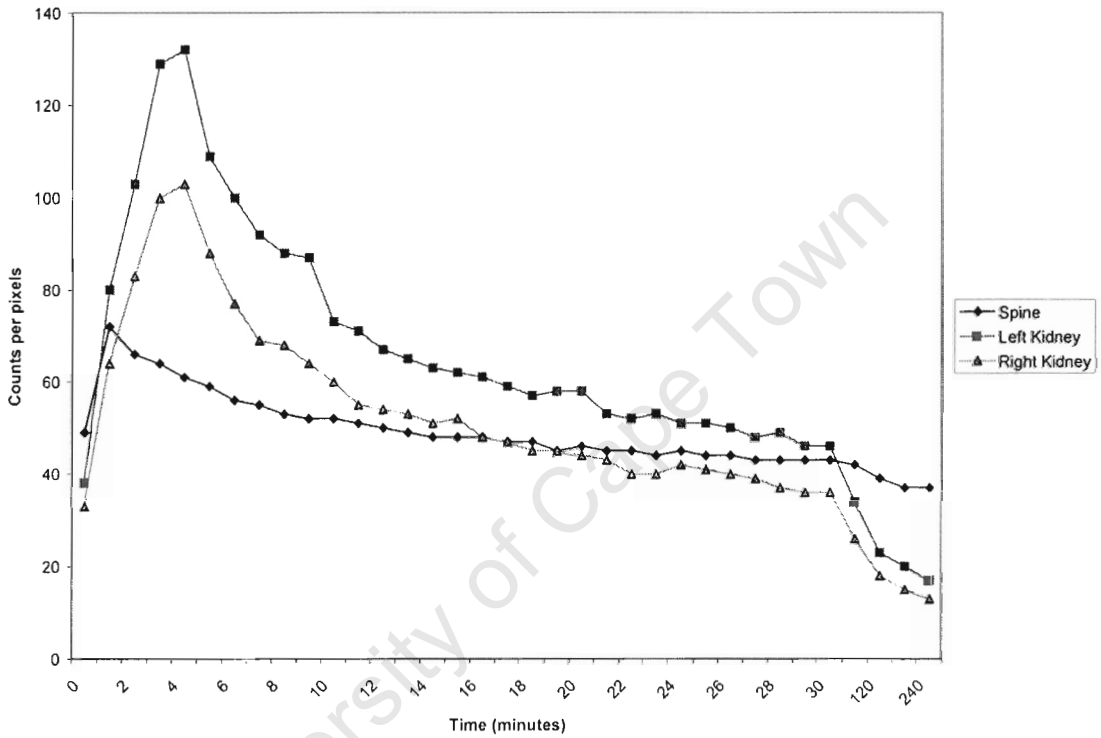

Figure 5.4.2(a). *Distribution and clearance of ^{99m}Tc-APDDMP within the spine and kidneys as observed in animal experiments [5]. Monitored as count per pixel for a duration of 4 hours, which included a 30 minute dynamic study followed by a static study up to 4 hours.*

5.5 Conclusion

In normal blood plasma only 0.1% of APDDMP remained complexed with Sn^{II}. Furthermore, this 0.1% of APDDMP (i.e. complexed with Sn^{II}) accounts for only 2.8% of the total Sn^{II} in blood plasma (*Figure 5.4.1a*). 95.1% of APDDMP was taken up by Ca^{II}. Histidinate and cysteinate complexed about 38.3% and 11.7% of Sn^{II} respectively – besides the binary complexes they've formed in combination with other ligands. Due to the extent of hydrolysis of Sn^{II} (38.3%), the dissociation of the Sn^{II}-APDDMP complex in blood plasma is mainly attributed to competition by Ca^{II}, and to a smaller degree Mg^{II}, for the APDDMP ligand. Thereby displacing the Sn^{II} ions into the blood plasma where it hydrolyses, as opposed to the scavenging of the Sn^{II} ions by in vivo ligands. The tin-ions that are not immediately hydrolysed are then complexed by a variety of ligands resulting in a large distribution of Sn^{II} species within blood plasma. However, the plasma mobilisation effect of APDDMP – which is only observed for Ca^{II} – is negligible (*Figure 5.4.1c*).

The behaviour of Sn^{II} and APDDMP in blood plasma was best depicted by the second hypothesis – the Sn^{II} clears rapidly relative to APDDMP. The results of the first postulate – in which the rapid clearance of APPDMP with respect to Sn^{II} was tested – served to confirm the second hypothesis.

The rationale behind the method used was to "starve" the complex of one of its components. The ligand is usually administered in excess – in this instance with a metal-to-ligand ratio of 1:10. Because of the abundance of ligand available for complexation, any change made to the ligand concentration should not affect the extent of complexation to a large degree. However, this only stands if competition for Sn^{II} by other ligands is negligible. This is proven by the first postulate, in that the percentage of complexed [APDDMP] to the total concentration increases – since the total ligand concentration is being lowered. This should still ensure the survival of the radiopharmaceutical for delivery at the target tumour, because of a fixed interaction between APDDMP and Sn^{II}. Hence, beyond the amount of APDDMP that was compensated for competition by other

ligands (i.e. the excess) the complex does not dissociate readily. Therefore, the Sn^{II} does not favour complexation with physiologically occurring ligands over APDDMP.

On the other hand, competition of a second kind must be tested, whereby the metal-ions in blood plasma compete against Sn^{II} for APDDMP. Upon injection the excess APDDMP binds to the physiological metal-ions, and further displaces the Sn^{II} ion from the complex. The effect would be similar to that of the second hypothesis, in which the ratio of Sn^{II}-to-APDDMP that remains complexed increases as the available [Sn^{II}] is decreased. Understandably, the percentage of the total Sn^{II} concentration that is complexed decreases since its capacity to counteract the competition of other metal-ions is reduced. The drop in the percentage of [APDDMP] that remains complexed supports this – the competition of the metal-ions outweighs the Sn^{II} ion's chances of forming complexes.

Rapid clearance of the entire complex would be mainly due to metabolism. The third assumption only confirmed predictions made above. Although both the Sn^{II}-ion and APDDMP concentrations are decreased there was still a clear increase in the ratio of complexation. Since it has been shown that the extent of complexation is independent of the [APDDMP], it stands to reason that the mere drop in the available Sn^{II} ion concentration hinders its survival within the Sn^{II}-APDDMP complex.

APDDMP's affinity for Ca^{II} could be too high. Most likely the Sn^{II} ions are displaced by the Ca^{II} ions present in blood plasma, adversely affecting delivery of the radionuclide to the bone tumour. Instead, the radioactive tin-117m ($^{117m}Sn^{II}$) is flushed out via the kidneys in the form of histidinate and/or cysteinate complexes, accounting for more than 50% of the Sn^{II} in the blood plasma. However, the APDDMP ligand could still continue the journey towards the tumour, but without the active ingredient $^{117m}Sn^{II}$ – and with Ca^{II} ions instead – having been hijacked. Due to the extent of hydrolysis of Sn^{II} (about 40% of the tin(II)-ions) it would also be reasonable to expect to see considerable uptake by the liver or the reticuloendothelial system, as reported for studies conducted on Sn^{II}-chloride by Srivastava *et al* [2]. Srivastava also noted the difficulty of working with tin-based

compounds at pH7.4, as the reproducibility of results was hampered by the ease at which tin hydrolyses (both Sn^{II} and Sn^{IV}), as well as the ease of oxidation of Sn^{II}.

5.6 References

[1] J. R. Zeevaart, D. R. Jansen, M. F. Botelho, A. Abrunhosa, C. Gomes, L. Metello, Z. I. Kolar, G. C. Krijger, W. K. A. Louw, and I. C. Dormehl, *Journal of Inorganic Biochemistry,* 2004, **98,** 1521-1530.

[2] S. C. Srivastava, G. E. Meinken, P. Richards, P. Som, Z. H. Oster, H. L. Atkins, A. B. Brill, F. F. Kapp Jr, and T. A. Butler, *Int. J. Nucl. Med. Biol.,* 1985, **12**, 167-174.

[3] J. R. Zeevaart, W. K. A. Louw, Z. I. Kolar, J. M. Wagener, N. V. Jarvis, R. A. M. Claessens, *Journal of Radioanalytical and Nuclear Chemistry,* 2003, **257**, 83-91.

[4] J. R. Duffield, D. R. Williams, and I. Kron, *Polyhedron*, 1991, **10**, 377-387.

[5] Unpublished data obtained from animal studies (baboons) as conducted by J. R. Zeevaart.

[6] J. R. Zeevaart, N. V. Jarvis, W. K. A. Louw and G. E. Jackson, *J. Inorg. Biochem.,* 2001, **83**, 57-65.

[7] J. R. Zeevaart, N. V. Jarvis, I Cukrowski and G. E. Jackson, *S. Afr. J. Chem.,* 1997, **50**, 189-194.

[8] R. A. M. J. Claessens and Z. I. Kolar, *Langmuir,* 2000, **16**, 1360-1367.

[9] J. M. Wagener and N. V. Jarvis, *S. Afri. J. Chem.*, 1995, **48**, 85.

CONCLUSION AND FUTURE WORK

6.1 Conclusion

The conventional techniques for developing and evaluating radiopharmaceuticals involved the random selection of a metal-ion and ligand combination with the hope of a positive outcome. The method involved a series of extensive animal trials. By pooling the vast variety of analytical tools available for elucidating novel systems, the chances of making more educated predictions are enhanced as to the behaviour of prospective therapeutic agents, as illustrated in this thesis to a small degree. In this study glass electrode potentiometry was combined with a computer simulated model of blood plasma (ECCLES) to effectively evaluate the in vivo behaviour of a potential radiopharmaceutical, Sn^{II}-APDDMP, thereby predicting the effectiveness of the drug without having to pursue animal experiments. The outcome of which can later be validated by a limited number of well-planned animal studies.

Radioactive tin-117m (^{117m}Sn) was identified as a suitable nuclide because of its favourable radiation characteristics, affording low radiotoxicity to the more sensitive healthy bone marrow. This is favourable as it allows for an increase in the administered dose with minimal side-effects. Preliminary 'cold' experiments were conducted with stable forms of Sn^{II} and Sn^{IV} for the potentiometric determination of the equilibria with the respective ligands of choice.

Two fairly new phosphonate ligands were studied, as these are regarded as having good bone affinity, and hence expected to aid in the accumulation of the drug in regions of high bone-turnover – as is characteristic of tumours. The ligands being: *N,N,-dimethylenephosphonate-1-hydroxy-4-aminopropylidene-diphosphonate (APDDMP)* and *N,N',N'-trimethylenephosphonate-polyethyleneimine (PEI-MP).*

The complexation equilibria that were observed were that of Sn^{II}-APDDMP and Sn^{IV}-PEI-MP. Complexation studies of APDDMP with those metal-ions that occur in blood plasma in high concentration namely Ca^{II}, Mg^{II} and Zn^{II} were also studied. The analyses of titration data by ESTA produced satisfactory results, and reasonably low Hamilton R-Factors and standard deviations. The calculated functions: $\overline{Z}_H$, $\overline{Z}$, and $\overline{Q}$ were close to the experimentally observed values, and representative distributions of equilibria were obtained. The table below (Table 6.1) shows the dominant species of each system as they occurred at the physiological pH 7.4. All the complexes that form at pH 7.4 are highly charged (negative; as high as 6-) for all of the systems under investigation. For the radiopharmaceuticals considered, PEI-MP predominantly formed hydrolysed complexes, whereas with APDDMP, 51% of the species that formed at pH 7.4 were hydroxides with the exception of two complexes: $[Sn^{II}\text{-APDDMP}]^{5-}$ (48%) and $[Sn^{II}_2\text{-APDDMP}]^{3-}$ (1%). In the formation of complexes between APDDMP with Ca^{II}, Mg^{II} and Zn^{II} the distribution at physiological pH was somewhat mixed for the three systems, with hydroxide species being very prominent.

The blood plasma modelling program ECCLES was used as a means of evaluating the in vivo performance of APDDMP and, in essence, explain the bio-distribution of Sn^{II}-APDDMP as observed in a study conducted on rats [1]. The animal studies revealed a considerably high kidney and bladder uptake, and excretion. Three hypotheses were tested by studying trends in the percentage complexation of the Sn^{II} metal-ion and ligand concentrations as calculated by ECCLES. The exact values were not as significant to this study, but rather the overall trends in ratios and relative concentrations of the metal-ion and ligand were utilized to draw the necessary conclusions. The metal-to-ligand ratios of the complexed Sn^{II} and APDDMP were compared, as the ratios within the administered drug were gradually altered. The hypotheses were established to ascertain whether dissociation of the Sn^{II}-APDDMP complex(es), due to susceptibility of either the Sn^{II} ion or the ligand, was responsible for the observed renal uptake, or even due to rapid clearance of the complex as a whole. The calculations proved that the complex is not able to withstand the competition within blood plasma and dissociates before it reaches the target. This is due to the rapid clearance of the radioactive tin-117m ($^{117m}Sn^{II}$), as

observed by *Srivastava et al* [2] and *Zeevaart et al* [1]. APDDMP has a stronger affinity for physiological metal-ions such as Ca^{II}, which resulted in the dissociation of the radiopharmaceutical, whereupon the $^{117m}Sn^{II}$ was flushed out via the kidneys, bound to histidinate and cysteinate ligands in blood plasma. The change in the levels of APDDMP within blood plasma was minimal, or slower, upon dissociation of the drug, whilst the total Sn^{II} concentration decreased.

Therefore, based on the conclusions derived from the ECCLES calculations, which substantiated the animal studies, $^{117m}Sn^{II}$-APDDMP would not be a very effective radiopharmaceutical for the treatment of metastatic bone cancer. However, ^{117m}Sn remains a favourable radionuclide for consideration as a component for bone-seeking radiopharmaceuticals. ^{117m}Sn-PEI-MP (Sn^{II} and/or Sn^{IV}) radiopharmaceuticals could hold more promising results. Initial studies have been pursued to establish the formation constants [3, 4, 5,] of PEI-MP as prospective drugs. Future efforts should be focused toward characterizing $^{117m}Sn^{IV}$-PEI-MP behaviour within blood plasma, and validation by animal trials. Chapter 4 reports the formation constants for Sn^{IV}-PEI-MP determined in this study. The ligand forms relatively stable complexes with Sn^{IV}, which could possibly survive the conditions of blood plasma. The complexes that form at pH 7.4 are less diverse than with APDDMP. Hence it would be more specific in its action, with hopefully less side-effects. The dominant species $[Sn^{IV}_2L(OH)_5]^{2-}$, accounts for approximately 60% of the Sn^{IV}.

Table 6.1: *The dominant species of each system at pH7.4, and their mole fraction percentage (I = 150mM NaCl and T = 25°C).*

System	Dominant Species at pH 7.4	Mole Fraction Percentage at pH 7.4	Chapter
Sn^{II}-APDDMP	$[Sn^{II}\text{-APDDMP}]^{5-}$	48%	2
	$[Sn^{II}_2\text{-APDDMP(OH)}]^{4-}$	32%	
	$[Sn^{II}_2\text{-APDDMP(OH)}_2]^{5-}$	16%	
	$[Sn^{II}\text{-APDDMP(OH)}]^{6-}$	3%	
	$[Sn^{II}_2\text{-APDDMP}]^{3-}$	1%	
Ca^{II}-APDDMP	$[Ca^{II}_2L]^{3-}$	69%	3
	$[Ca^{II}_2L(OH)]^{4-}$	27.5%	
	$[Ca^{II}_2LH]^{2-}$	3.5%	
Mg^{II}-APDDMP	$[Mg^{II}_2L(OH)]^{4-}$	52.0%	3
	$[Mg^{II}_2L]^{3-}$	39.0%	
	$[Mg^{II}_2LH]^{2-}$	7.5%	
	$[Mg^{II}_2L(OH)_2]^{5-}$	1.5%	
Zn^{II}-APDDMP	$[Zn^{II}_2L(OH)]^{4-}$	54.0%	3
	$[Zn^{II}_2L(OH)_2]^{5-}$	40.0%	
	$[Zn^{II}L(OH)]^{6-}$	5.0%	
	$[Zn^{II}_2L]^{3-}$	1.0%	
Sn^{IV}-PEI-MP	$[Sn^{IV}_2L(OH)_5]^{2-}$	60.0%	4
	$[Sn^{IV}_2L(OH)_4]^{1-}$	37%	
	$[Sn^{IV}_2L(OH)_3]^{0}$	3%	

6.2 Future Work

The distribution of the APDDMP ligand, solely, in blood plasma remains to be verified by animal studies, since only the radionuclide (^{117m}Sn) could be detected. It is possible that APDDMP on its own could have localized on bone tissue, and more specifically accumulated at the tumour site. Zeevaart *et al* [6] successfully demonstrated that APDDMP is, in fact, a good bone seeker, having achieved a bone uptake of 82.2% in animal experiments conducted with ^{99m}Tc-APDDMP. Alternatively, this can be determined by synthesizing APDDMP with a radioactive-phosphorous label (^{32}P) so as to trace the bio-distribution of the ligand – injecting Sn^{II}-APDDMP containing a stable isotope of tin(II), and thereby purely monitor the localisation of the ligand.

With APDDMP the formation of neutral species at pH 7.4 were successfully avoided, as compared to APD, $[MLH]^0$ [8,9]. However, the increased charge introduced by the additional methylenephosphonate groups (two) did little to enhance the delivery of the radionuclide ($^{117m}Sn^{II}$) to bone, let alone the tumour site. Although liver uptake was effectively minimized, the complexes that do form at pH 7.4 are too highly charged – predominantly $[ML]^{5-}$ – for favourable bone uptake (*Table 6.1*). The affinity that APDDMP exhibits for Ca^{II} hinders the efficacy of the prospective radiopharmaceutical ($^{117m}Sn^{II}$-APDDMP).

An alternative approach to APDDMP could be to functionalize APD with groups that can enhance the stability of the complex without necessarily affecting the charge of the species. By increasing the complex stability, all complexes form more readily at lower pH, essentially shifting the complex formation down the pH scale. In so doing, the neutral species, $[MLH]^0$, that would typically predominate at pH 7.4 – as with APD – would make way for the $[ML]^-$ complex, which becomes present to a larger extent. This can possibly be achieved by adding two *N,N*-dimethylethanamide (or *N,N*-dimethylacetamide) groups at the amine of APD, hence a new potential ligand called APDDAM (*Figure 6.1*).

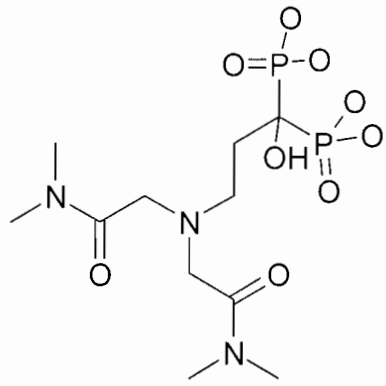

APDDAM

***Figure 6.1**: Molecular structure of the ligand APDDAM: N,N-di(N',N'-dimethylethanamide)-1-hydroxy-4-aminopropylidene-diphosphonate.*

ECCLES calculations of Sn^{IV}-PEI-MP could not be pursued, as the blood plasma model for Sn^{IV} has not yet been established. The formation constants should be determined for the binding interactions of Sn^{IV} with the variety of ligands typically found in blood plasma and included in the ECCLES database before any preliminary predictions can be made pertaining to the *in vivo* performance of prospective Sn^{IV}-PEI-MP radiopharmaceuticals. However, extensive research has already been conducted on the PEI-MP with various metal-ions, including Sn^{II} [4]. The inclusion of these formation constants for PEI-MP into the ECCLES database will giver some insight into the interaction of the ligand itself within blood plasma. *Figure 6.2* shows the blood plasma speciation of PEI-MP, incorporating data obtained from *Zeevaart et al* [4] into ECCLES. Once again a high affinity of the ligand for Ca^{II} is observed. Interesting to note is that the ligand also exists as uncomplexed protonated species H_2PEIMP, HPEIMP and H_3PEIMP, although to a small degree. This could mean that calcium will not displace the tin-ion from the PEI-MP complexes as easily as it did with APDDMP. Because, it would be expected that any free ligand occurring in the blood plasma would be easily occupied by Ca^{II}-ions, as was the case of APDDMP. Being a polymer, PEI-MP invokes steric hindrance for access of larger metal-ions as opposed to protons (H^+-ions) – upon dissociation of the Sn-PEI-MP complex. The blood plasma speciation of Sn^{IV} will give

further insight as to the susceptibility of the Sn^{IV}-PEIMP radiopharmaceutical, whereupon predictions can be made as to whether the complex dissociates within blood plasma and why, or why not.

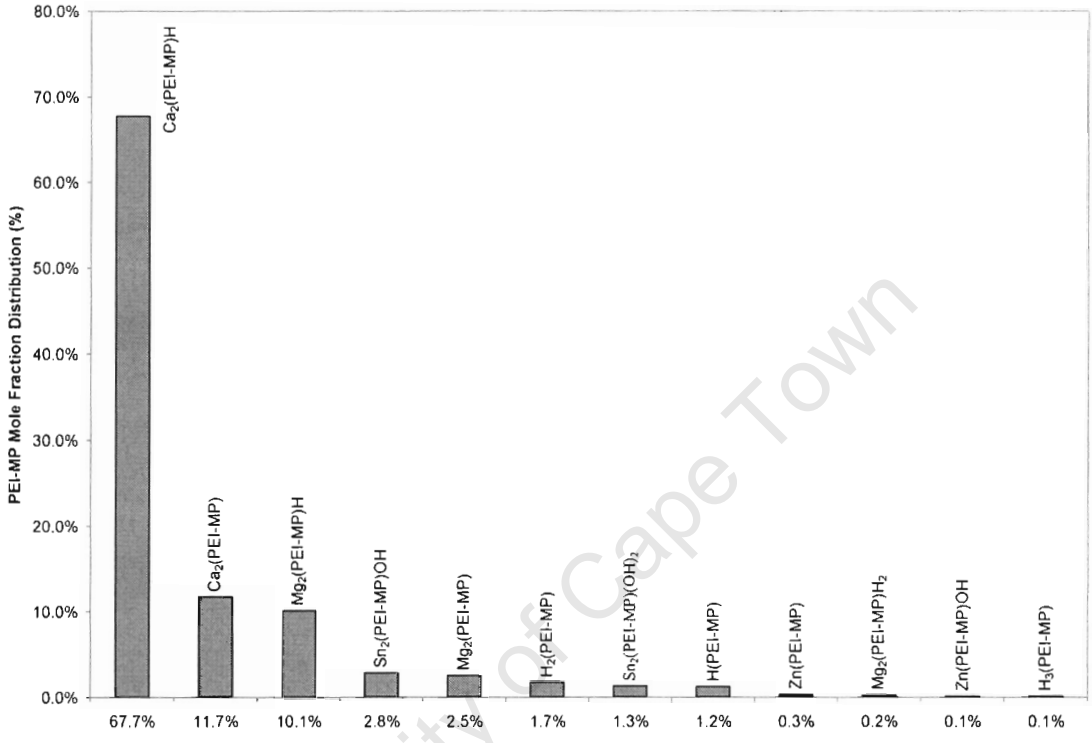

Figure 6.2: *Speciation of PEI-MP in normal blood plasma,* $[Sn^{II}] = 8.5\times10^{-6}\,mol.dm^{-3}$ *and* $[PEI\text{-}MP] = 8.5\times10^{-5}\,mol.dm^{-3}$.

A further aspect for inclusion in the ECCLES blood plasma modelling could be the consideration of mixed-metal species. These are similar to the binuclear complexes observed within the speciation models reported above, such as Sn^{II}_2-APDDMP and Sn^{IV}_2-PEI-MP$(OH)_3$, but instead contain two different metal-ions – for example $Sn^{II}Ca^{II}$-APDDMP. The likelihood exists that these type of species could form, however their formation constants have yet to be determined experimentally. Future studies could include the measurement the equilibrium constants for the mixed systems of the major physiological metal-ions, namely Ca^{II}, Mg^{II} and Zn^{II}, with Sn^{II} and Sn^{IV} for both ligands APDDMP and PEI-MP

Experiments pertaining to Sn^{IV}-PEI-MP were mainly complicated by the inevitable hydrolysis of Sn^{IV} in solution resulting in the formation of precipitate, which hampered the potentiometric analyses. As considered in Chapter 4, the dual-burette method has to be modified and refined, in which the Sn^{IV} (in acid medium to retard hydrolysis) is titrated against the ligand in solution whilst maintaining fixed pH with a second burette containing alkaline solution, typically 0.05M NaOH. However, with the current technique, a reasonable model was obtained. PEI-MP could still be the subject of future research, since – based on the results obtained here – it would effectively have a reduced liver uptake as opposed to Sn^{II}-APDDMP, given that the dominant species is moderately charged, $[Sn^{IV}_2L(OH)_5]^{2-}$. PEI-MP has good bone-seeking capabilities, as illustrated in pharmacokinetic and biodistribution studies of ^{99m}Tc-PEI-MP [7]. Therefore, reasonable deposition and accumulation of $^{117m}Sn^{IV}$-PEI-MP in bone can be expected. As with APDDMP, predictions can be made of the behaviour of the Sn^{IV}-PEI-MP radiopharmaceutical in blood plasma using ECCLES as soon as the Sn^{IV} model is in place. Animal studies will give some practical insight as to the biodistribution of $^{117m}Sn^{IV}$-PEI-MP. Blood plasma modelling of Sn^{II}-PEI-MP was performed by Zeevaart *et al* [4], and revealed promising results, with 82.8% of the Sn^{II} remaining bound to PEI-MP.

Like PEI-MP, which is essentially the polymer of EDTMP, other ligands that exhibit an affinity for calcium, and hence hydroxyapatite, can be polymerized. For example, a derivative of HEDP. In so doing, continue to exploit the enhanced permeability and retention effect, whereby the polymer can be expected to accumulate selectively in regions of increase bone turnover for effective delivery of the radionuclide.

As the general understanding grows, through persistent probing and refining of techniques, more accurate predictions can be made – effectively making it possible to design radiopharmaceuticals that are more efficient, with minimal side-effects. Better ligands can be synthesized, or the existing ones modified to enhance the delivery of radionuclides to tumours for pain palliation and the eventual eradication of the cancer. Making advances toward the ultimate cure. The search continues.

6.3 References

[1] J. R. Zeevaart, D. R. Jansen, M. F. Botelho, A. Abrunhosa, C. Gomes, L. Metello, Z. I. Kolar, G. C. Krijger, W. K. A. Louw, and I. C. Dormehl, *Journal of Inorganic Biochemistry,* 2004, **98**, 1521-1530.

[2] S. C. Srivastava, G. E. Meinken, P. Richards, P. Som, Z. H. Oster, H. L. Atkins, A. B. Brill, F. F. Kapp Jr, and T. A. Butler, *Int. J. Nucl. Med. Biol.,* 1985, **12**, 167-174.

[3] N. V. Jarvis, J. R. Zeevaart, J. M. Wagener, W. K. A. Louw, I. C. Dormehl, R. J. Milner, and E. Killian, *Radiochim. Acta*, 2002, **90**, 237-246.

[4] J. R. Zeevaart, W. K. A. Louw, Z. I. Kolar, J. M. Wagener, N. V. Jarvis, R. A. M. J. Claessens, *Journal of Radioanalytical and Nuclear Chemistry,* 2003, **257**, 83-91.

[5] J. R. Zeevaart, W. K. A. Louw, Z. I. Kolar, E. Killian, F. E. Jansen van Rensburg, I. C. Dormehl, *Arzneim.-Forsch/Drug Res.*, 2004, **54**, 340-347.

[6] J. R. Zeevaart, N. V. Jarvis, W. K. A. Louw and G. E. Jackson, *J. Inorg. Biochem.,* 2001, **83**, 57-65.

[7] I. C. Dormehl, W. K. A. Louw, R. J. Milner, E. Kilian and F. H. A. Schneeweiss, *Drug Res.*, 2001, **54**, 258-263.

[8] J. R. Zeevaart, PhD Thesis, *'Metal ion speciation in Blood Plasma as a Tool in Predicting the in vivo Behaviour of Potential Bone-Seeking Radiopharmaceuticals', Delft University of Technology,* 2001, Delft University Press, The Netherlands.

[9] J. R. Zeevaart, N. V. Jarvis, W. K. A. Louw, G. E. Jackson, I. Cukrowski, C. J. Mouton, *Journal of Inorganic Biochemistry, 1999,* **73**, 265-272.

[10] B. K. Shcherbakov, F. I. Bel'skii, M. P. Komarova, Y. M. Polikarpov, T. Y. Medved, M. I. Kabachnik, Izv. Akad. Nauk. SSSR Ser. Khim., 1982, **3,** 560-564.

[11] J. R. Zeevaart, W. K. A. Louw, N. V. Jarvis and J. M. Wagener, *J. Lab. Comp. Radiopharm.,* 2001, **44**, S799-S801.